A CLOUD AND BUBBLE CHAMBER STUDY OF PROTON-PROTON INTERACTIONS AT 970 Mev

by

J. G. Hill

A thesis submitted for the degree of

Ph.D. (Special Regulations)

University of Birmingham

October, 1959

AT THE BEHEST OF THE UNIVERSITY, THE FOLLOWING PAGES OF THIS THESIS HAVE NOT BEEN SCANNED:

Appendices.

(1) Proton-proton interactions at 970 Mev (Proc.Roy.Soc.A, 251, 218, 1959)

For reference only.

(2) Proton-deuteron interactions at 970 Mev (Proc.Roy.Soc.A, 251, 233, 1959)

(3) 9-inch liquid hydrogen bubble chamber in a pulsed magnetic field

(Nucl.Instrum. and Methods, 4, 26, 1959)

SYNOPSIS

Chapter I describes an experiment to study proton-proton interactions at 970 Mev. A high pressure diffusion cloud chamber was filled with hydrogen at 25 atmospheres and operated in the proton beam from the Birmingham synchrotron. A pulsed magnetic field of 13,000 oersted, applied to the chamber, enabled momenta of primary and secondary particles to be measured. 1029 events were observed due to the interaction of protons with protons. Of these, 565 events were attributed to elastic collisions and are discussed in terms of the optical model of the nucleus, giving a radius of interaction of $0.9 \pm 0.1 \times 10^{-13}$ cms. Information from 458 inelastic events is compared with the statistical theory of pion production due to Fermi, and the isobar theory due to Peaslee. The results for positive pion production support Peaslee's theory but there are certain anomalies in the neutral pion production.

Chapter II contains a description of a 9" diameter liquid hydrogen bubble chamber for use with the Birmingham synchrotron. Details are given of the chamber and expansion system along with the cryogenic, vacuum, high pressure and optical systems and the method for obtaining a pulsed magnetic field. The operation of the apparatus is discussed and an enclosed system for filling the chamber with deuterium is described. Finally,

possible experiments that may be performed are mentioned.

CONTENTS

PREFACE

The author joined the Birmingham diffusion cloud chamber group in September 1956. He was immediately engaged in the operation of the cloud chamber for the experimental run described in Chapter I. During the following few months he made a detailed study of the momentum spectrum of the primary beam from photographs taken during the experiment. For the major part of the next 18 months he measured the relevant properties of over one half of the interactions observed in hydrogen, the remainder being measured by his supervisor, Dr. L. Riddiford, and Dr. A.P. Batson. Also during this time he took an active part in the operation of the cloud chamber with gas fillings of helium and nitrogen, and helped to investigate the possibility of using a pencil beam of protons.

Over the past 12 months his main interest has been with the liquid hydrogen bubble chamber, although a further study has been made of the cloud chamber experimental results (Chapter I, section 3). His prime concern has been the development of an enclosed system for filling the bubble chamber with deuterium, which has been tested successfully with hydrogen. Considerable time has also been spent helping to improve the operation of the chamber with liquid hydrogen and, in particular, modifying the excitation system which provides the pulsed magnetic field.

INTRODUCTION

Although to date there is no satisfactory theory of nuclear forces, the most promising, and partially successful approach, has been on the basis of field theory. This approach has been extremely successful in an explanation of electromagnetic forces, where modern field theory indicates that the forces between charges arise from the virtual exchange of photons. In this case, because of the infinite range of electromagnetic forces, the quantum exchanged, the photon, has zero rest mass. However, nuclear forces are finite in range so that on this theory there is a virtual exchange between nucleons of particles of finite mass. Yukawa (1935) predicted an exchange particle of about 300 electron masses in order to account for the range and strength of nuclear forces. In 1947 this particle, known as the pi-meson or pion, was observed in nuclear emulsions (Lattes et al., 1947) which had been exposed to cosmic rays. At energies greater than about 400 Mev pion production becomes important in nucleon-nucleon collisions, so that it is of interest to investigate inelastic (pion-producing) processes in an attempt to study the nature of nuclear forces.

Because of the complexity of field theory calculations, theories of pion production at present are phenomenological in nature. Brueckner (1952), in an analysis of early experiments on pion-nucleon scattering, introduced the concept of a nucleon isobar to explain the observed variation of total cross-section with energy and the charged pion multiplicity. This idea of "isobaric" states of the nucleon had been suggested from

meson theory, and Brueckner showed that a state with T = 3/2 could account for the anomalous features of the experimental results. Later this approach was extended to cover photomeson production and single meson production in nucleon-nucleon collisions (Brueckner and Watson, 1952). In the latter case, for an interaction of the type

$$N + N \longrightarrow N + N + \pi$$

it is postulated that an intermediate stage is the excitation of one of the nucleons to an "isobaric" state with T = 3/2 and that this isobar subsequently decays into a nucleon and a pion.

A statistical theory of pion production has been proposed by Fermi (1950, 1953, 1954). He supposes that when two high energy nucleons collide their kinetic energy is released in a small volume of radius equal to the Compton wavelength for a pion. He includes a factor to allow for the Lorentz contraction of this sphere at high energies. During the interval of time in which this state exists a number of reactions involving the creation and destruction of pions can take place. Fermi takes the extreme view that statistical equilibrium is reached, because of the strong interaction in the pion field, and that the final number of particles created is governed by statistical laws. He neglects the restrictions imposed by the conservation of angular momentum and assumes that all possible final states are formed with a probability proportional to the statistical weight of the final state. He points out that complications arise due to the identity of some particles, and that allowance should be made for the multiplicity of states introduced by particle spin. He considers the production of a single meson and shows

that angular momentum conservation introduces a small correction. He gives the relative probability for each reaction to occur, and also the ratio of double to single pion production at a given energy. A comparison with experimental results on neutron-proton scattering at 2.2 Bev (Fowler et al., 1954) indicates that the latter ratio is too small. If the one adjustable parameter of the theory, namely the interaction volume, is increased the observed double to single pion ratio can be reproduced. However, the total inelastic cross-section now becomes more than double that observed.

Block (1956) points out that in applying Fermi's statistical theory of meson production to Cosmotron and Bevatron energies, an exact relativistic evaluation of the phase space integral for the final many-particle system is required. He gives formulae which are applicable to 2, 3, 4 and 5-body final states. Curves are given for the momentum spectra of any one particle at several incident nucleon energies. He has also derived expressions for the Q-values which would be observed between pairs of particles in the final system. The results for a 3-body final state (two nucleons and a pion) are compared with the results of the present experiment in section 2(vi) of Chapter I.

Kovacs (1956) has modified Fermi's theory to take into account the interaction between particles in the final state. He considers nucleon-nucleon and pion-nucleon interactions separately and neglects pion-pion interactions. This separation, which he regards as approximate, is justified on the grounds that the pions leave the field of interaction fairly quickly, while the slowly moving nucleons are still within the range of their mutual forces. The two nucleons are assumed to be in a

relative S-state after the interaction. This assumption although plausible near the threshold energy for a reaction is doubtful when applied to high energies, where higher l-values are expected to contribute. The meson-nucleon interaction is treated by a method suggested from meson-nucleon scattering in which a strong resonant interaction is known for the system with $T = J = 3/2$. The effect of the nucleon-nucleon interaction is that higher pion multiplicities are favoured when compared with the statistical theory, since the nucleons are left in a low energy state. The pion-nucleon resonance modifies these multiplicities in the appropriate energy region. In particular, double meson production is enhanced at the expense of single meson production at energies around 1.5 Bev. This model gives a better interpretation of neutron-proton scattering at Cosmotron energies (Fowler et al., 1954) than that due to Fermi. Kovacs' theory, unlike the one discussed below due to Lindenbaum and Sternheimer, does not predict angular and energy distributions for a particular reaction.

Peaslee (1954) has deduced the charged and neutral pion ratios in single and double meson production at a given energy, by applying the hypothesis of charge independence to the model of isobaric states of the nucleon, first suggested by Brueckner and Watson. Peaslee supposes that the isobar is well separated from the unexcited nucleon (single meson production) when the isobar decays, and therefore he neglects any subsequent interactions between the final nucleons. This assumption is rather questionable since the lifetime of the isobar will only be of the order of 10^{-23} secs., so that for a velocity of 0.1 c the separation of

the isobar and the nucleon will be only 0.6×10^{-13} cm., whereas the range of the nucleon-nucleon force is known to be of the order of 1×10^{-13} cm. Peaslee's ratios have been compared with the results on neutron-proton and proton-proton scattering at Brookhaven (Fowler et al., 1954; Morris et al., 1956). Better agreement is obtained than with the corresponding values from the statistical theory, and further the importance of the isobaric state with $T = J = 3/2$ is brought out.

Lindenbaum and Sternhiemer (1957) have given a detailed quantitative model for pion production in nucleon-nucleon collisions in the energy range 0.8 - 3.0 Bev, via the excitation of one or both nucleons to an isobaric state. The relative probability for a final state is taken to be proportional to the final two-body phase space factor multiplied by the relative probability for formation of one or two isobars with $T = 3/2$. The second factor is related to the observed total cross-section for the scattering of positive pions in hydrogen. The total isotopic spin and its z-component are considered to be conserved throughout the process. In addition the mass of each isobar is regarded as variable, and equal to the total energy in the centre of mass system of the pion and nucleon resulting from the isobar decay. The angular distribution of the isobars is treated for two cases: isotropic, and forward and backward in the centre of mass system. The curves used in the present experiment (Chapter I, section 2(vi)) are, however, independent of these assumptions. The decay of the isobar is assumed isotropic in its own centre of mass frame. By supposing that the isobar is well separated from the other

nucleon or isobar when it decays, the final state interaction with the other particles is neglected. This questionable assumption, according to the authors, is best left to the test of experiment.

Predictions are given at various energies for the energy and angular distributions, Q-values and angular correlations of the final particles in single and double pion production. In general the experimental results at Brookhaven on neutron-proton and proton-proton scattering favour the isobaric nucleon model rather than the statistical model.

Lindenbaum and Sternhiemer point out the important differences between their theory and that due to Kovacs mentioned above. Kovacs' phase space factors correspond to multibody collections of two nucleons and a pion (3-body) for single pion production, and two nucleons and two pions (4-body) for double pion production. On the other hand Lindenbaum and Sternheimers' phase space factors are for two bodies; one nucleon and one isobar for single pion production, and two isobars for double pion production. Furthermore, the resonant interaction is built into the moving isobars which can be quite energetic, thus overcoming the restriction in Kovacs' theory of S-state nucleons. Kovacs does not give detailed information on individual inelastic interactions, so that a further comparison cannot be made.

Mandelstam (1958) has given a resonance model for pion production in nucleon-nucleon collisions at fairly low energies. He assumes that production takes place into a few angular momentum states only, and that the matrix element for each particular transition is constant except for factors due to the final state pion-nucleon and nucleon-nucleon interactions.

He considers the outgoing pion in a resonant (3/2, 3/2) state with one of the nucleons. This assumption will not be accurate near threshold energy where S-state production predominates. The other nucleon is assumed to be in either an S-state or a P-state with respect to the centre of mass system. From angular momentum and parity considerations Mandelstam finds it necessary to introduce 6 parameters. These parameters are fixed from experimental observations on deuteron and total positive pion production in proton-proton collisions from threshold energy up to 660 Mev. A correction is introduced to take into account the possibility of production and reabsorption of real mesons. Unless this is done, the calculated cross-sections can rise above the theoretical maxima for the processes involved.

Although the calculated total cross-sections, especially for positive pion production, agree fairly well with experiment at energies as high as 900 Mev, Mandelstam states that this should not be taken to indicate that the assumption of S and P waves with no D-state production is a good one at high energies. He considers that his results give a good account of pion production, both total and differential, up to an energy of 660 Mev, except, as mentioned above, near threshold energy. The value of 660 Mev is arbitrarily chosen and equals the maximum energy of protons from the Russian synchrocyclotron. The ratio of the positive pion production to that for neutral pion production is predicted fairly accurately for energies up to 660 Mev at which energy the calculated ratio is 3.9. The difference between this value and that of Peaslee (1954) is partly due to the mass difference between the positive and neutral pion and partly to the inclusion of interference effects between

the outgoing nucleons.

For the complete analysis of pion production, it is required that each event is completely determined thus enabling angle and energy correlations between particles to be obtained. This is most readily achieved using visual techniques. Nuclear emulsions have been used at energies up to 8.5 Bev. Near the energy of the experiment described in Chapter I Hughes et al. (1957) have studied proton-proton interactions at 925 Mev. Most other experiments have used hydrogen-filled diffusion cloud chambers. Proton-proton interactions have been studied at 810, 1500 and 2750 Mev by Morris et al. (1956), and at 650 Mev by Batson and Riddiford (1956). Pion production in neutron-proton collisions at maximum neutron energies of 1.5, 2.2 and 6.2 Bev have been studied by Wallenmeyer (1957), Fowler et al. (1954) and Holmquist (1958) respectively. All these experiments give some support to the theory of pion production via an intermediate isobar state with T = 3/2. However, because of the small number of events involved, the statistical certainty of the results of these experiments is not high. In more recent years the diffusion cloud chamber has been superseded by the liquid hydrogen bubble chamber. Experiments to date using these chambers have been performed mainly to study the production and interaction of strange particles. However, single pion production has been investigated using pion beams in bubble chambers. Borelli et al., (1959) have studied the following reaction of 960 Mev negative pions in hydrogen:

$$\pi^- + p \rightarrow \pi^+ + \pi^- + n$$

An analysis of 239 events shows good agreement with the isobar model.

The experiment described in Chapter I is a cloud chamber study of proton-proton interactions at 970 Mev. The total number of events analysed is greater than in any of the experiments mentioned above, so that a comparison of the inelastic results with the statistical and isobar theories is possible with a better statistical accuracy. The cross-sections for the possible reactions at this energy, and the angular distribution of the elastic scattering, have been determined. The results of this experiment along with those of a similar experiment (Batson et al., 1959; see appendix) on the scattering of protons by deuterium have stressed how worth-while it is to perform experiments using a bubble chamber with fillings of liquid hydrogen and liquid deuterium. In Chapter II a description is given of a 9" diameter bubble chamber (Colley, Kinson and Riddiford, 1959; see appendix) that has been designed to operate in a pulsed magnetic field. It is indicated how results of greater statistical and experimental certainty may be obtained.

CHAPTER I

THE DIFFUSION CLOUD CHAMBER

FIGURE 1

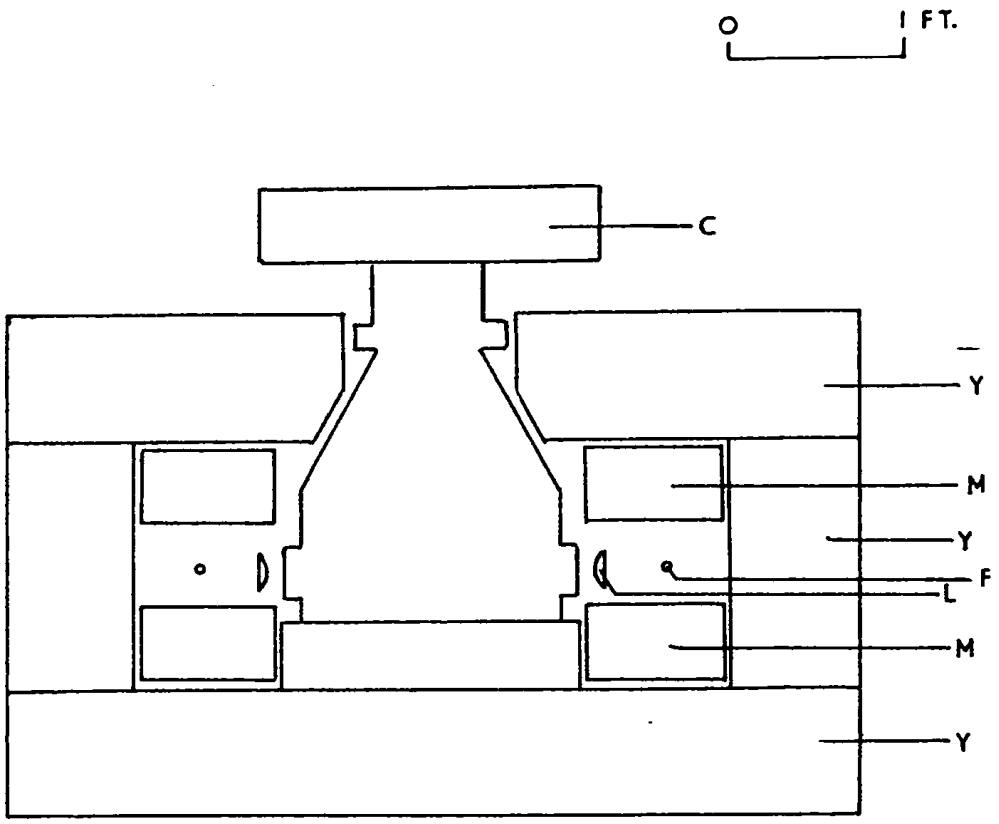

C CAMERA
Y MAGNET YOKE
M MAGNET COILS
F FLASH TUBE
L COLLIMATING LENS

THE CLOUD CHAMBER AND ANCILLARY EQUIPMENT

SECTION 1

THE CLOUD CHAMBER

A high pressure diffusion cloud chamber in a pulsed magnetic field (Batson et al., 1956) was operated with a hydrogen gas filling at a pressure of 25 atmospheres. Figure 1 shows the general construction of the chamber and of the magnet assembly which supplied the magnetic field.

The chamber was 18" in diameter and under normal operating conditions had a sensitive region at the bottom of the chamber approximately 2" deep. The base of the chamber was cooled to about -55°C by circulating methanol which had passed through a heat exchanger immersed in a freezing mixture of solid carbon dioxide and methanol. The temperature gradient was maintained and controlled by means of three electrical heaters situated as shown in Figure 2. The temperature of the source of methyl alcohol vapour was about 23°C. Five copper-constanton thermocouples located as shown in Figure 2 were used to measure the temperature distribution. A clearing field was applied between pulses to remove ions which would deplete the vapour supply to the sensitive region and also facilitated the removal of old tracks. This circular electrode positioned as in Figure 2 was normally maintained at a potential of -1000 volts, but was removed

FIGURE 2.

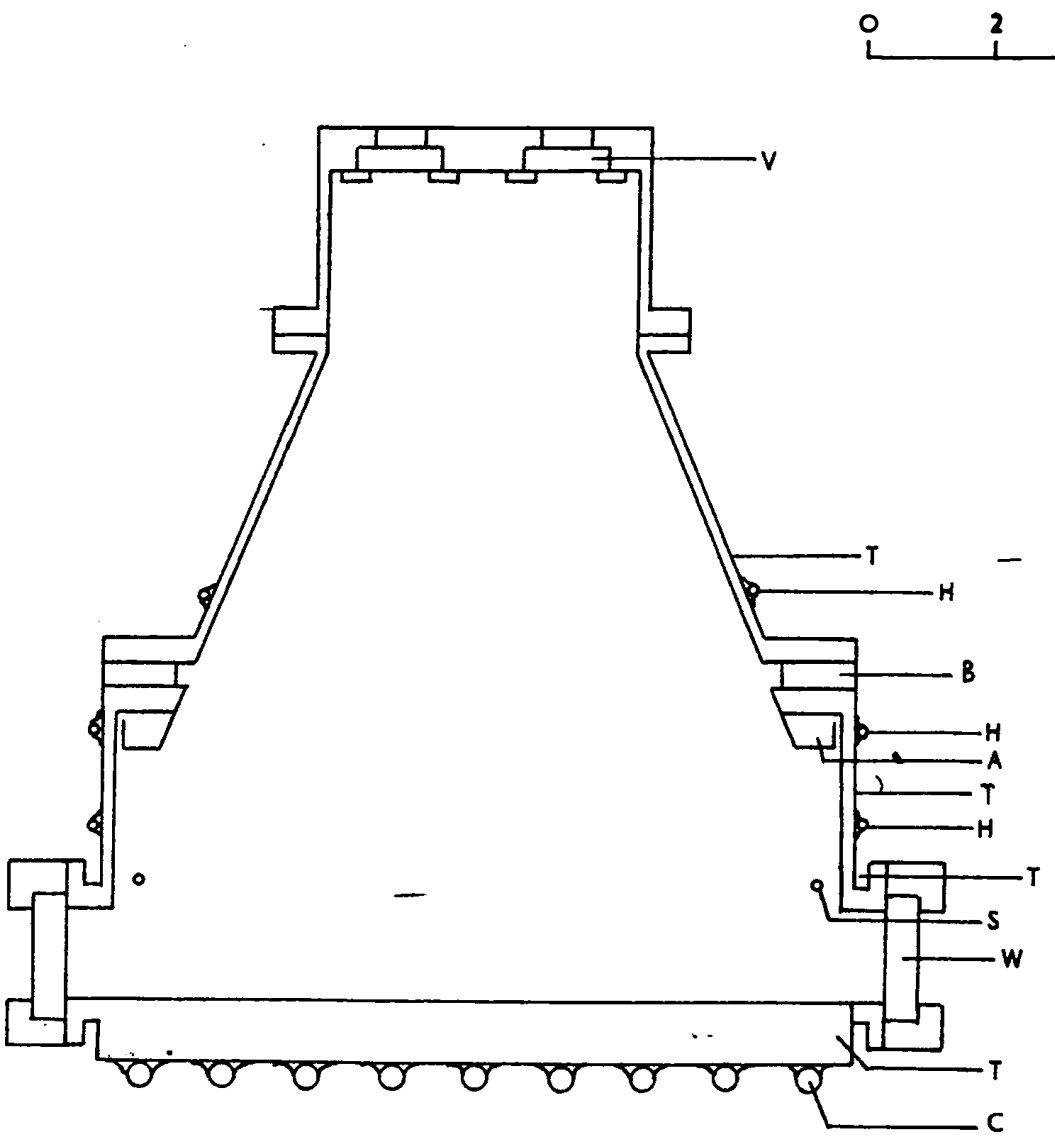

V VIEWING WINDOW
T THERMOCOUPLE
H HEATER
B BAKELITE SPACER
A ALCOHOL RESERVOIR
S SWEEPING FIELD ELECTRODE
W ILLUMINATION WINDOW
C COOLING SPIRAL

THE CLOUD CHAMBER

4 secs. before the pulse of particles entered the chamber to prevent old cosmic ray tracks, made extremely diffuse by the action of the field, from forming an unpleasant background.

For the photography of events a camera was placed at the top of the chamber. The sensitive region was illuminated through the side windows at the bottom of the chamber, as shown in Figure 1; the light source consisted of two 200 joule xenon-filled flash tubes, one on each side of the chamber. Stereoscopic pairs of photographs were taken on 60 mm. wide type 5G91 recording film (by Ilford Limited) every time a pulse of particles passed through the chamber. The camera lenses(type Dalmac wide-angle) subtended an angle of approximately 10^{o} at the centre of the sensitive region.

The cloud chamber was placed in a pulsed magnetic field of 13000 oersted which made possible measurements of momenta of particles photographed within it. The pulsed operation minimised power consumption and avoided overheating of the coils. The general features of the coil boxes and seven ton yoke assembly are shown in Figure 1. The coils were excited from a 500 kW d.c. generator normally used to supply the magnet of the Nuffield Laboratory 60" cyclotron. This generator supplied about 500 amps. at 400 volts. peak to the magnet. The coils were cooled by forced air from a fan mounted on the magnet trolley. The magnetic field in the

sensitive region of the chamber was measured under steady-state and pulsed conditions. The steady-state measurements were made with search coils and a Grassot fluxmeter, and also by Mr. H.R. Shaylor using the proton resonance apparatus designed by him for use in the magnet of the 60" cyclotron. All methods agreed to within 1%. The pulsed field was observed by using a simple Miller integrator circuit to integrate the signal from a large search coil. The measurements of the magnetic field under steady-state and pulsed conditions agreed to within 2%. The spatial variation of magnetic field in the sensitive region was measured under steady state conditions by a difference coil method using a fluxmeter. These latter measurements were important for making a correction to the momentum measurements.

It was necessary to relate the sequence of operation of the cloud chamber to the synchrotron cycle. Synchrotron timing is derived from a precision rotating condenser which controls the frequency of the accelerating potential of the machine. Light flashes from mirrors attached to this condenser are used to regulate the speed of a synchronous motor, which drives a cam used to time the radio-frequency power amplifier. The cloud chamber timing was derived mainly from a series of microswitches operated by cams attached to a shaft suitably geared to the shaft of the

synchronous motor. The magnet timing was adjusted so that the peak of the magnetic field was coincident with the passage of the particles through the chamber. This was achieved by displaying the signal from the magnetic field integrator and the pulse from a scintillation counter in the particle beam on an oscilloscope. This adjustment was not critical as the magnetic field had a fairly broad peak. The cam-switches were also used to control the film wind-on between photographs, and removed the clearing field at the appropriate time. The flash tubes were triggered directly from a pulse from one of the mirrors attached to the precision rotating condenser.

FIGURE 3

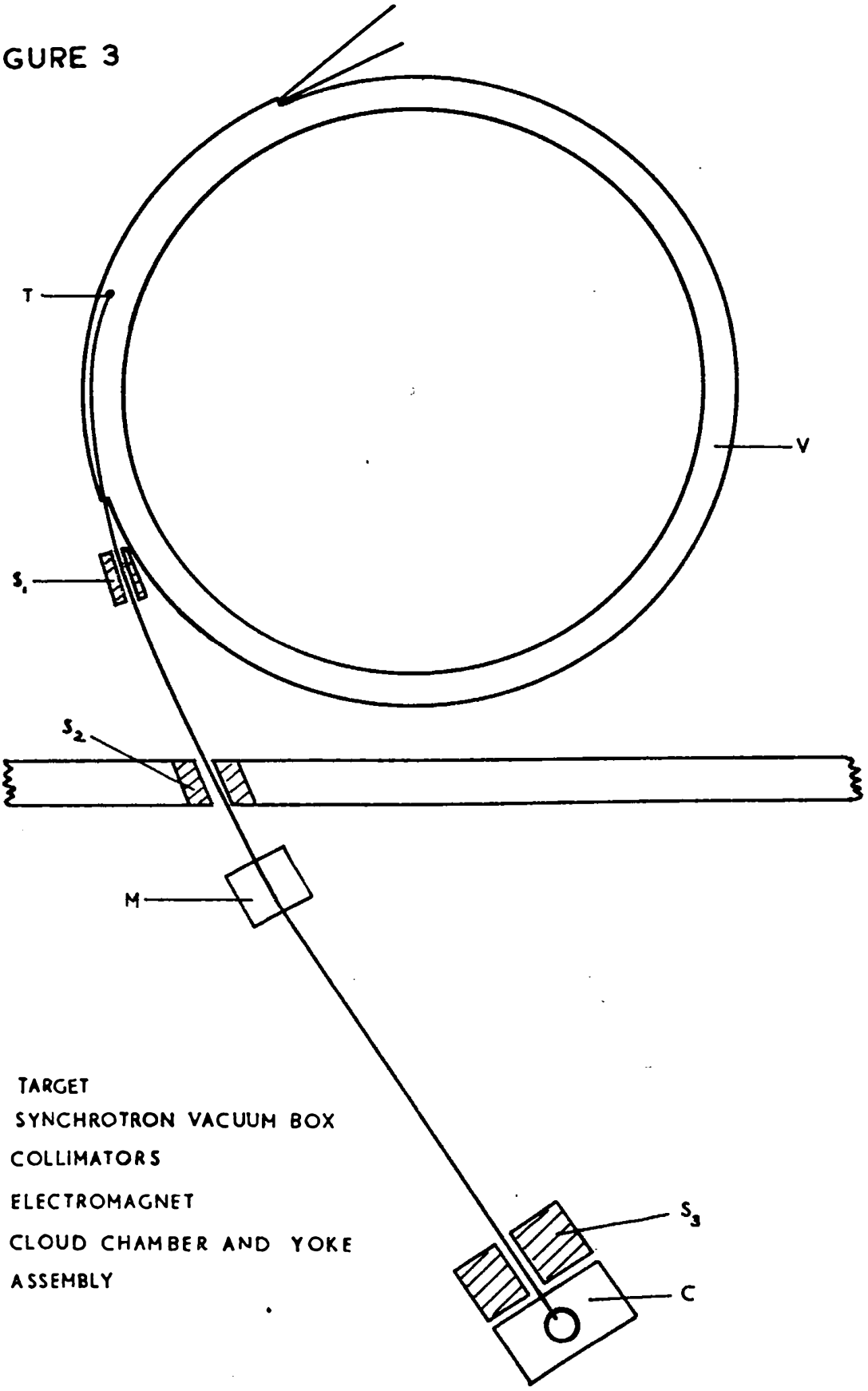

T TARGET
V SYNCHROTRON VACUUM BOX
S COLLIMATORS
M ELECTROMAGNET
C CLOUD CHAMBER AND YOKE ASSEMBLY

EXPERIMENTAL ARRANGEMENT

SECTION 2

THE PROTON-PROTON EXPERIMENT

(see also Appendix)

(i) Experimental Arrangement

Figure 3 shows the arrangement used for obtaining a monoenergetic beam of protons in the sensitive region of the cloud chamber. S_1 was a heavy alloy collimator situated close to the point of exit of the scattered beam from the synchrotron vacuum box. S_2 was a lead collimator in the main shielding wall between the synchrotron and the experimental room. On passing through collimators S_1 and S_2 the proton beam traversed the gap of a long electromagnet, M, which gave a magnetic field of about 8,000 oersted. This along with the fringing magnetic field of the synchrotron produced considerable momentum selection of the beam and thus reduced the low energy and neutral particle content of the beam. The primary beam finally encountered a third collimator S_3 in front of the cloud chamber. This collimator, of cross section 8" x 3/8", defined the beam to a thin horizontal slab about the median plane of the sensitive region of the chamber. This ensured that the secondary particle tracks from an interaction were at least 3 cm. long.

The Birmingham proton synchrotron (Moon, Riddiford and

Symonds, 1955) accelerates about 3 x 10^9 protons to an energy of 980 Mev once every ten seconds. The beam used in the present experiment was obtained by switching off the radio-frequency accelerating potential at the peak of the magnetic field and allowing the circulating beam to spiral outwards in the decreasing magnetic field onto a target placed near the outside wall of the vacuum box. Particles scattered at about 4^o to the initial direction were selected by the system of collimators. Under these conditions the primary beam energy was expected to be about 970 Mev with a small spread about this value. The most suitable beam intensity in the chamber was 30-40 protons per pulse. Above this number the sensitivity of the chamber was impaired because of the large amount of ionisation, and also subsequent scanning and measurement of photographs was hindered. As the scattered beam would normally be greatly in excess of this, it was reduced by means of an adjustable stop in the vacuum box.

A careful investigation was carried out of the momentum spectrum of the primary beam. Curvatures of a sample of primary tracks recorded on film during the experimental run were measured using a microscope. This technique has been described by B.B. Culwick (1957). It was found necessary to make corrections to these measurements to allow for:

FIGURE 4

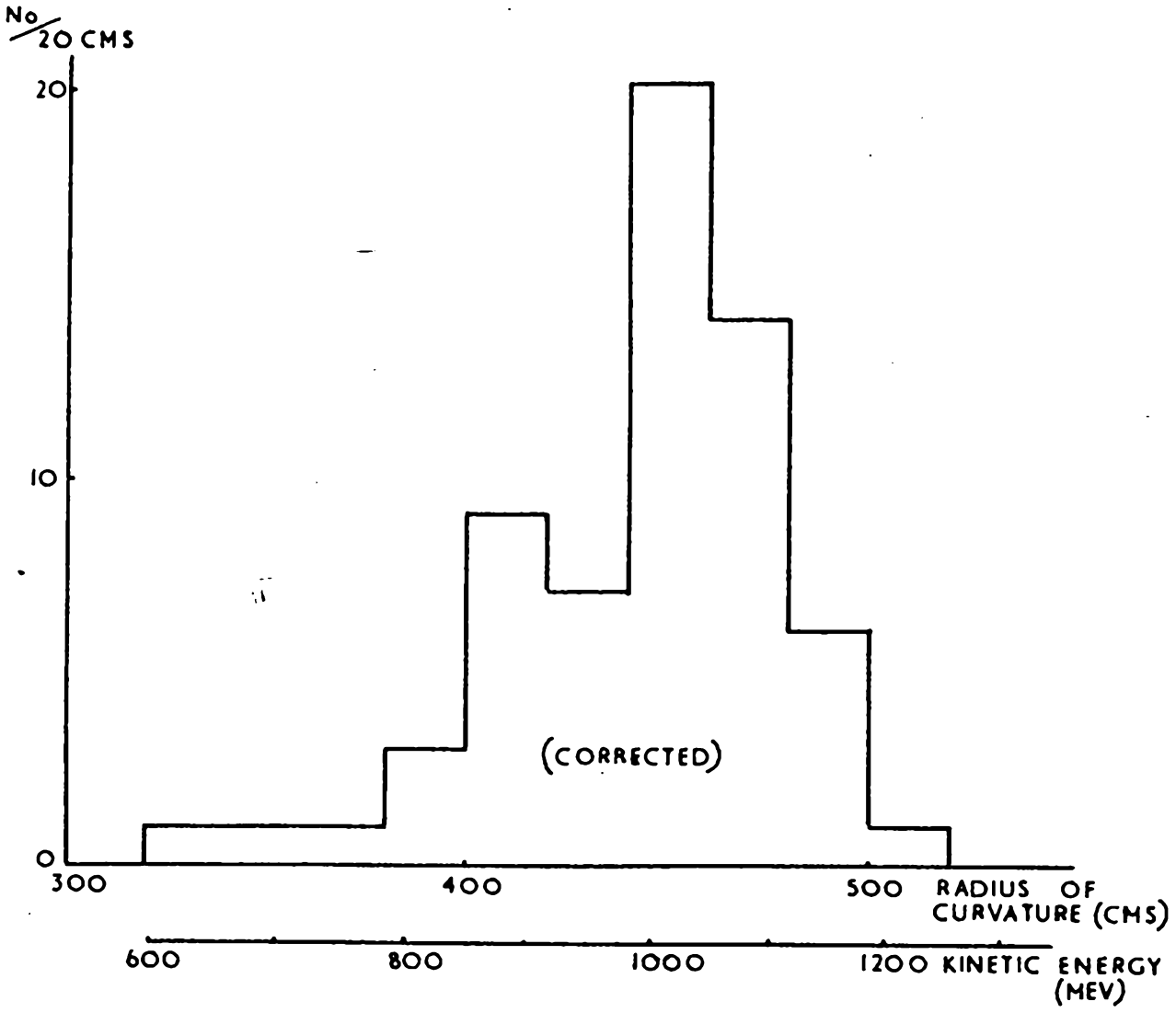

MOMENTUM SPECTRUM OF PRIMARY PROTONS

(1) optical distortion

(2) spatial variation of magnetic field, and

(3) gas motion between the instants of particle entry and photography.

Figure 4 shows the corrected momentum spectrum obtained as a result of this investigation. The spread at half-height is just over 5% and the mean radius of curvature is consistent with an energy of 970 Mev. Since a primary beam energy of about 970 Mev with a spread of a few per cent was expected under the beam arrangement used, it was evident that the incident energy was fairly well defined and that the remaining spread in momentum did not entirely represent an actual spread in incident momentum.

(ii) Technique of Measurement

For the measurement and analysis of events the processed film was replaced in the camera and reprojected to its original size onto a reprojection table. The condenser lenses used for this purpose also acted as pressure plates when the film was being exposed during the experimental run. A sheet of white cardboard was fixed to the top of the reprojection table in order to give good contrast between the tracks and the rest of the image. The table could be moved vertically and horizontally in the directions perpendicular to the beam

direction. It could be tilted about a horizontal axis up to an angle of 75°, and also completely rotated about a vertical axis. In this way the two stereoscopic images of a track could be brought together and aligned, and the dip angles, curvatures and relative angles could be determined in the manner described below. Reprojection in this manner eliminates the effects of optical distortion. This technique has been described by Batson et al. (1956).

The films were first of all scanned carefully and frames on which events occurred were marked. A smaller single-lens reprojector was used for this purpose. For the measurement of an event, a film was placed in the camera and a corresponding pair of frames, on which an event occurred, was located accurately in the camera. This was possible since the diaphragm in front of the film had been made the limiting stop in the reprojection system. The film was adjusted until the circular images of the frames fitted exactly into the circular images of the diaphragm of the reprojection system. Care was taken to ensure that the two images of the point of interaction of the event coalesced.

An interaction in hydrogen always appeared as a two-pronged event. Each event was tested for coplanarity. To do this, the table was rotated until its horizontal axis was

in the primary beam direction. The table was then tilted until the two images of one of the secondary tracks lay parallel and very close together. Any deviation from parallelism of the two images of the other secondary track indicated that the event was not coplanar. The angle (ϕ) through which the table had been tilted was recorded. It was, of course, the same for both secondary tracks of a coplanar event. The images were then coalesced and the table was locked in position by a system of foot-operated electromagnets. Using one photograph only, since this gave a finer image, tangents to the primary and the secondary track at the point of the event were drawn on the white cardboard top of the table. The angle (θ) between these lines was measured with a protractor. This procedure was repeated for the other secondary track. For a secondary track with an azimuthal angle (ϕ) greater than 75° it was not possible to adjust the table to measure this angle or the scattering angle (θ) directly. In this case the table was set in the horizontal position and adjusted in height until the two images of the point of interaction coincided. The scattering angles in the horizontal plane from the two images were then measured. From these measurements and others described later it was possible to compute the azimuthal angle (ϕ) and the scattering angle (θ).

The dip angle (δ) of each track was measured by aligning

the two images with the horizontal axis perpendicular to the track. The technique of bringing the track images parallel was again employed. The images were then coalesced and the table was clamped in this position so that the curvature of the track in space could be measured. Again, using only one of the stereoscopic images, the track image was compared to a set of standard curves marked in ink on stiff white cardboard. The standard curves were laid systematically alongside the track image and a careful scrutiny of the narrow gap between the two curves was made. The greatest and least curvatures which fitted the track were recorded, together with the length of the track. The table was then clamped in the horizontal plane and adjusted in height until the centres of the track images coincided. The lengths of the track images in the horizontal plane were measured. This procedure was repeated for the other two tracks of the event.

The ionisation density of the secondary tracks relative to the primary was assessed; allowance was made for the dip angle if this was large. The apparent ionisation density usually varied along the length of a track and in particular increased with height. This was probably due to an increase in either sensitivity or illumination with height in the chamber. For this reason an estimation was only made in the region close to the point of interaction of the event. The

position of the event in the sensitive region was recorded. This information is required for the calculations on tracks with $\phi > 75^{\circ}$.

The coplanarity test, in conjunction with measurements of scattering angle and estimation of ionisation density, was sufficient in the majority of cases to identify those events that were elastic. In the case of elastic events, it was in general not necessary to measure the track curvature. For the majority of inelastic events accurate curvature measurements were also made on the film image with a microscope, using the method described by B.B. Culwick (1957). It was necessary to make several corrections to these microscope measurements. The image recorded on film is a conical projection onto a horizontal plane, so that a correction was necessary to convert the curvature measured on the microscope to the curvature in space. This geometrical correction has been dealt with by K.H. Barker (1954). In calculating the momentum of a dipping track from its curvature, account was taken of the fact that the particle moved in a component of the vertical magnetic field. Corrections were made to the curvature measurements to allow for optical distortion and spatial variation of magnetic field. For all but a few secondary tracks the effects of gas motions were small.

The accuracy to which the azimuthal angle (ϕ) and dip

angle (δ) could be measured depended largely upon the nature of the secondary track, but in general they could be determined to within about 2° for tracks longer than about 2 cms. The scattering angle (θ) could be determined to within 1°, again provided that the tracks were not too short. The probable error in a momentum measurement is inversely proportional to the square of the track length. Typical figures for a track 10 cm. long in space (1.25 cm. on the film), quoting the range within which the momentum can lie, are given in Table 1.

TABLE 1

Error in typical momentum measurements

Radius of curvature in space (cms)	Momentum (MeV/c)	Reprojection Table	Microscope
65	260	± 6%	± 3%
300	1170	± 25%	± 10%

(iii) Analysis of Data

(a) Identification of events

Over 20,000 pairs of photographs were taken during the experiment and 1,029 events due to proton-proton interactions were found. A small number of "stars" were found. These are from the interactions with the carbon and oxygen nuclei of

PLATE I

the small percentage of methyl alcohol vapour present in the cloud chamber.

At this energy the possible processes which can occur in proton-proton scattering are:

(1) $p + p \longrightarrow p + p$ elastic scattering

(2) $\longrightarrow d + \pi^+$

(3) $\longrightarrow n + p + \pi^+$

(4) $\longrightarrow p + p + \pi^\circ$

(5) multiple pion production

} inelastic scattering

Plate 1 shows an example of an elastic event in which the scattering angle of the right hand track is 22°. An example of an inelastic event of type 4 is shown in plate II. The computational analysis described in section 2 (iii)(b) gives a value of 8° for the scattering angle of the neutral pion.

The thresholds for single and double pion production are respectively about 290 Mev and 590 Mev. If double pion production is significant then 4-pronged events of the type

$$p + p \longrightarrow p + p + \pi^+ + \pi^-$$

and 2-pronged events of the type

$$p + p \longrightarrow n + n + \pi^+ + \pi^+$$

should have been observed. No 4-pronged events were observed and only one possible example of a 2-pronged event with two charged pions was noted. The cross section for double pion

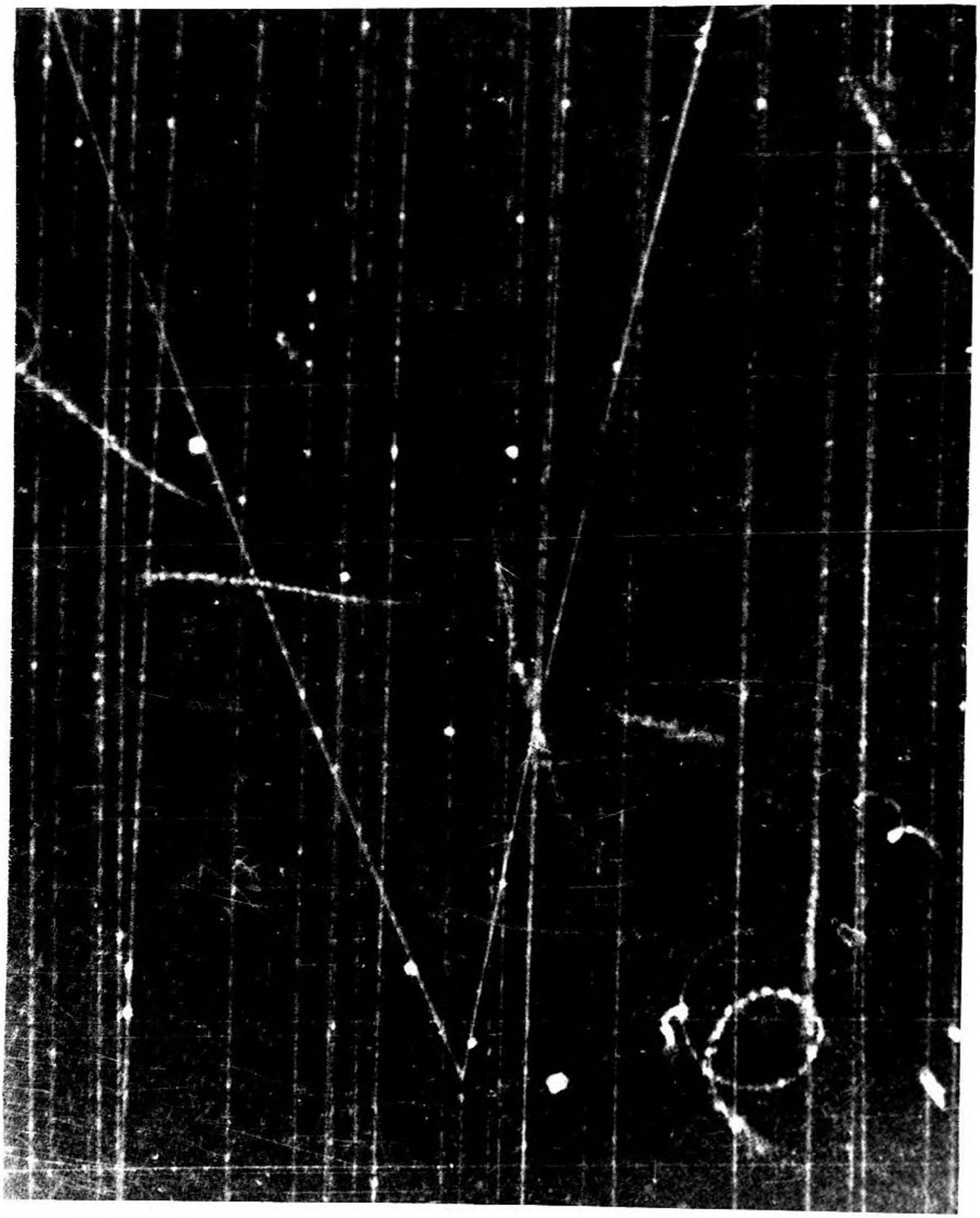

PLATE II

production is therefore assumed to be very small at this energy, a result which is supported by a similar experiment of Morris et al. (1956).

Elastic events are the easiest to identify. At this energy the angle between the two secondary tracks must lie between 78° and 90°. An elastic event must also be coplanar. Occasionally it is possible to show that an event which satisfies the above conditions is not elastic from a consideration of the ionisation densities and momenta for the secondary tracks, which are calculable from the kinematics of the reaction.

All 2-pronged events which did not satisfy the requirements for an elastic event were regarded as inelastic collisions The inelastic events were sub-divided as far as possible into categories (2), (3) and (4). If either of the secondary tracks is identified as a pion then it must be of type (2) or (3). For events of type (2), which involve deuteron formation, the event must be coplanar and the angle of the deuteron cannot be greater than about 16°. Also, since there are only two secondary particles, the pion angle is determined for a given deuteron angle. If both secondaries are identified as protons, then the event must be of type (4). The nature of the particle producing a given track could usually be identified from a consideration of the curvature of the track and

its ionisation density relative to the primary track. Since a 970 Mev proton is a nearly minimum ionising particle, any track with a droplet density appreciably greater than the primary track was considered as at least twice minimum ionisation density. This was found to be a reasonable criterion from a study of elastic events. The energies corresponding to a twice minimum ionising track are 245 Mev and 35 Mev for a proton and pion respectively.

Sternheimer (1954) has shown that at this energy a nucleon cannot be ejected at an angle greater than 58° to the primary direction in processes involving single pion production. Consequently any track at an angle greater than 58° must be a pion. Further, it can be shown that the maximum nucleon energy at a given angle decreases to about 50 Mev as the scattering angle increases to 58°, whereas the maximum pion energy decreases much more slowly with angle. Thus a track could often be identified from its ionisation density and angle alone. It is possibly easier to recognise events of type (2) and (3), because of the arguments given above. An additional factor is that for events of type (4), <u>both</u> secondary particles must be identified as protons.

In some cases where identification was not possible by the above arguments, an event could often be identified from the kinematics of the reaction, providing useful momentum

measurements were available. For instance, pions of energy greater than 640 Mev cannot be produced in nucleon-nucleon collisions at this energy, so that a particle of high momentum ejected close to the forward direction must be a proton. Finally, it was possible to identify many events by the computational techniques described in the following section.

(b) Further analysis

Of the 1029 events analysed, 1023 were identified by the methods described above. 565 of these were identified as elastic events. The remaining 458 were sub-divided as shown in Table 2.

TABLE 2

Partial Cross sections

		Number of events	Cross Section (mb)
(1)	Elastic	565	25.8 ± 0.9
(2)	$p + p \rightarrow d + \pi^+$	4	0.2 ± 0.1
(3)	$p + p \rightarrow n + p + \pi^+$	328	16.4 ± 0.7
(4)	$p + p \rightarrow p + p + \pi^0$	85	4.3 ± 0.5
(5)	either (3) or double pion production	2	
(6)	Unidentified inelastic	39	
(7)	Completely unidentified	6	

For 345 of these events, in which the momentum of at least one secondary particle was well-measured, a further analysis was made. From this momentum, and the directions of the two charged secondary particles, the event was completely determined, assuming a primary proton energy of 970 Mev. The computations were performed on a Ferranti "Pegasus" digital computer, which was programmed by Dr. A.P. Batson. The details of the method of analysis are as follows.

Suppose that the primary momentum and total energy are $\underline{k}$ and E, and that the momenta of the final particles (energies E_1, E_2, E_3) are $\underline{k}_1$, $\underline{k}_2$ and $\underline{k}_3$. Then, from the conservation of energy and momentum

$$E = E_1 + E_2 + E_3 \qquad (1)$$

and

$$\underline{k} = \underline{k}_1 + \underline{k}_2 + \underline{k}_3 \qquad (2)$$

where E, E_1, $\underline{k}$, $\underline{k}_1$ and the direction (θ_2, ϕ_2) of $\underline{k}_2$ are known.

If we define a new vector $\underline{q} = \underline{k} - \underline{k}_1$ where $E_q = E - E_1$, and if $\underline{q}$ makes an angle ψ with $\underline{k}$, then

$$k_2 = \frac{qA\cos\psi \pm E_q\left\{A^2 - 4m_2^2(E_q^2 - q^2\cos^2\psi)\right\}^{1/2}}{2(E_q^2 - q^2\cos^2\psi)} \qquad (3)$$

where

$$A = (E_q^2 - q^2) + (m_2^2 - m_3^2)$$

and

$$q\cos\psi = \left[(k - k_1\cos\theta_1)\cos\theta_2 - k_1\sin\theta_1\sin\theta_2\cos(\phi_1 - \phi_2)\right]$$

The two values of k_2 were compared with the experimentally determined value and, where possible, the appropriate value was selected. Then k_3 , Θ_3 and ϕ_3 were determined from equation (2). Where no choice was possible, subsequent calculations were carried out on both values.

The angles and energies of all particles were computed in the centre of mass system. If the dashed parameters are those in the centre of mass system, then from the Lorentz transformations

$$E' = \gamma(E - v k \cos\Theta) \tag{4}$$

$$k' \cos\Theta' = \gamma(k \cos\Theta - v E) \tag{5}$$

and

$$k' \sin\Theta' = k \sin\Theta \tag{6}$$

where $\gamma = (1 - v^2)^{-\frac{1}{2}}$ and v is the velocity of the centre of mass system. Thus E', and hence k' , is obtained directly from equation (4). Θ' is then determined by equation (5). The angle (α) between each two particles in the centre of mass system was calculated from

$$\cos\alpha_{12} = \cos\Theta_1' \cos\Theta_2' + \sin\Theta_1' \sin\Theta_2' \cos(\phi_1 - \phi_2) \tag{7}$$

Finally, the Q-value between each two particles was obtained. This is defined as the kinetic energy of the two particles in the coordinate system of their <u>own</u> centre of mass, and

$$(Q_{12} + m_1 + m_2)^2 = m_1^2 + m_2^2 + 2(E_1' E_2' - k_1' k_2' \cos\alpha_{12}) \tag{8}$$

The computer was also made to calculate the error in each quantity consequent upon the errors in the measurement

FIGURE 5

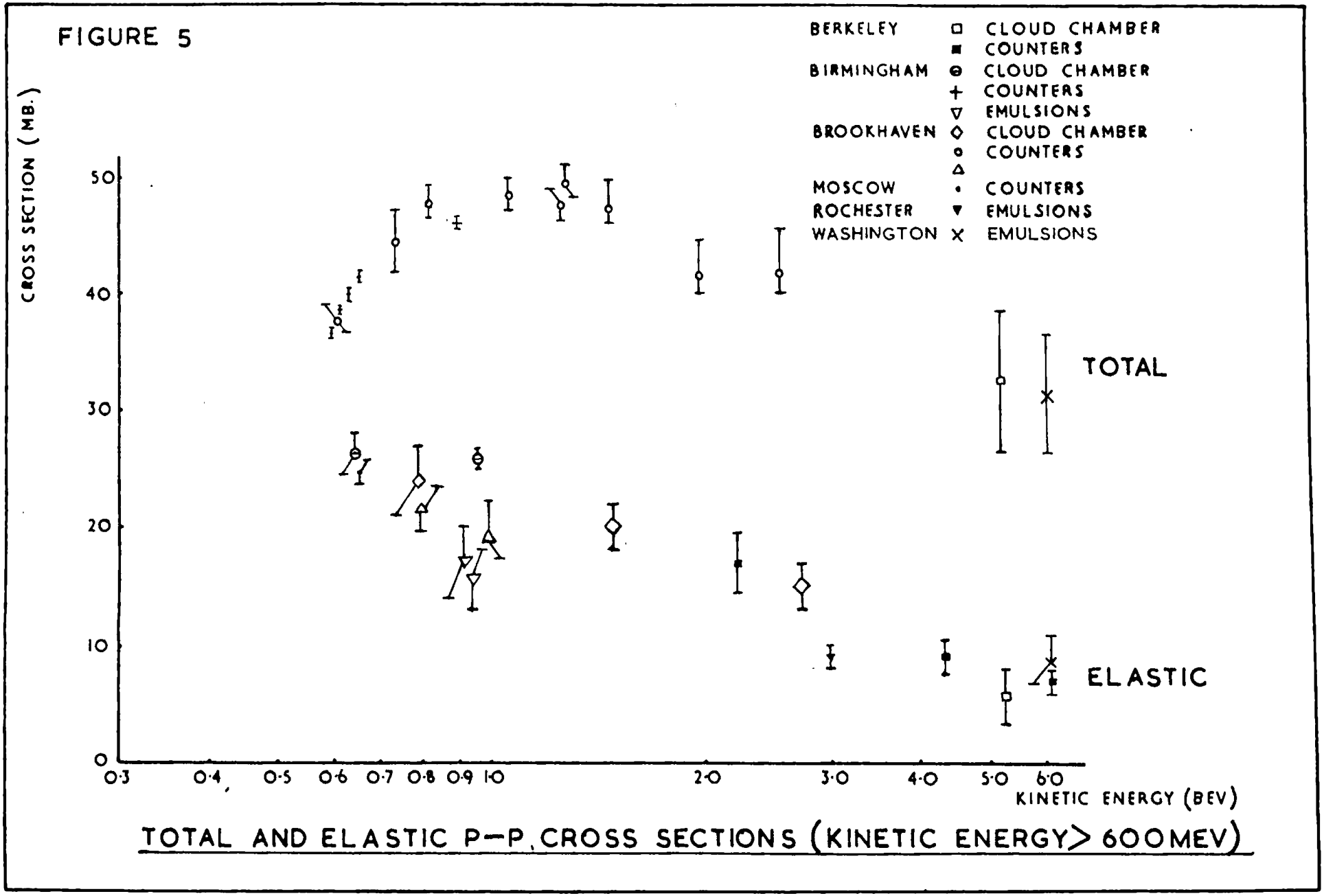

TOTAL AND ELASTIC P–P CROSS SECTIONS (KINETIC ENERGY > 600 MEV)

of k_1 . This was achieved by performing calculations on 3 values of k_1 corresponding to the measured value with upper and lower limits.

273 events of type (3) and 72 events of type (4) in which only one value of k_2 was acceptable were computed as described above. A discussion of the results is given in section 2(vi).

The computer was also used to help in the identification of those uncertain events in which fairly accurate momentum measurements were available. The event was presented to the computer with different mass assignments and a comparison was made between the calculated and measured values of k_2 . In this way positive identification of the event was obtained in nearly all cases.

(iv) Cross Sections

The total cross section for proton-proton scattering in this energy region has been determined by Chen et al. (1956) and Hutchinson, Law and White (1959). A weighted mean of their values gives a cross section of 46.7 ± 0.5 mb at 970 Mev. These values of the total cross section along with the results of other workers (Dzhelepov et al., 1955; Wright et al., 1955; Kalbach et al., 1959) are given in Figure 5 for energies above 600 Mev. No attempt has been made in this

experiment to measure the total cross section since the uncertainty in the result would be very much larger than that quoted above.

Normalising to the above cross section, the elastic and partial inelastic cross sections are obtained from the relative numbers of each type of event. The results, based on certain events, are shown in Table 2. The quoted errors are from the standard deviations of the numbers of events.

The ratio of the number of elastic to inelastic events is 1.23 ± 0.08. From the numbers of certain events (Table 2) a value 3.9 ± 0.6 is obtained for the ratio $\sigma (p + p \rightarrow n + p + \pi^+)$ to $\sigma (p + p \rightarrow p + p + \pi^0)$. This value is compared with that from other experiments in Table 3.

TABLE 3

The ratio $\sigma(p+p \rightarrow n+p+\pi^+) : \sigma(p+p \rightarrow p+p+\pi^0)$

Research Group	Energy (Mev)	
Batson & Riddiford, 1956	650 ± 100	3.8 ± 1.0
Dzhelepov et al., 1955	657 ± 2	2.9 ± 0.5
Morris et al., 1956	810 ± 100	$17. \pm 8$
Hughes et al., 1957	925	4.5 ± 1.5
The present experiment	970	3.9 ± 0.6

The value of this ratio can be calculated from the statistical theory of pion production, proposed by Fermi

(1953, 1954), and the isobar theory due to Peaslee (1954). The details of these theories are discussed in the Introduction. By making the assumption that all final states are equally possible, Fermi predicts a ratio of 3. If pion production proceeds through an excited state of the nucleon, of isotopic spin T = 3/2, as postulated by Peaslee, then the ratio should be equal to 5. However, Mandelstam (1958) has made calculations at energies up to 660 Mev using a more detailed form of isobar theory, in which the interaction between the nucleons and the mass difference of the charged and neutral pion are taken into account. He shows that values of the ratio intermediate between 3 and 5 may be obtained, and calculates a value of 3.9 at 660 Mev. The Russian value does, however, lend support to the statistical theory.

An additional consideration is the suggestion made in section 2(iii)(a) that the identification of events with charged pion production is easier than for events with neutral pion production. In view of the 39 unidentified inelastic events there may be therefore a bias in the ratio π^+/π° which would make this ratio too large.

The cross section for reaction

$$p + p \longrightarrow d + \pi^+$$

is compared with the results of other workers (Durbin et al., 1951; Fields et al., 1954; Stadler, 1954; Mescheryakov et al.

FIGURE 6

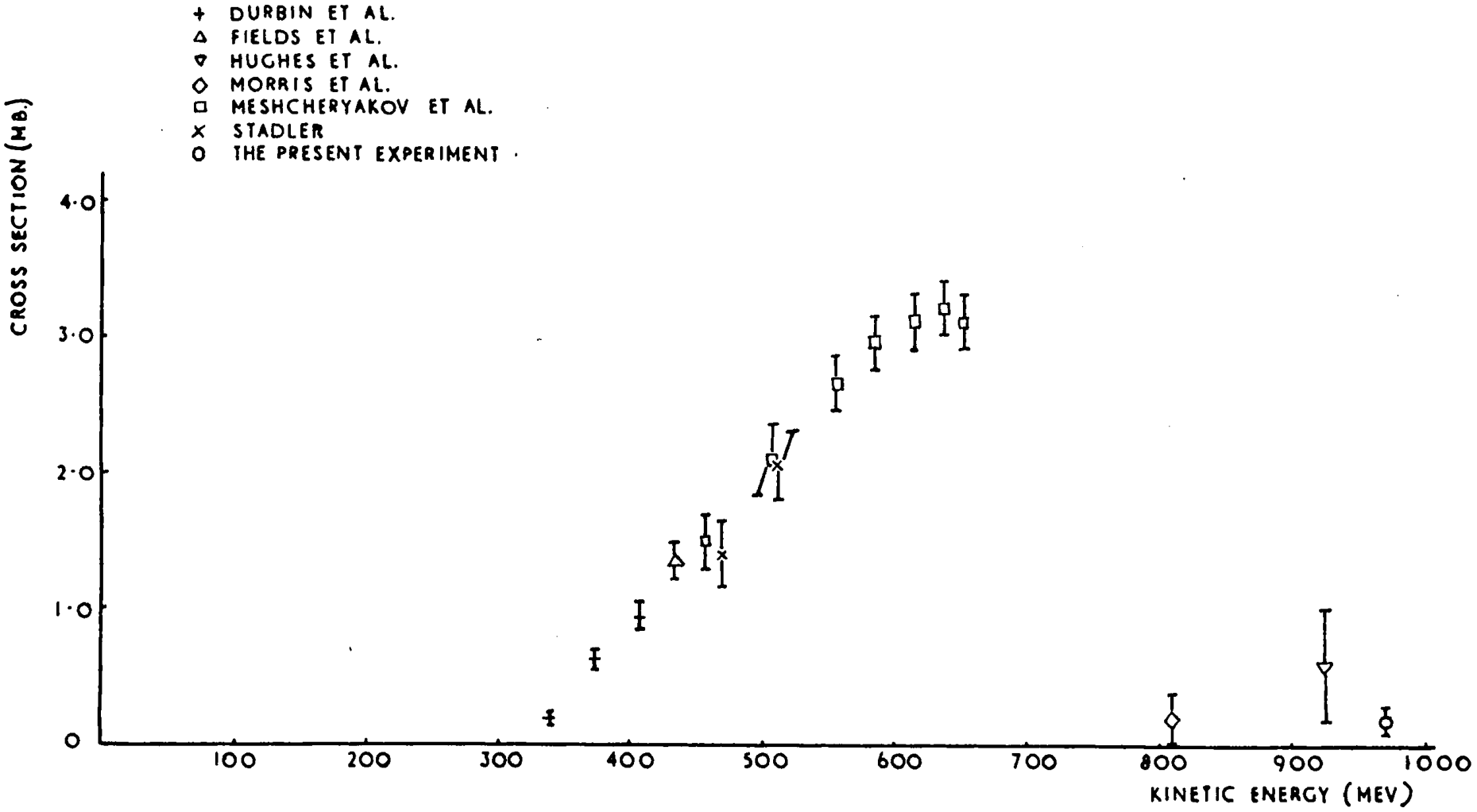

TOTAL CROSS SECTION FOR REACTION $P + P \rightarrow D + \pi^+$

1955; Batson and Riddiford, 1956; Morris et al., 1956; Hughes et al., 1957) in Figure 6. The result of this experiment along with other results at high energies confirms the suggestion from the Russian data that the reaction goes through a resonance at about 650 Mev. This resonance is expected if the reaction proceeds through an excited nucleon state of isotopic spin 3/2 (Mandelstam, 1958). However, Mandelstam's theory shows the limitations of Peaslee's isobar theory since Peaslee neglects interactions between nucleons, which is clearly unrealistic in the case of deuteron formation.

An investigation was made of the variation in azimuthal angle of the elastic events from 16 films, representing about one quarter of the total number of films. The distribution was seen to be non-uniform for scattering angles of less than 20° in the laboratory system. The results are shown in the solid histogram in Figure 7. The secondaries from the inelastic events were also found to be non-uniform in azimuth. An independent search was made for this effect by the counter group in this laboratory (Booth et al., 1958). They investigated the elastic scattering at 14° using a scintillation counter arrangement. No asymmetry in azimuth was found. As a result of these investigations a careful rescan of the 16 films was undertaken.

The original scan of all films was carried out by a

FIGURE 7

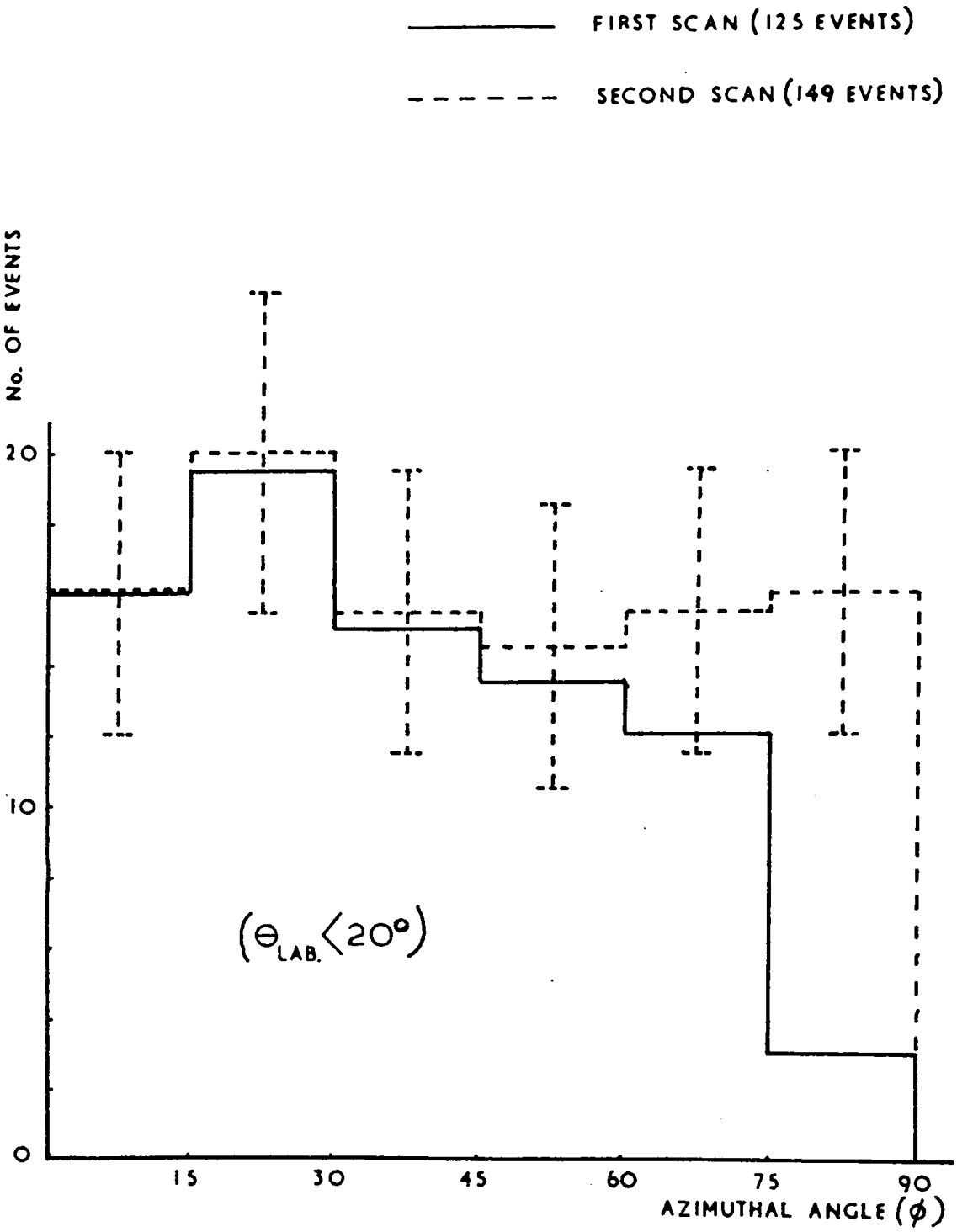

AZIMUTHAL DISTRIBUTION OF ELASTIC EVENTS FROM RESCANNED FILMS

single observer who looked at one frame only of each stereoscopic pair of photographs. The careful rescan was carried out by 4 observers, each scanning 4 films. Both frames were observed by a general area scan and also by looking along the primary tracks. 50 new events were found in a total of 285. This represents a total scanning efficiency of 82½% for the first scan. The effect of the new elastic events found in the sample is to make the distribution uniform in azimuth, as shown by the broken line of Figure 7. The azimuth distribution of inelastic events is still not quite uniform when the new events are included.

It is, therefore, probable that the quoted elastic to inelastic ratio is rather high. This, in turn, would make the elastic cross section high, a fact which is indicated by the measurements of other workers at this energy as shown in Figure 5. The number of events contained in the rescan sample was too small to show whether or not the π^+/π^o ratio is affected by the scanning loss.

(v) Elastic Scattering Results

The angular distribution in the centre of mass system of the 565 elastic scattering events is shown by the full line in Figure 8. A correction was made to this distribution to take into account the preferential loss of events at small

FIGURE 8

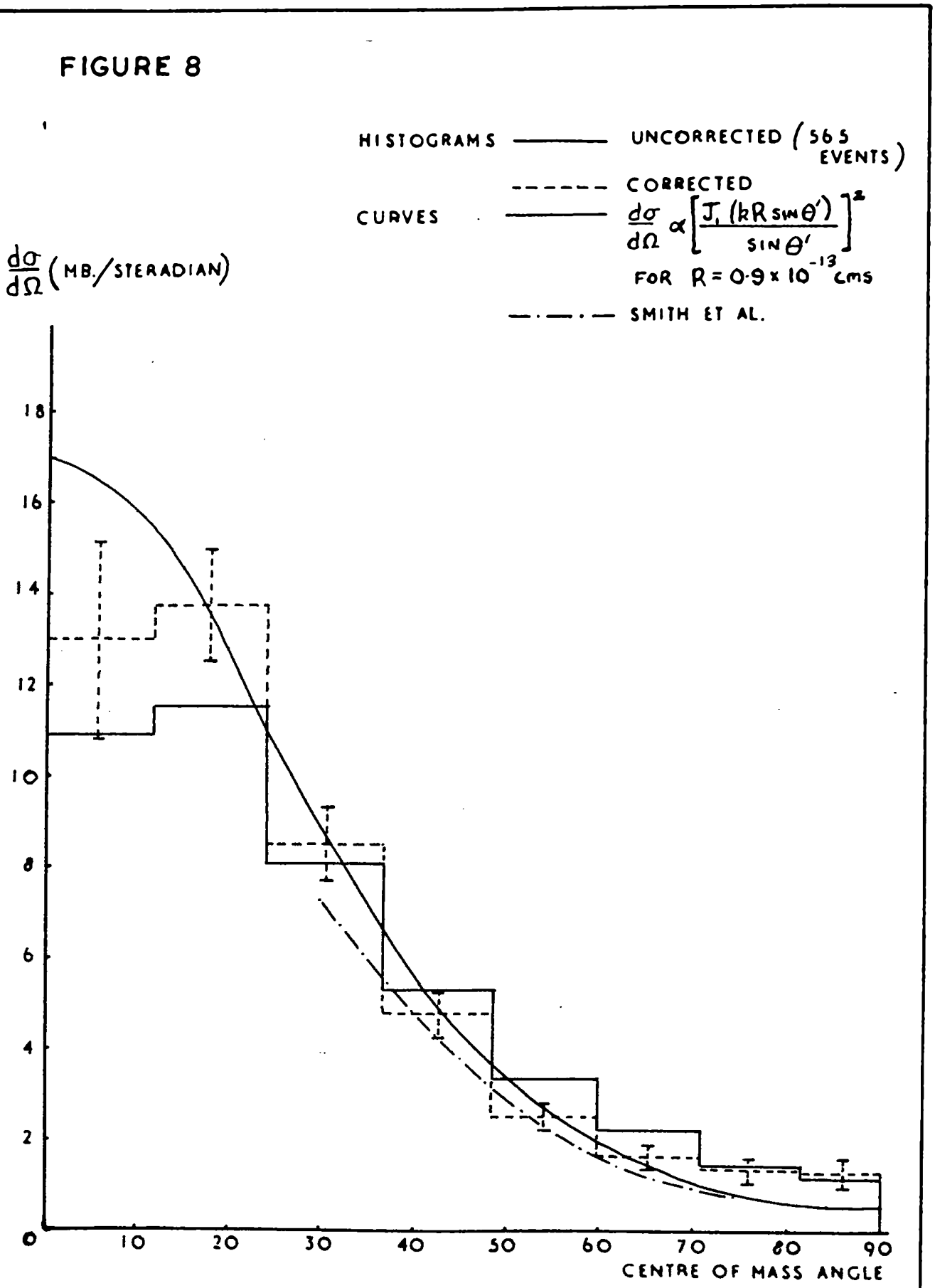

ELASTIC ANGULAR DISTRIBUTION

scattering angles. Azimuthal distributions were plotted for 8 ranges of scattering angle corresponding to 5° intervals in the laboratory system. For θ less than about 20° in the laboratory system there was a clear indication of events lost at large azimuths.

Since the loss of events increased fairly uniformly with azimuth, a straight line of the form

$$y = a + bx$$

was fitted to each distribution by using the method of least squares. The most probable value of the intercept a was found, which corresponds to the number of events in the first azimuthal angle interval. Assuming no loss of events in this first interval, the number of events in each scattering angle range was calculated assuming an isotropic distribution in azimuth. The corrected distribution is shown by the dotted line in Figure 8. Standard deviations, calculated from the observed number of events, are also shown. The angular range is plotted from 0° to 90°. Since the system consists of two identical particles, the angular distribution must be symmetrical about 90° in the centre of mass system. Coulomb scattering is only appreciable for θ less than about 2° in the laboratory system. Because of the loss of events at small angles there is considerable uncertainty in the number of events in the first scattering angle interval ($\theta = 0^{\circ} - 5^{\circ}$). A correction for Coulomb scattering is not therefore

considered worthwhile, since it would only affect this first interval.

The elastic differential cross section has been measured around this energy by several workers (Morris et al., 1956; Duke et al., 1957; Smith et al., 1955). The results of Smith et al. are also shown in Figure 8. Their results agree well with the corrected value obtained in this experiment, though their data does not extend to angles less than 30°. The peak in the forward direction is in marked contrast to the isotropic distribution found at energies below about 400 Mev.

This effect has been interpreted as diffraction scattering of the incident particle wave, and discussed in terms of the optical model of the nucleus. This treatment was first used by Fernbach, Serber and Taylor (1949) to describe the interaction of 90 Mev neutrons with complex nuclei. The results of Smith et al. have been treated by Serber and Rarita (1955), who regarded the proton as an opaque sphere. For such a model the total cross section is equal to $2\pi R^2$, where R equals the radius of the sphere. Using a value for the total cross section at 1,000 Mev from the Brookhaven counter group (Chen et al., 1956) they deduced a value of R. From this value they obtained an angular distribution, which fitted the experimental results extremely well. Cork et al. (1957) have compared elastic angular distributions at 2.24, 4.40 and 6.15 Bev with the prediction of a simple optical model. They find

good agreement with experiment.

The fact that the anisotropy in the elastic scattering begins to appear when pion production becomes important suggests that there is some relation between the two effects. It is postulated that a large cross section for inelastic processes, i.e. particle absorption, causes the struck proton to appear as an opaque sphere to the incident particle wave. Fernbach, Serber and Taylor show that for a completely opaque sphere of radius R, the angular distribution of the elastically scattered protons in the centre of mass system will be of the form

$$\frac{\partial\sigma}{\partial\Omega} \propto \left[\frac{J_1(kR\sin\theta')}{\sin\theta'}\right]^2 \qquad (9)$$

where k = wave number of the incident proton wave in the centre of mass system

J_1 = a first order Bessel function

For scattering from an opaque sphere, the elastic (diffraction) cross section and the inelastic (absorption) cross section are both equal to πR^2. This is approximately the case in this experiment.

Expression (9) for $\partial\sigma/\partial\Omega$ is a rather sensitive function of kR and a good fit to the data of this experiment is obtained for $R = 0.9 \times 10^{-13}$ cms. The possible errors in this

value of R are difficult to specify, but can be estimated roughly by inserting different values of kR into equation (9), and comparing the distribution obtained with the experimental results. The equation is only exact for small angle scattering and in fitting the curve to the data, most weight has been given to the results at angles from 12^{o} - 60^{o}. Little weight was given to the value in the first angular interval because of the loss of events at small scattering angles. The value of R obtained in this way is shown in Table 4 along with values from other experiments.

TABLE 4

Radii from the Optical model

(opaque sphere)

	Energy (Mev)	Radius (fermis)	Experimental technique
Morris et al. 1956	810	0.93	Cloud chamber
J.Dowell, 1958	930	0.85 ± 0.05	Propane bubble chamber
P.Duke et al. 1957	925	0.9 ± 0.1	Emulsions
The present experiment	970	0.9 ± 0.1	Cloud chamber
* Serber & Rarita 1955	1000	0.88	Counters
Cork et al., 1957	2240	0.931	Counters
	4400	1.015	
	6150	1.072	

* These workers used the results of Smith et al. (1955).

All the results are in good agreement and indicate that the effective radius of the interaction in proton-proton collisions at these energies is about $(0.8 - 1.0) \times 10^{-13}$cm. It should be noted that expression (9) is only strictly true for $kR \gg 1$, whereas in the present case $kR = 3.1$ for $R = 0.9 \times 10^{-13}$cm. It is interesting to compare these results with those of Chambers and Hofstadter (1956) who have deduced

the size of the charge distribution of the proton from scattering experiments with high energy electrons, and give a value for the r.m.s. radius of $0.77 \pm 0.10 \times 10^{-13}$ cm.

A model has been given by G.E. Brown (1958) for proton-proton scattering in the Bev region. He analyses the scattering at 1 Bev in terms of an interaction which is taken to be a hard core of radius 0.45 fermis together with an external absorption of Gaussian form. J. Dowell (1958) of this laboratory has studied proton-proton elastic scattering at 930 Mev in a propane bubble chamber. He shows that Brown's model fits his data fairly well and further indicates that a good fit can be made to the angular distribution of the present experiment.

(vi) Inelastic Scattering Results

As mentioned in section (iii)(b) a detailed analysis was carried out on 345 inelastic events. The results from this analysis will now be compared with the predictions of the theories of pion production due to Fermi and Peaslee. These theories are mentioned in some detail in the Introduction. The predictions at high energies have been calculated by Lindenbaum and Sternheimer (1957) for the isobar theory and by Block (1956) for the statistical theory. The predictions of these theories concerning the cross sections have been dealt with in section (iv).

FIGURE 9

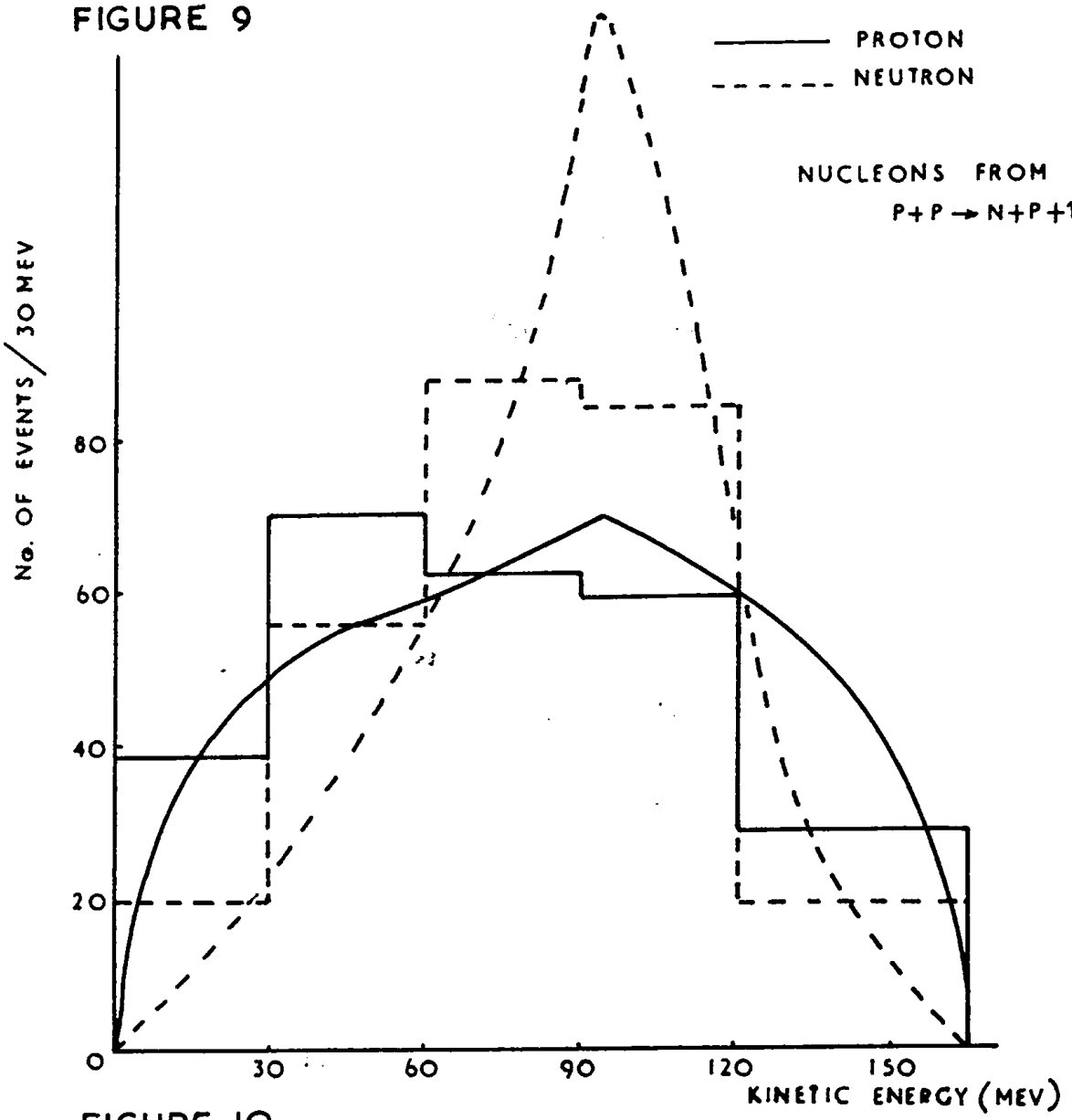

FIGURE 10

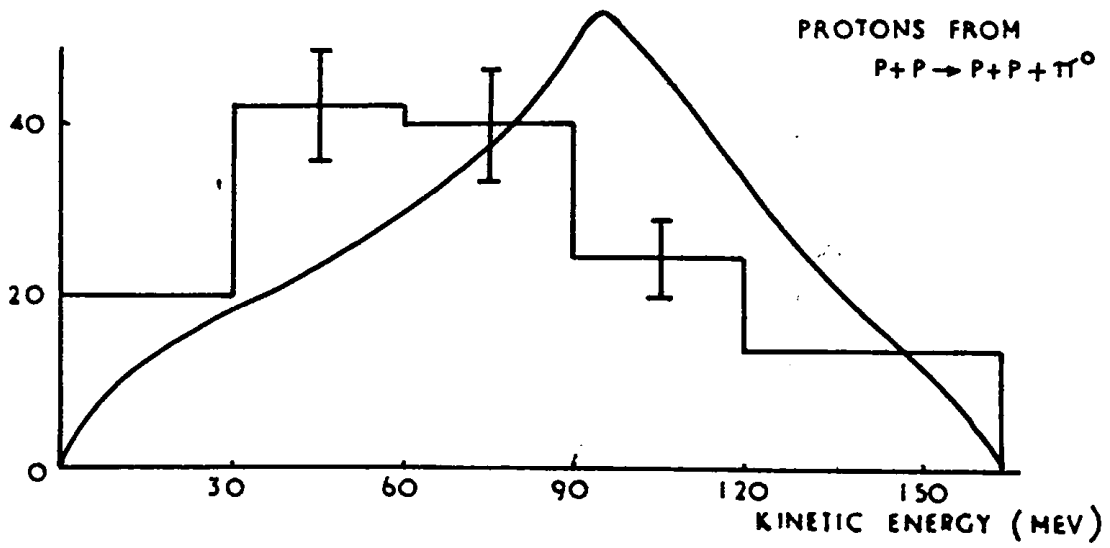

NUCLEON ENERGY SPECTRA

(a) The reaction $p + p \rightarrow n + p + \pi^+$

If pion production occurs through an intermediate state of $T = 3/2$, then a study of the reaction

$$p + p \rightarrow n + p + \pi^+$$

will be of interest, since the $p\pi^+$ system is a pure $T = 3/2$ state, whereas the $n\pi^+$ system is predominantly a $T = \frac{1}{2}$ state. This means that in most cases the $T = 3/2$ isobar decays into a proton and a positive pion, and thus the nucleon energy spectra will differ. Also the pion-nucleon particle correlations (Q, α defined in section (iii)(b)) will be different for the $p\pi^+$ and $n\pi^+$ systems. The statistical theory requires that these distributions should be identical, as the statistical weights depend only on the masses of the particles involved.

The kinetic energy spectra of the nucleons in the centre of mass system are given in Figure 9. The two curves are the predicted distributions at 1 Bev for neutron and proton from the isobar theory, calculated from Lindenbaum and Sternheimer's data. The data appear to be fairly well described by the theory. In making a detailed test for agreement allowance must be made for the broadening of theoretical distributions due to measurement errors. This broadening is not known exactly so that the χ^2-test (see, for example, Davies, 1957) is not applicable. However, the t-test (Davies, 1957) which compares the arithmetic means of the theoretical and experimental distributions can be used. If it is assumed that the broadening of the theoretical distributions is unbiased, then a valid comparison is obtained. The significance of the t-value is measured as a probability, which is obtained

FIGURE 11

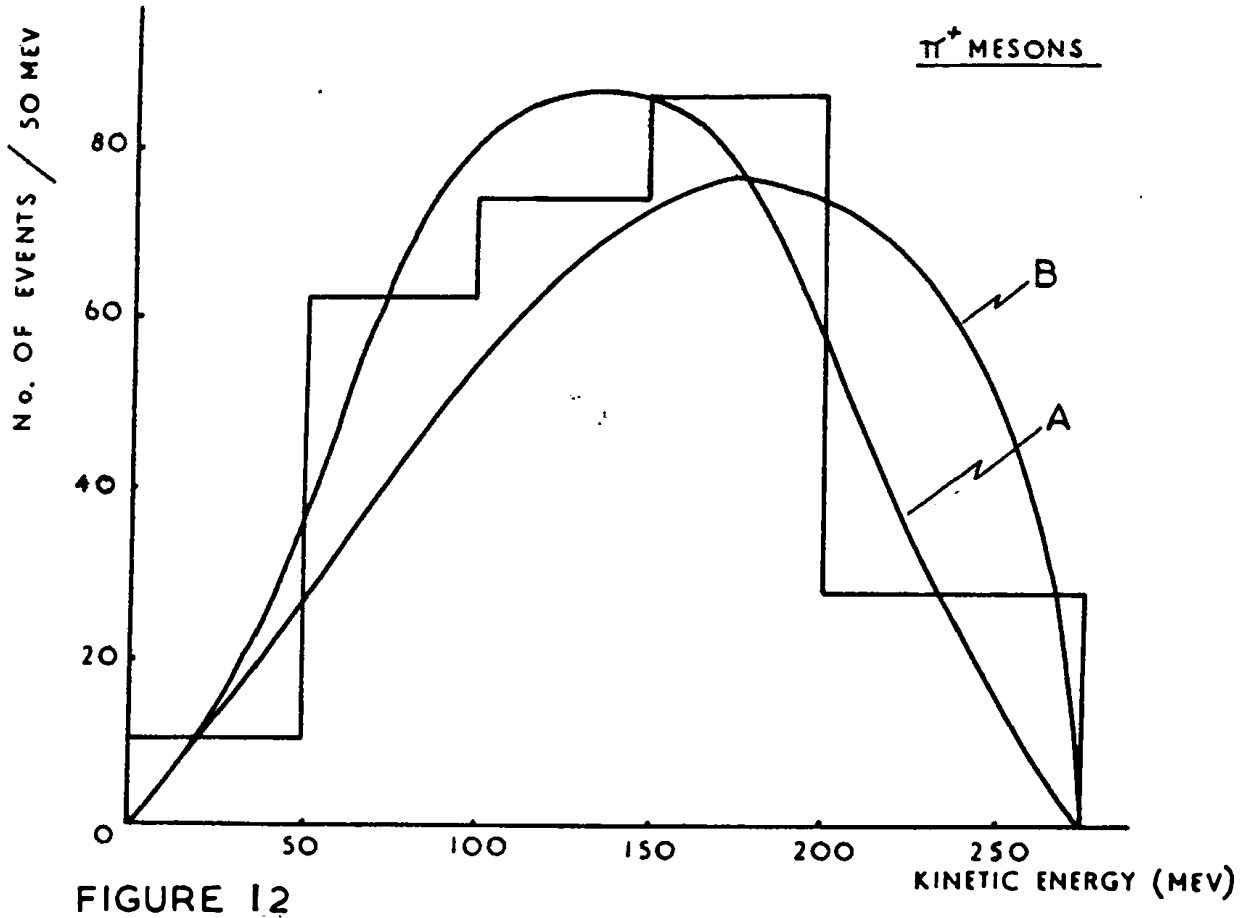

FIGURE 12

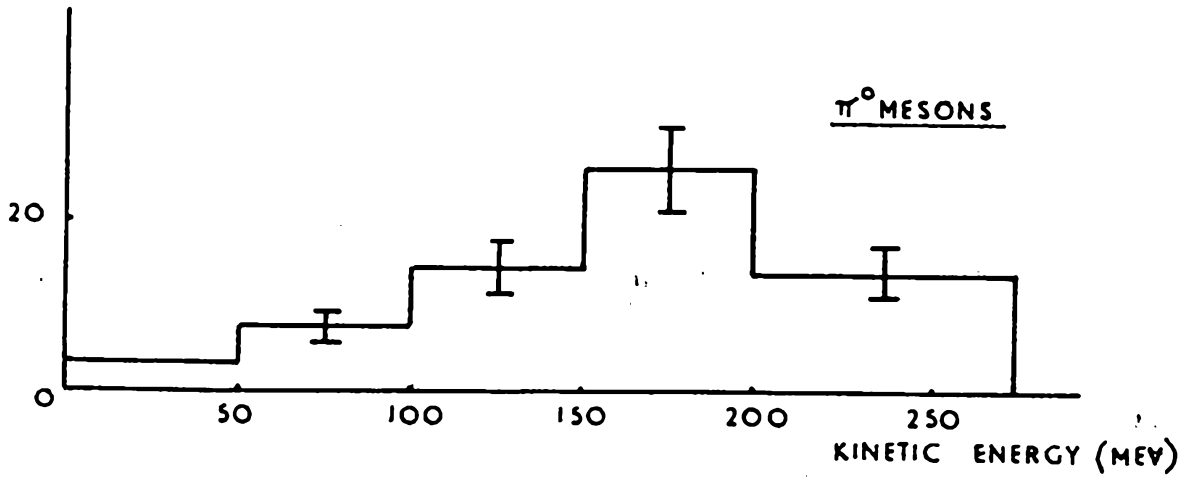

PION ENERGY SPECTRA

from standard tables (see, for example, Davies, 1957). When this test is applied, the t-value obtained for the neutron distribution compared with the isobar prediction indicates disagreement (probability 0.2%). The larger t-value for the proton distribution also indicates disagreement. The statistical theory predicts that the two nucleon distributions should be identical. The probability of this being true from the present data is less than 0.1%, evaluated from a χ^2-test on the two distributions. In this case the χ^2-test is valid since a comparison is made between two experimental distributions that have been compiled in the same way. The kinetic energy spectrum of the positive pions is shown in Figure 11, together with the predicted distributions from the isobar theory (A) and the statistical theory (B) at 1 Bev. The t-test indicates no disagreement with the isobar theory (probability 15 - 20%) but strong disagreement with the statistical theory (probability $\ll$ 0.1%).

The Q-value distributions between proton and pion, and neutron and pion are shown in Figure 13. Also shown are the theoretical distributions from the isobar theory, curve A, and statistical theory, curve B. The predicted distributions for $Q_{n\pi^+}$ do not differ greatly, so that a choice between the theories is not possible. The experimental distribution for $Q_{p\pi^+}$ agrees well with the prediction of the isobar theory, (probability 45 - 50%), but disagrees with the statistical theory (probability $\ll$ 0.1%). Again, the statistical theory predicts identical distributions for $Q_{p\pi^+}$ and $Q_{n\pi^+}$. A χ^2-test gives a 0.1% probability of these distributions being identical. An isobar theory prediction for the distribution of Q-values between the two nucleons is not yet available.

FIGURE 13

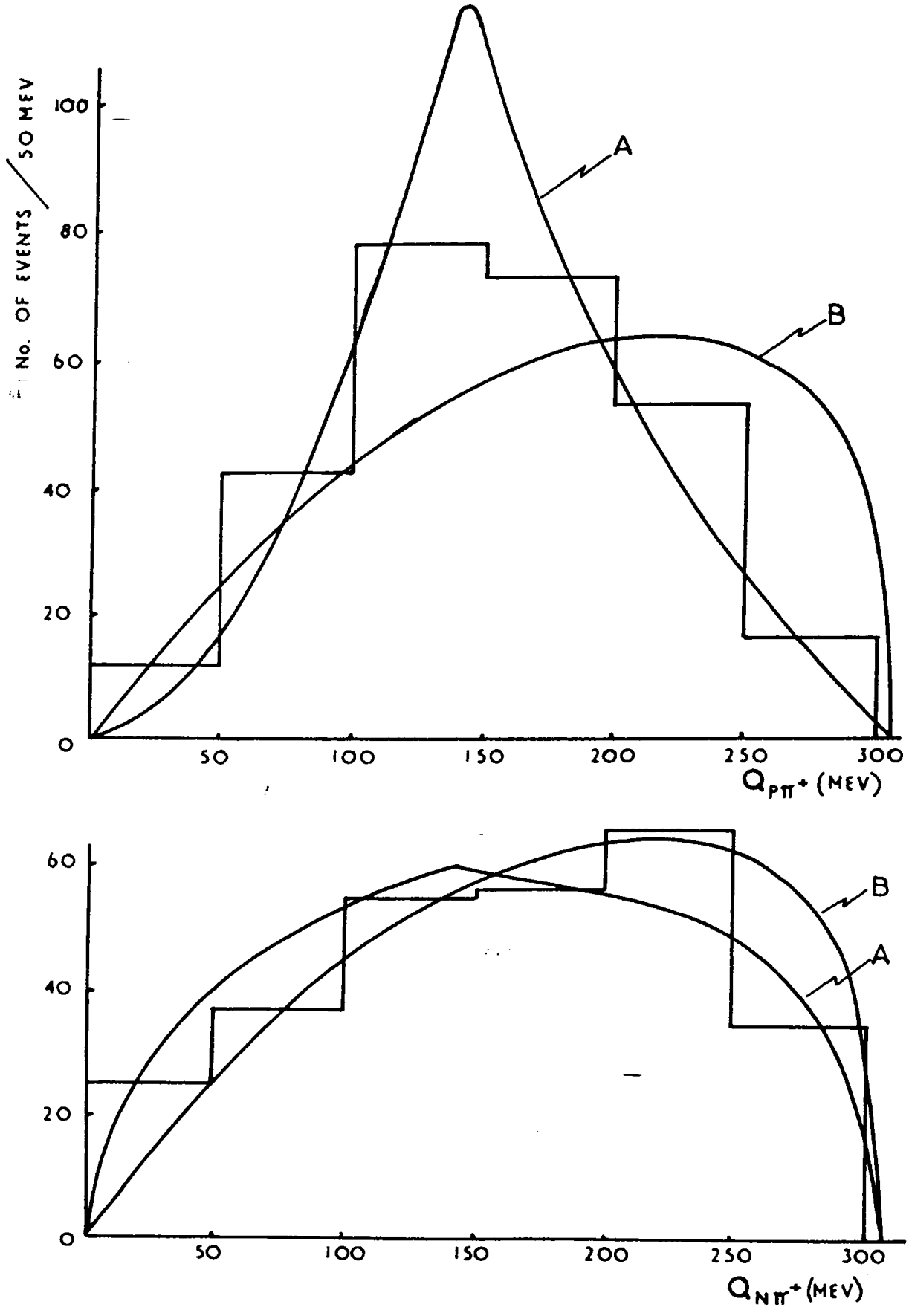

Q-VALUE DISTRIBUTIONS

The angular distributions of the secondary particles in the centre of mass system must be symmetric about 90°, since the initial interaction is between two identical particles. This is found in the results of the present experiment, except for the proton angular distribution, in which there is some loss at forward angles between 0° and 30°. Such particles would tend to move forward with high momentum in the laboratory system, and in general this momentum would not be accurately measured. Therefore, unless the pion momentum was well determined, such an event might not be included in the present sample. The neutron angular distribution is identical, within the statistics, to that of the backward-going protons, and therefore there is no evidence from the present experiment of any difference in the nucleon angular distributions. The neutron angular distribution, folded about 90°, is shown by the solid line of Figure 15. The angular distribution of the positive pions is shown by the solid histogram of Figure 14. A χ^2-test to measure the probability that the results are a sample from an isotropic distribution gives a value of only 2.5%.

The angular correlations (α) between each two particles in the centre of mass system have also been calculated. There is a preference for the nucleons to be emitted in opposite directions. Since the nucleons take most of the momentum, and also because of the angular distributions of the nucleons, this effect is to be expected. The distribution of angles between pion and each nucleon are given in Figure 16. The distributions should follow curves A and B on the isobar theory, whereas the statistical theory predicts that the distributions should be identical, and of a shape very similar to curve B. These distributions are rather similar

FIGURE 14

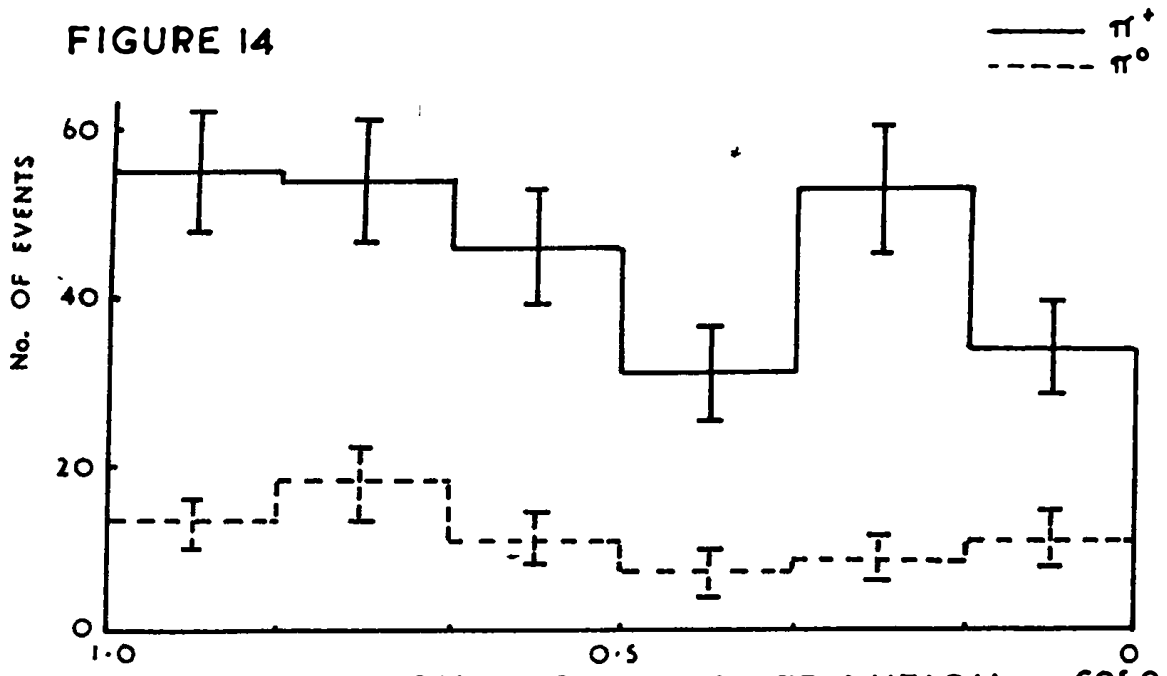

PION ANGULAR DISTRIBUTION

FIGURE 15

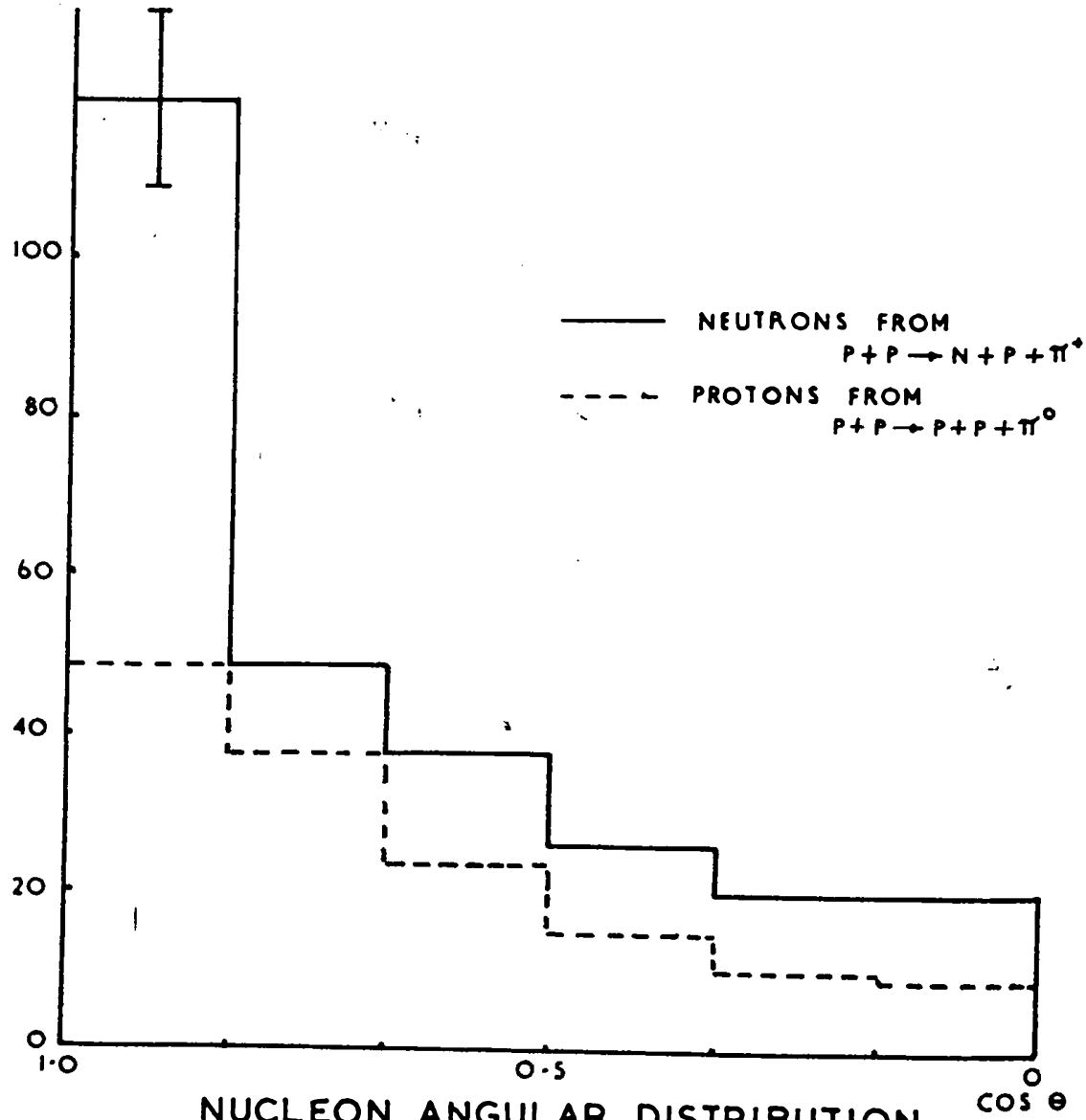

NUCLEON ANGULAR DISTRIBUTION

at this energy, and the data are not sufficiently determined to make a test between the two theories.

Although the sample of 273 events may be a biased one, as noted above in the case of the proton angular distribution, it is difficult to conceive that this should produce a large bias in the results. This is especially true of the Q-value distributions, since they represent a quite complicated function of the measured quantities.

(b) The reaction $p + p \rightarrow p + p + \pi^o$

The angular distributions of the neutral pions and protons from the 72 events of the type

$$p + p \rightarrow p + p + \pi^o$$

are shown by the broken lines in Figures 14 and 15. Within the statistics, these distributions are similar to those found for the nucleons and positive pions from the reaction

$$p + p \rightarrow n + p + \pi^o$$

The kinetic energy spectrum of the neutral pions in the centre of mass system is shown in Figure 12. This distribution is significantly different from the spectrum of the positive pions given in Figure 11; a χ^2-test on the two distributions gives a probability of only 1.5% that they are random samples of the same distribution. The neutral pion spectrum is peaked at higher energy, and has roughly the same shape as the statistical theory prediction. The disagreement with the isobar theory is also apparent in the centre of mass energy spectrum of the secondary protons, shown in Figure 10, in which the solid curve is the predicted distribution from the isobar theory. The low mean energy of

FIGURE 16

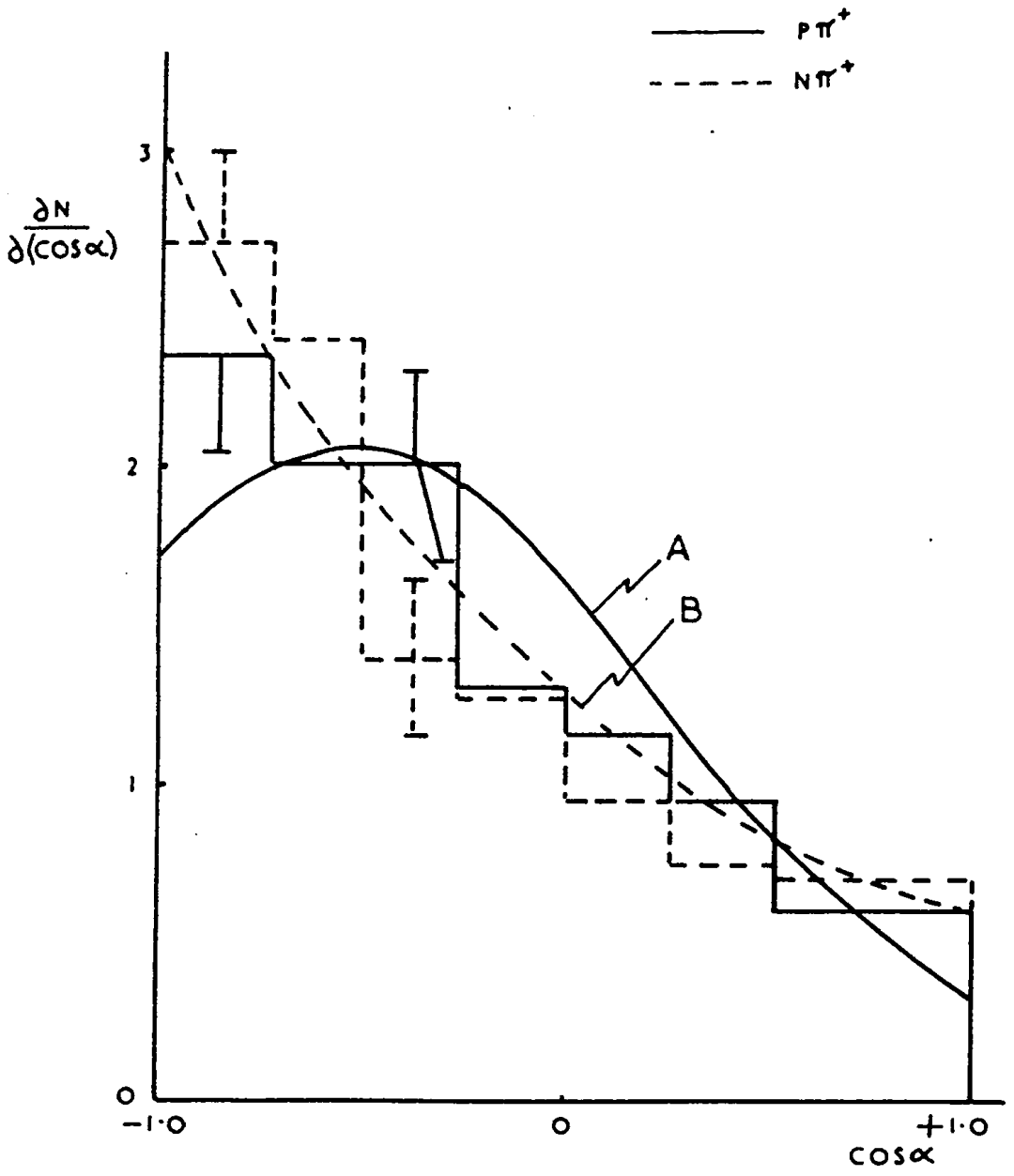

PION-NUCLEON ANGULAR CORRELATION

the protons compared to the predicted value is a reflection of the high mean energy of the pions.

(c) Conclusions

The results for the reaction

$$p + p \rightarrow n + p + \pi^+$$

disagree with the predictions of the statistical theory. The pion energy spectra and the Q-value distributions agree well with the isobar theory. Although the nucleon energy spectra show disagreement, they lie much closer to the predictions of this theory. The disagreement may not be as large as indicated by the t-test above, since the theoretical curves are for an incident energy of 1 Bev, and the present sample omits some fast protons (section 2(vi)(a)). The above results do therefore give support to the concept of the $T = 3/2$ isobar as an intermediate stage in pion production.

It is not expected that Lindenbaum and Sternheimer's model will give a precise description of pion production because of the simplifying assumptions. In particular, they consider that the assumption of no final state nucleon interaction is best put to the test of experiment. With larger numbers of events, the improved statistics should enable a more critical comparison to be made with the isobar theory. For example, the assumptions concerning the angular distribution of the isobar (see Introduction) may be tested by analysis of the nucleon and pion angular distributions. It is clear from Mandelstam's model, which is applicable at lower energies, that refinements can make appreciable changes in the theoretical predictions. This is evident, for example, when his results

concerning the ratio of positive to neutral pion production are compared with that due to Peaslee (section 2(iv)).

It appears that the energy spectra of the secondary particles from the reaction

$$p + p \rightarrow p + p + \pi^{o}$$

do not agree well with those from positive pion production. Any conclusions drawn from these results must be very tentative as the sample consists of only 72 events. In section 2 (iii)(a) a suggestion was made that the identification of events with charged pion production is easier than for events with neutral pion production. In view of the 39 unidentified inelastic events, an appreciable bias may therefore exist in the above sample. However, these results are interesting in the light of information obtained in an experiment on proton-deuteron scattering at 970 Mev (Batson et al., 1959, see appendix), in which the cross-section for the reaction

$$p + n \rightarrow p + n + \pi^{o}$$

was found to be higher than that expected from the other nucleon-nucleon inelastic cross-sections. Baldin and Kabir (1958) and Yamaguchi (1958) have independently proposed the existence of a neutral pion of isotopic spin zero. Although the possible anomalies on neutral pion production in this experiment might be explained in terms of such a particle, there is no experimental evidence to date to substantiate its existence.

SECTION 3

Further Study of Proton-Proton Scattering

A further study was made of the 565 elastic and the 328 positive pion producing events in order to

(i) check whether or not there was any indication of parity violation in pion production, and

(ii) to look at some features of certain angular distributions in the positive pion producing events in order to obtain, if possible, additional information on the preference of the secondary particles for particular angular momentum states.

To evaluate the possible simulation of such effects resulting from polarisation of the primary protons, a check was first made on the right-left asymmetry in the distribution of the secondaries from both the elastic and the positive pion producing events.

(i) Primary Beam Polarisation

If the primary beam is polarised, there will exist a right-left asymmetry for the elastically scattered protons. In an elastic scattering the secondary proton of smaller scattering angle (θ_L) is considered to be the scattered

FIGURE 17

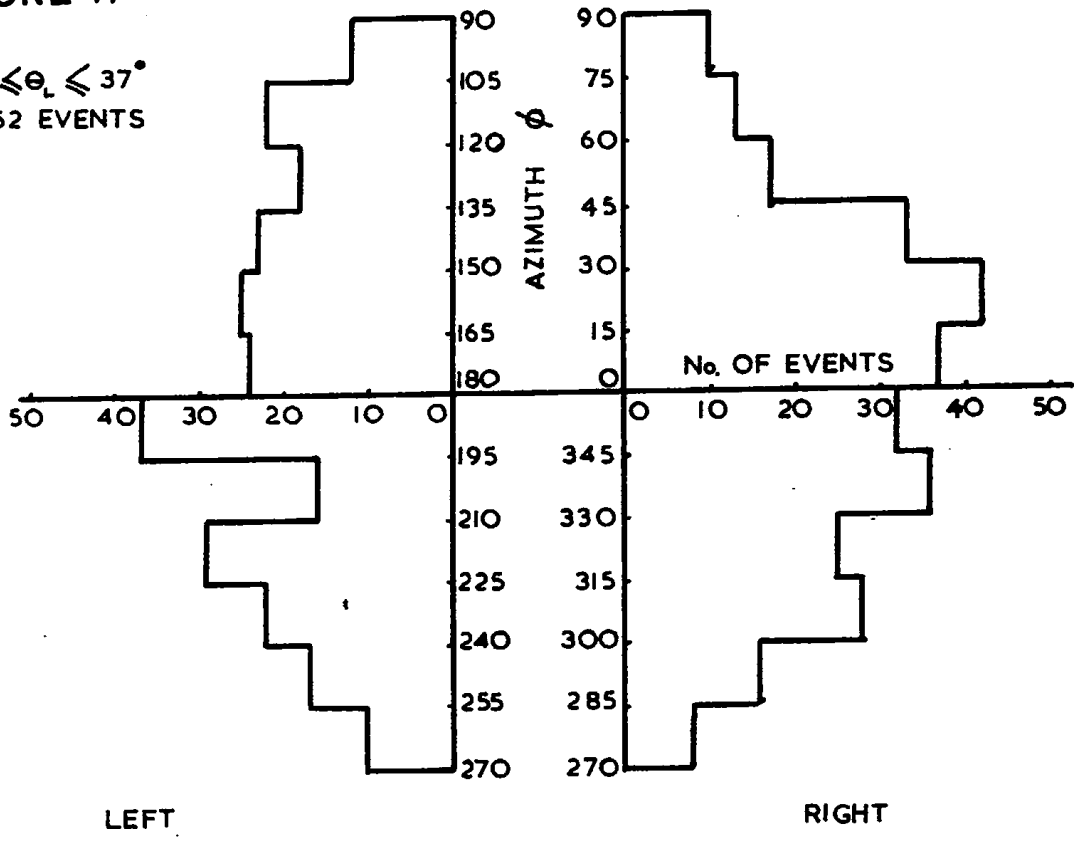

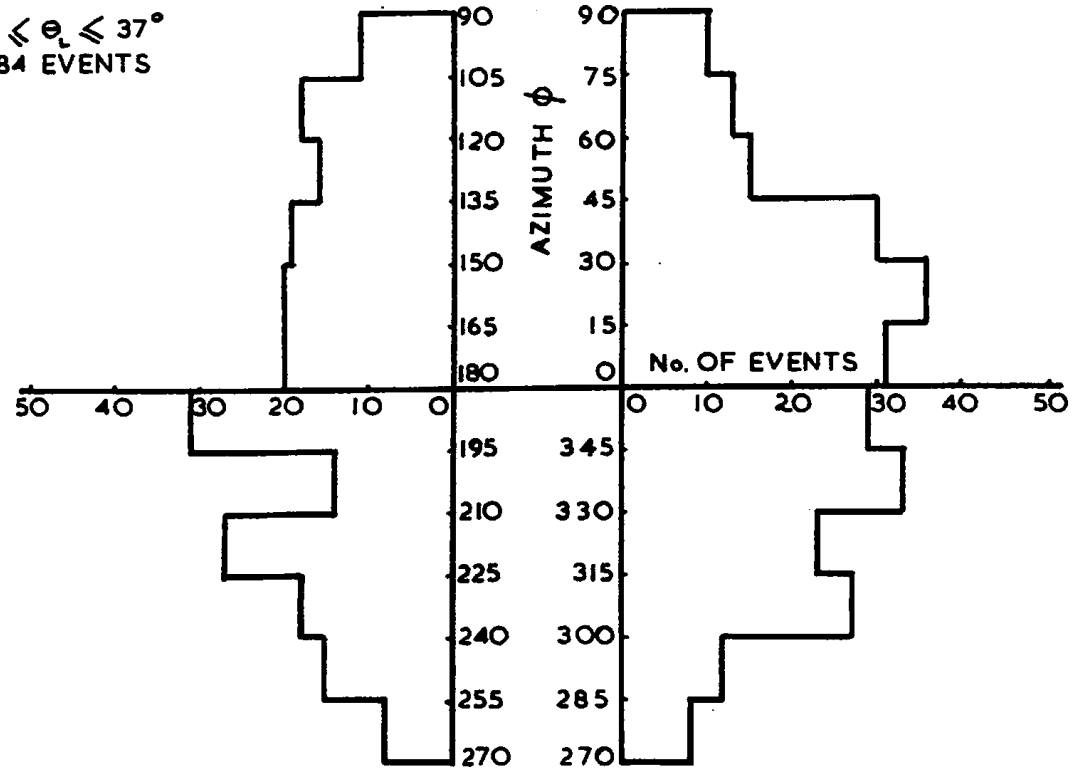

AZIMUTHAL DISTRIBUTIONS OF ELASTIC EVENTS

proton and the other the recoil proton.

Before proceeding with the analysis, the distribution in azimuth of the elastic events was examined. In Figure (17), histograms of the azimuthal distributions are given for events selected according to the following limits on θ_L :

(a) $0^\circ \leq \theta_L \leq 39^\circ$ 552 events

(b) $7^\circ \leq \theta_L \leq 39^\circ$ 484 events

The cut-off at 7° in (b) was introduced to remove the bias due to small angle scanning losses. The 39° limit represents the angle in the laboratory system at which the polarisation falls to zero ($\theta_L = 39^\circ$ corresponds to $\theta_{CM.} = 90^\circ$).

The measured asymmetry (ϵ) is defined as follows (see, for example, Wolfenstein, 1956):

$$\epsilon = \frac{R - L}{R + L}$$

where R, L are the numbers of particles scattered to the right and left respectively. In computing the asymmetry only events with $315^\circ \leq \phi \leq 45^\circ$ and $135^\circ \leq \phi \leq 225^\circ$ were used. No attempt was made to correct for scanning bias and for the dependence of polarisation on azimuthal angle, because the two corrections were small over the range of azimuth chosen. In any case, the dependence of scanning bias on azimuth was approximately the reciprocal of the dependence of polarisation, so that the scanning bias tended to compensate for the

azimuthal variation of polarisation.

Table 5 shows the computed asymmetries for the selections on θ_L given in (a) and (b) above.

TABLE 5

	L	R	ϵ	$\Delta = \frac{R-L}{\sqrt{R+L}}$	p
(a)	154	205	0.14	2.69	0.01
(b)	131	182	0.16	2.88	0.005

Δ is the difference between R and L in units of standard deviations and p is the probability of the given R - L asymmetry occurring by purely statistical fluctuation. Although the statistics are poor, the values of p are sufficiently small to conclude that,

(a) the incident beam was polarised, and

(b) polarisation is produced in proton-proton elastic scattering at 970 Mev.

A measurement of the primary beam polarisation has been made in this laboratory by means of a counter experiment (M. Huq, 1958), giving a value of about 1/3. Measurements of polarisation in elastic proton-proton scattering have been made at lower energies (Mescheryakov et al., 1957). By

averaging the Russian results at 635 Mev over the range of scattering angle of (b) in Table 5, using the differential cross section as a weighting factor, a value of about 1/3 is inferred for the average polarisation at 970 Mev. This inference is justified since, although the cross section for proton-proton scattering varies considerably from 450 Mev to 635 Mev, the average polarisation as well as the dependence of polarisation on scattering angle remain practically unchanged. This value of 1/3 in conjunction with the primary beam polarisation predicts an asymmetry of about 0.11, which is to be compared with the observed value of 0.16 (Table 5).

For the inelastic events, no significant R - L asymmetries were found in the azimuthal distributions of the secondary particles. It was therefore assumed that a check for parity violation in meson production would not be affected by polarisation effects.

(ii) Parity conservation in Pion Production

Since it was suggested (Lee and Yang, 1956) and subsequently verified experimentally (Wu et al., 1957; Garwin et al., 1957; Friedman and Telegdi, 1957) that conservation of parity was violated in weak interactions, this law has been questioned in the case of strong interactions. Although there is good evidence for parity conservation in strong

FIGURE 18(a)

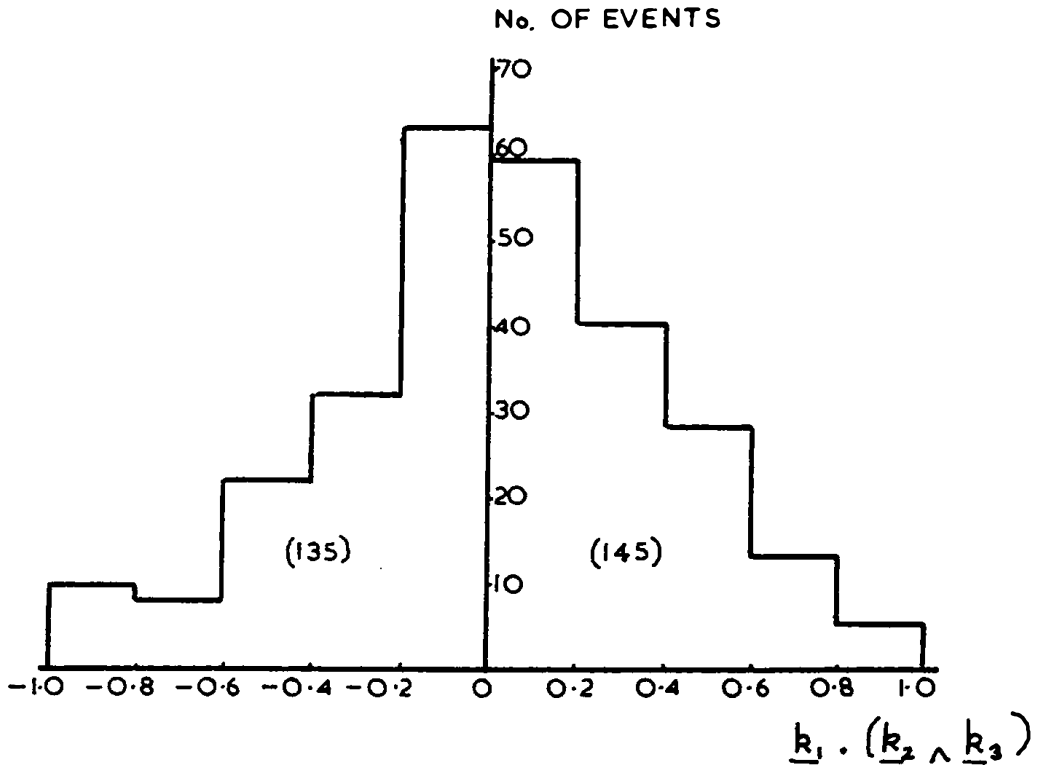

FIGURE 18(b)

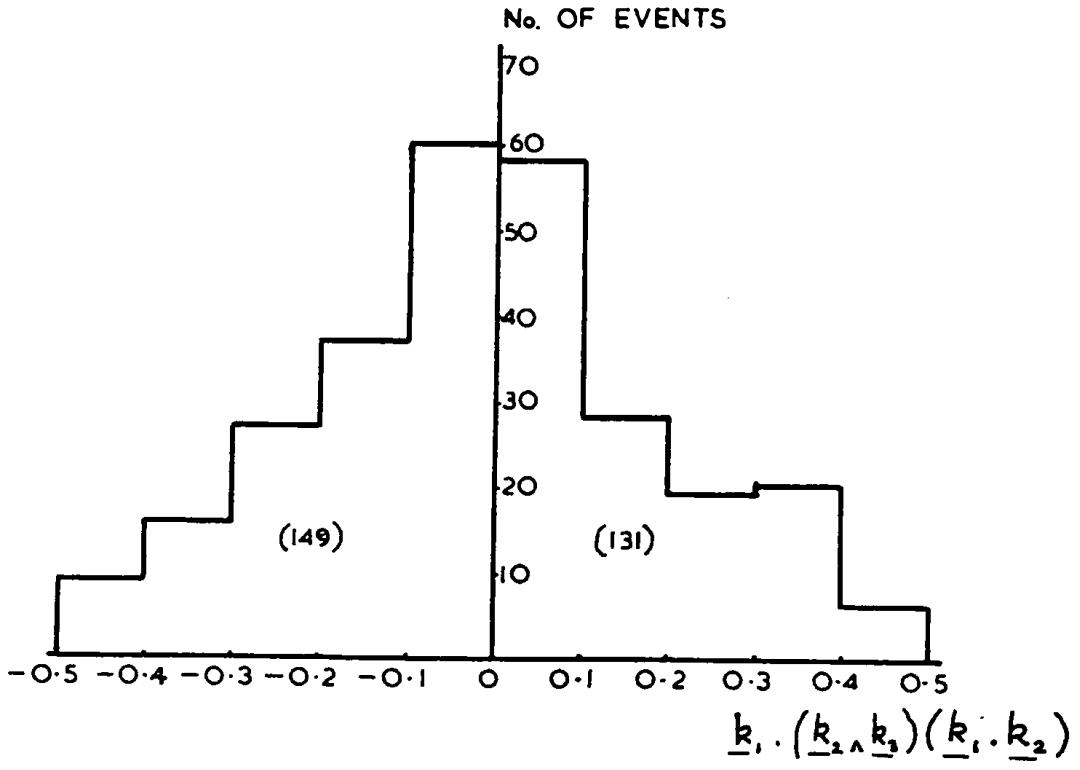

PSEUDOSCALAR PRODUCTS

interactions at low energies (Tanner, 1957; Wilkinson,1958) there is at present little information at high energies. Bubble chamber experiments at Berkeley (Crawford et al., 1959) have shown how small any parity non-conserving effect must be in the production of strange particles. At Rochester, Heer et al., (1958) have bombarded aluminium with 209 Mev polarised protons and looked for an up-down asymmetry in positive mesons produced, which would indicate violation of parity conservation. They deduce an upper limit to the parity-mixing coefficient of 2×10^{-3}. An attempt is being made at the suggestion of Bernadini and Lederman to find evidence for violation of the law in the production of neutral pions from carbon by 500 Mev polarised neutrons. It is hoped to find any parity violating term to an accuracy of 5 parts in 10^3.

The positive pion producing interactions

$$p + p \longrightarrow n + p + \pi^+$$

were analysed to detect any parity non-conservation. If parity is not conserved then pseudoscalar quantities should be present in the cross section. For parity conservation the average value of any such terms should vanish. If k_1, k_2 and k_3 are unit vectors in the directions of the incident proton, the emitted proton and the positive pion respectively, then possible pseudoscalar products which are most obviously suggested are:

FIGURE 18(c)

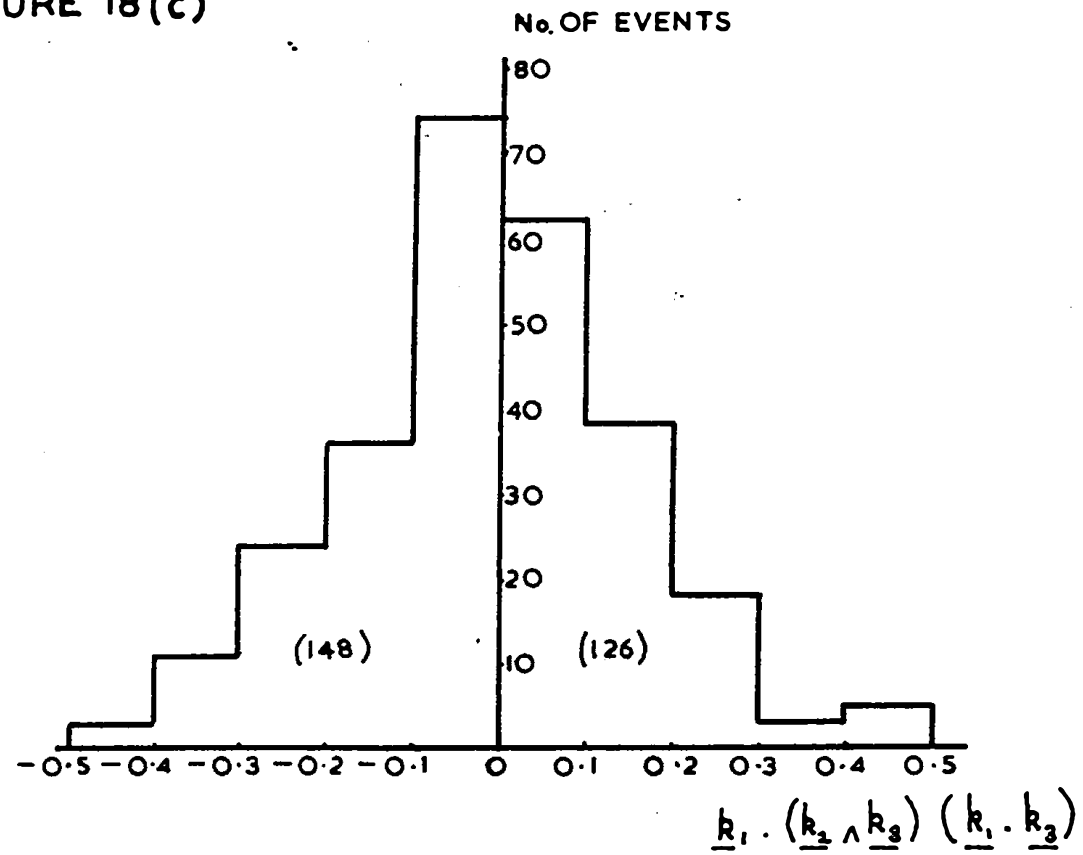

FIGURE 18(d)

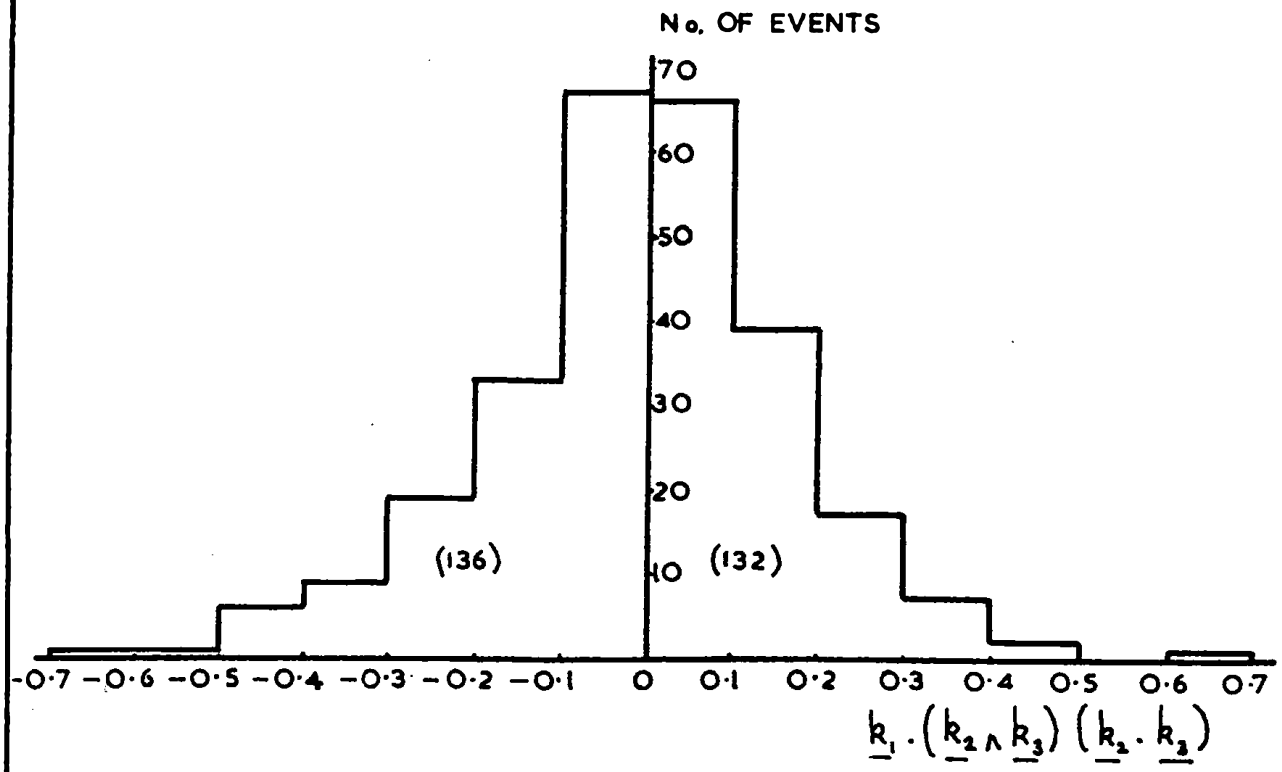

PSEUDOSCALAR PRODUCTS

(a) $\underline{k}_1 \cdot (\underline{k}_2 \wedge \underline{k}_3)$

(b) $\underline{k}_1 \cdot (\underline{k}_2 \wedge \underline{k}_3)(\underline{k}_1 \cdot \underline{k}_2)$

(c) $\underline{k}_1 \cdot (\underline{k}_2 \wedge \underline{k}_3)(\underline{k}_1 \cdot \underline{k}_3)$

(d) $\underline{k}_1 \cdot (\underline{k}_2 \wedge \underline{k}_3)(\underline{k}_2 \cdot \underline{k}_3)$

The above quantities were computed for each event for which directions of both charged secondary particles were known in the centre of mass system. The resulting distributions are shown in Figures 18(a), (b), (c) and (d). In the absence of strong polarisation effects, the identity of the two protons requires that, on the average, term (a) should vanish. Figure 18(a) shows this to be the case. A detailed statistical test, the chi-squared test (Davies, 1957), shows that there is no significant departure from symmetry. In executing this test, one half of the distribution is compared with the other half reflected in the y-axis and a measure of the probability of the two distributions being identical is obtained. An asymmetry in the distribution of any one of the terms (b), (c) and (d) would lead one to suspect a violation of parity. It is seen from figures 18(b), (c) and (d) that these distributions are symmetrical so that the average contribution of these terms to the cross section is nil. Again, for each distribution, a χ^2 - test shows that there is no significant departure from symmetry.

(iii) Further Angular Distributions

The results of section 2(vi) for the reaction

$$p + p \longrightarrow n + p + \pi^+$$

show that the concept of a T = J = 3/2 isobar as an intermediate stage in pion production is a reasonable one. G. Morpurgo (1958) has suggested that certain angular distributions of secondary particles in reactions involving single meson production might give information regarding the preference of the secondary particles for particular angular momentum states. These angular distributions might therefore be useful in confirming the existence of a J = 3/2 state isobar. As mentioned in section 2(vi), the T = 3/2 isobar decays most of the time into a proton and a pion. With this in mind, the appropriate angles in the centre of mass system of the proton and pion, defined below, were computed for each well measured event.

These angles are:

(a) χ , the angle between the pion direction and the line of flight of the isobar in the centre of mass frame of the isobar, and

(b) Φ , the angle between the production plane of the isobar and the decay plane in the centre of mass system of the isobar.

It is apparent that these angles are the same as those

FIGURE 19

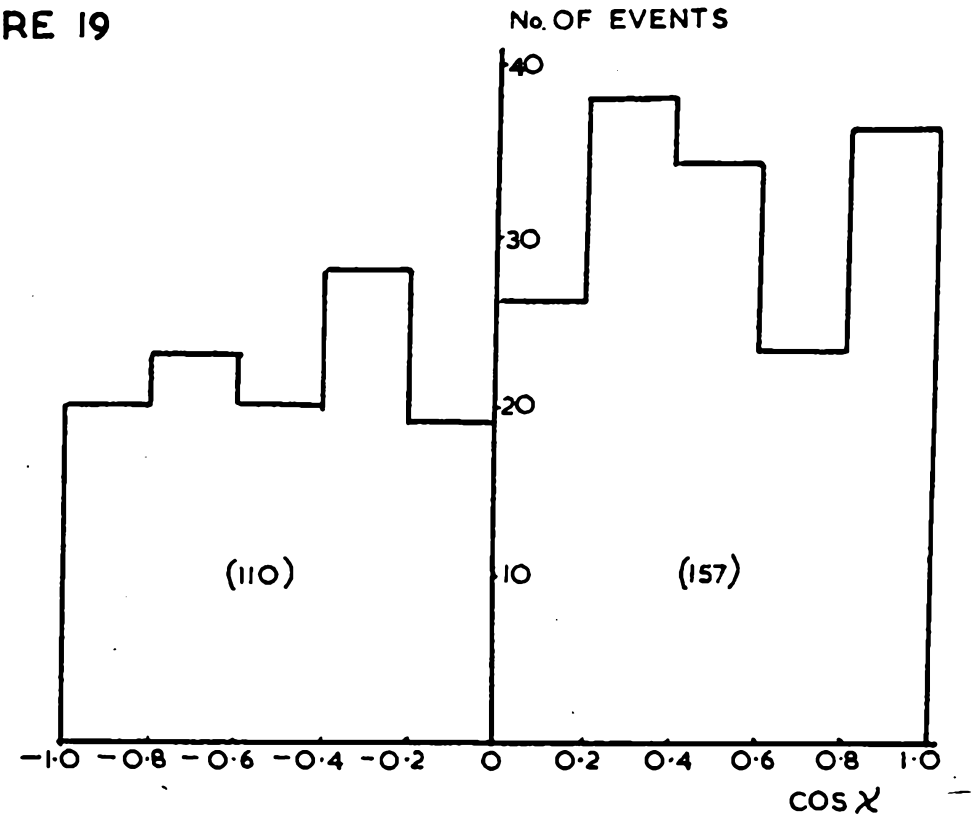

FIGURE 20

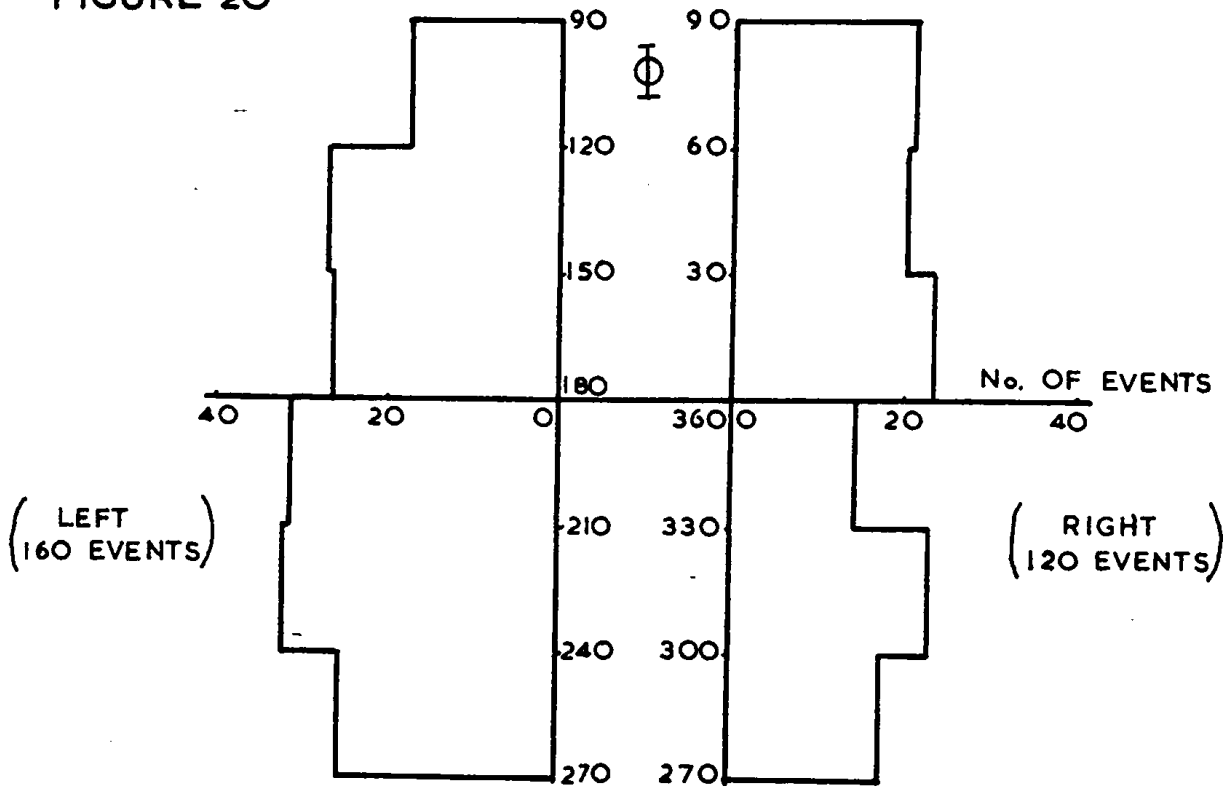

DISTRIBUTIONS IN χ AND Φ

considered in the reactions involving associated production of hyperons and K particles to get information on the spins of hyperons (Eisler et al., 1958). However, there are important differences (Morpurgo, 1958) to be noted when drawing an analogy between isobar and hyperon production. The angle χ is given by

$$\tan\chi = \frac{|\underline{k}_3| \sin(\pi - \alpha_{34})}{\gamma\left[|\underline{k}_3| \cos(\pi - \alpha_{34}) - \beta U_3\right]}$$

where $\underline{k}_3$ = momentum of the π^+ in the centre of mass system

α_{34} = opening angle between the pion and the neutron in the centre of mass system.

$\gamma = 1/\sqrt{1-\beta^2}$ and $\beta = v/c$, where v = velocity of the isobar.

U_3 = total energy of the pion in the centre of mass system.

These quantities were readily obtained from the information recorded on each well measured event.

The distribution in χ for 267 events is shown in Figure 19. The numbers shown on the histogram give a forward-backward asymmetry of 2.9 standard deviations, which indicates that the asymmetry is significant. The angle Φ is given by the following expression

$$\cos\Phi = \frac{(\hat{\underline{k}}_1 \wedge \hat{\underline{k}}_4) \cdot (\hat{\underline{k}}_3 \wedge \hat{\underline{k}}_4)}{|\hat{\underline{k}}_1 \wedge \hat{\underline{k}}_4|\,|\hat{\underline{k}}_3 \wedge \hat{\underline{k}}_4|}$$

where $\hat{k}_4$ is a unit vector in the direction of the neutron in the centre of mass system. This expression was calculated for 280 events and the resulting histogram is shown in Figure 20. The 0° - 180° axis corresponds to the production plane of the isobar. A significant left-right asymmetry of 2.4 standard deviations is obtained. There is no significant up-down asymmetry.

A theoretical investigation of these distributions has been carried out by Mr. L. Castillejo and Mr. G.P. McCauley of the Mathematical Physics Department. They have pointed out that it is not possible to draw the definite conclusions suggested by Morpurgo (1958). The situation is complicated by the effects of a final state interaction in the production process and of the polarisation of the incident proton beam. To allow for these it would be necessary to perform detailed calculations similar to those of Mandelstam (1958). The question as to whether or not the observed asymmetries in the χ and Φ distributions can be interpreted theoretically is still therefore an open one. However, it appears plausible that some asymmetry could arise from a bias introduced in selecting the events. As mentioned in section 2(vi)(a), events with protons of high forward momentum in the laboratory system would tend not to be well measured, and therefore would not be included in the sample on which the computations for χ and Φ were made.

CHAPTER II

THE LIQUID HYDROGEN BUBBLE CHAMBER

SECTION 1

Introduction

In high energy interactions there are often more than two secondary particles; a visual detector is therefore desirable in order to obtain complete information readily. A visual technique is also necessary in the search for a rare type of event. Nuclear emulsions make a poor target material since they consist of several elements, thus making the identification of events a difficult task. Cloud chambers have the advantage that they can present pure target materials; in particular they can be filled with hydrogen gas under several atmospheres pressure. In recent years, the development of liquid hydrogen bubble chambers has enabled a greater stopping power to be obtained in hydrogen; there is about a factor 30 in density between liquid and 25 atmospheres of gas. The resulting increase in rate of accumulation of events can only be exploited by using automatic analysis equipment in conjunction with an electronic computer. Bubble chambers can in principle be constructed with extremely large dimensions and do not suffer from the disadvantage, found in diffusion cloud chambers, of a limited sensitive region. Large size enables such a detector to be useful in the study of short-lived phenomena, such as strange particles, where both

production and decay processes may be observed on one photograph.

The discovery of the bubble chamber principle was made by Glaser (1952, 1953) during research designed to find a visual detector for use in conjunction with high energy accelerators. He discovered that the passage of a charged particle could be rendered visible as a string of bubbles in a superheated liquid. He achieved this by holding the liquid under pressure at a temperature above the normal boiling point and suddenly removing this pressure. Hildebrand and Nagle (1953) first operated a bubble chamber, in the form of a pyrex bulb of volume 3 cc., with a filling of liquid hydrogen. It is not possible to construct a "clean" chamber of this type with large dimensions because of the large pressures that have to be withstood. A composite chamber consisting of a metal body with flat windows sealed to it by gaskets can be constructed with large dimensions. Wood (1954) built the first chamber of this type using liquid hydrogen. He discovered that he could obtain tracks in his "dirty" chamber by expanding rapidly, in a few milliseconds, before boiling on the walls repressurised the system. Chambers currently used are of this composite type and the rapid expansion is not a disadvantage for use with pulsed accelerators.

Experience with the 18" diameter diffusion cloud chamber

(see Chapter I) showed that there was a need for a liquid hydrogen bubble chamber for use with the 1 Bev proton synchrotron at Birmingham. A 9" diameter bubble chamber should yield data ten times more rapidly than the cloud chamber. Further, the limited sensitive depth of the cloud chamber meant that accurate curvature measurements could not be made on tracks with large dip angles. When work commenced on the Birmingham chamber, no hydrogen chamber larger than 4 inches in diameter had been operated. Experience with this chamber (Parmentier and Schwemin , 1955) indicated that the largest volume feasible was about 5 litres, if a liquefier of around 100 litres per day output was to be installed at Birmingham. A cylindrical chamber 9" in diameter with a reasonable depth of 4" gives a volume of the required size. The results of the experiment described in Chapter I had stressed the importance of accurate curvature measurements on the photographs of secondary tracks. Because of the smaller diameter of the bubble chamber compared with the cloud chamber a magnetic field of at least 15,000 oersted was envisaged. The only available generator was the one that had been used for pulsing the cloud chamber magnet. Pulsed operation was again essential in order to cope with the power dissipated in the air-cored coils, which are needed to give a uniform field of 15,000 oersted over the chamber volume. Use of a hollow water-cooled

conductor was not possible because of the large number of turns. Owing to the low refractive index of liquid hydrogen small angle scattering of light is necessary, and a straight through optical system is simplest. An iron-cored magnet would have necessitated the use of "venetian blinds" or a retrodirective optical system. It will be seen below that the eddy currents attendant on the pulsed field determined to a large extent the detailed construction of the chamber. It has proved possible, however, to operate the chamber in fields as high as 22,000 oersted.

FIGURE 21

THE CHAMBER AND EXPANSION SYSTEM

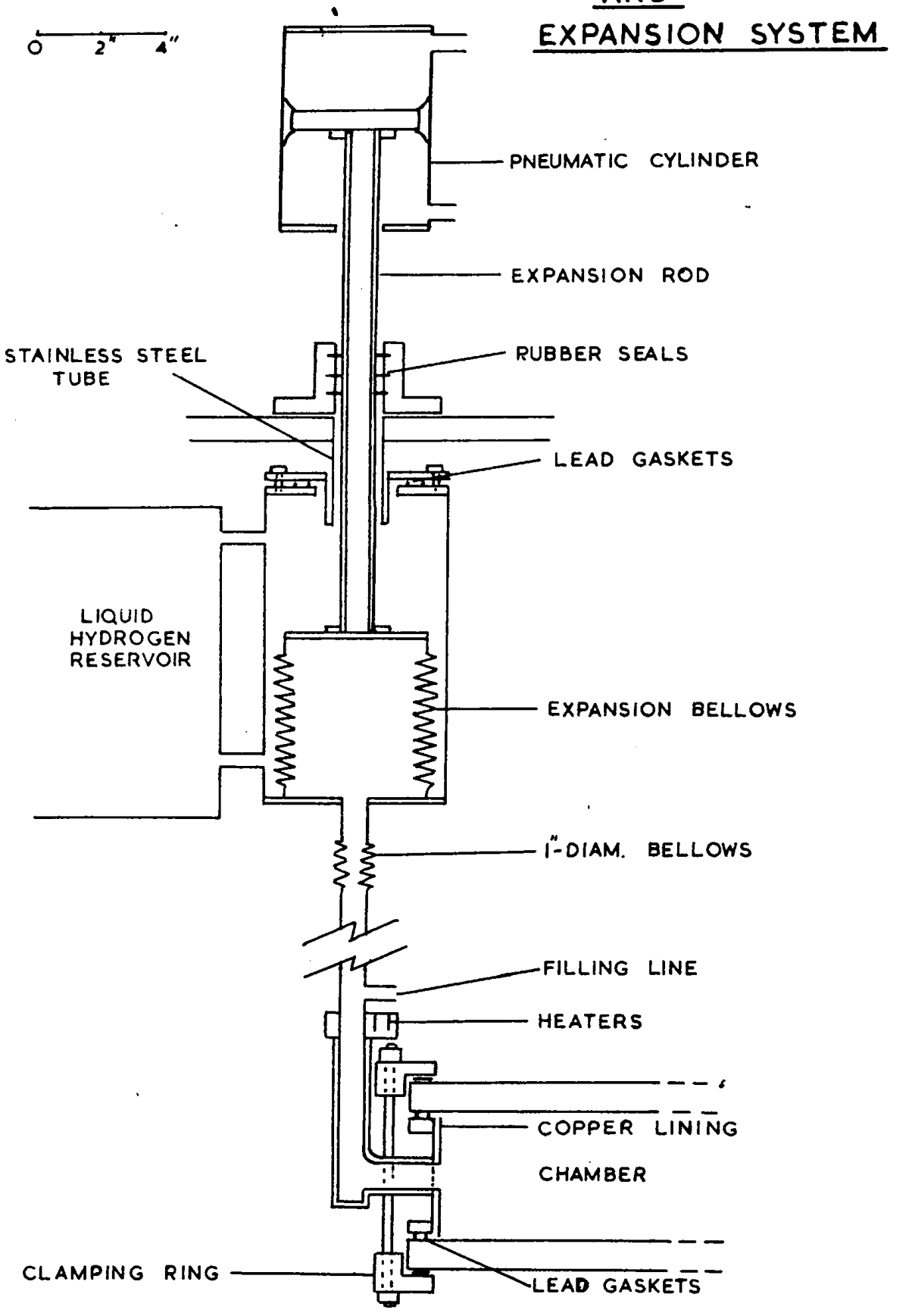

SECTION 2

The Apparatus

(see also Appendix)

(i) The chamber assembly and expansion system

The chamber consists basically of a stainless steel cylinder of 9" internal diameter formed by rolling a 4" wide plate and welding the join. This cylinder was machined to have a wall thickness of about 1/10" with flanges of rectangular cross section at both ends, as shown in Figure 21. Two concentric V-shaped grooves on the outer faces of both flanges serve to locate the gaskets sealing the chamber windows to the body. The gaskets are made from lead, or tin, drawn into wire 1 mm. in diameter, but they become squashed into the grooves when in position. During operation the space between each pair of gaskets is evacuated by means of a rotary oil pump.

Inside the chamber shell there is an oxygen-free copper lining 1/8" thick which is split vertically.to reduce eddy currents, and insulated from the main chamber by a sheet of "Melinex". Diametrically opposite the split, the lining is hard soldered to the expansion pipe positioned centrally in the chamber wall. The expansion pipe passes through the chamber wall and joins the bottom end of a pure copper block

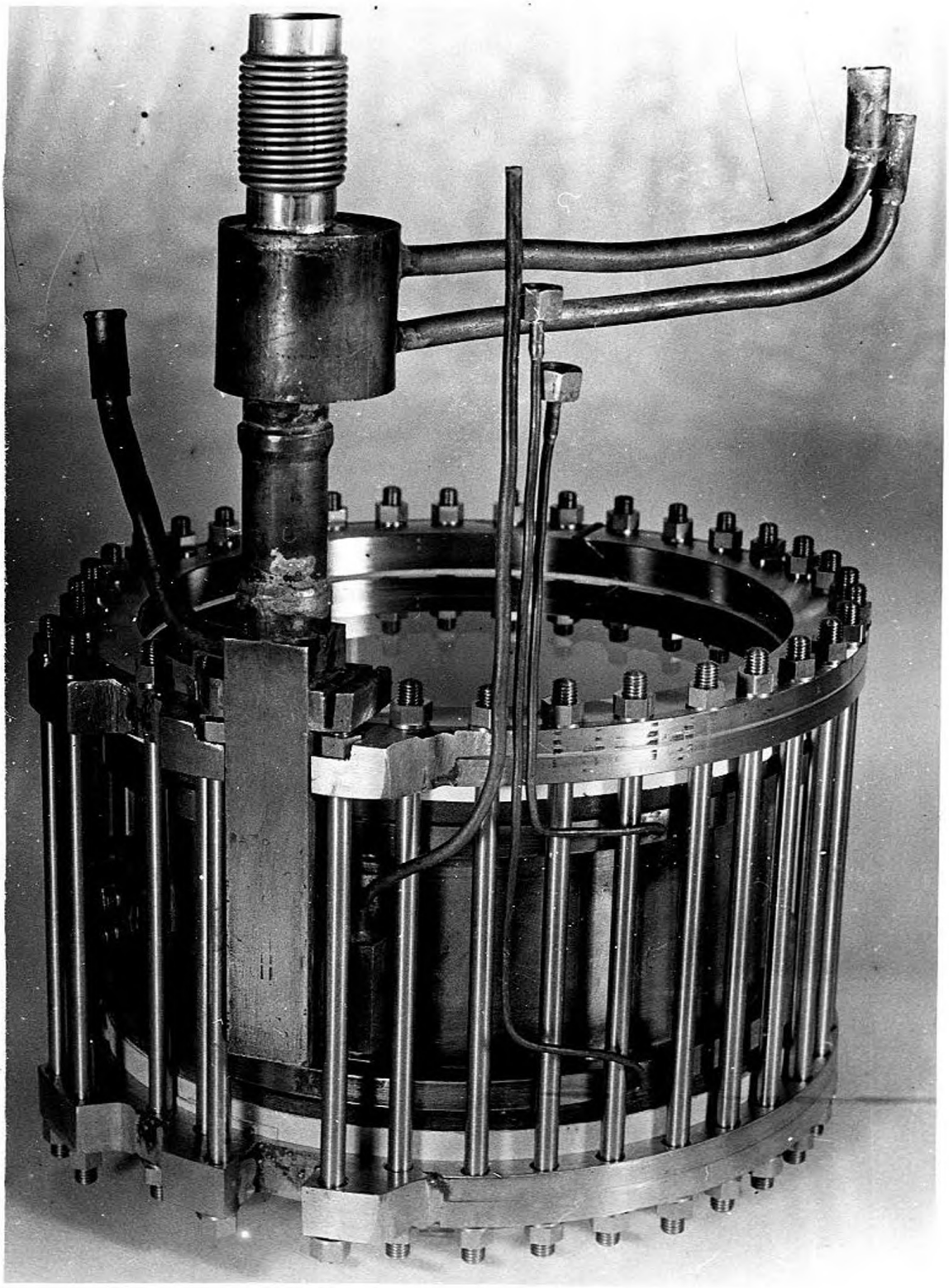

PLATE III

which runs vertically upwards. A 7/8" diameter hole through this block leads upwards to the expansion system and filling line as seen in Figure 21. The upper part of the expansion pipe is made from normal phosphorized copper which has a thermal conductivity about 20 times less than pure copper at liquid hydrogen temperatures. This serves as a heat leak between the heater blocks, placed at the top of the pure copper block, and the expansion system which is maintained at the temperature of the liquid hydrogen reservoir ($20^{o}K$). The two 25 watt heaters placed in slots enable the chamber temperature to be raised to its operating value. Plate III shows a general view of the chamber assembly. The small bellows at the top serves as a flexible connection for assembly purposes. Just below this is a boiler, which can be filled with liquid hydrogen from the reservoir. Although heat is conducted along the heat leak, an appreciable amount is transferred by convection in the liquid from the chamber to the expansion system.

The windows are made of toughened glass 3/4" thick by 10" in diameter and are held against the gaskets by clamping rings using 36 5/16" diameter stainless steel rods. This is clearly shown in Plate III. Also shown is a hydrogen vapour pressure thermometer soldered to the expansion pipe at the entrance to the chamber.

The expansion is performed by a 3-ply stainless steel bellows, 4" in diameter and 5" long. Attached to the top of the bellows is the control rod which is made of stainless steel and capable of withstanding the large forces experienced during expansion. The upper end of the control rod passes into a pneumatic cylinder 4" in diameter which is external to the vacuum tank. Compressed air at 150 p.s.i.g. holds down the piston and hence the bellows against the normal chamber pressure of 70-80 p.s.i.g. A 3/4" Barksdale valve (by Crescent Valve Co.Ltd.) opens the cylinder to the air for expansion when a suitable signal is applied (section 3). A further signal closes the valve and readmits the compressed air for the recompression stroke. The valve is shielded from the magnetic field by a soft iron cylinder. The inside of the bellows is common to the expansion pipe (Figure 21) and is normally full of liquid. Expansion takes place therefore directly on the liquid. Because of the smaller expansion ratio this system is more efficient than that employing a gas expansion. The bellows is enclosed in a 5" diameter cylinder which is common to the liquid hydrogen reservoir and allows liquid to circulate behind the bellows. The cylinder is suspended from the top plate of the apparatus by concentric stainless steel tubes (Figure 21) designed to minimise the heat input. The rubber seals on the control rod shaft are

FIGURE 22

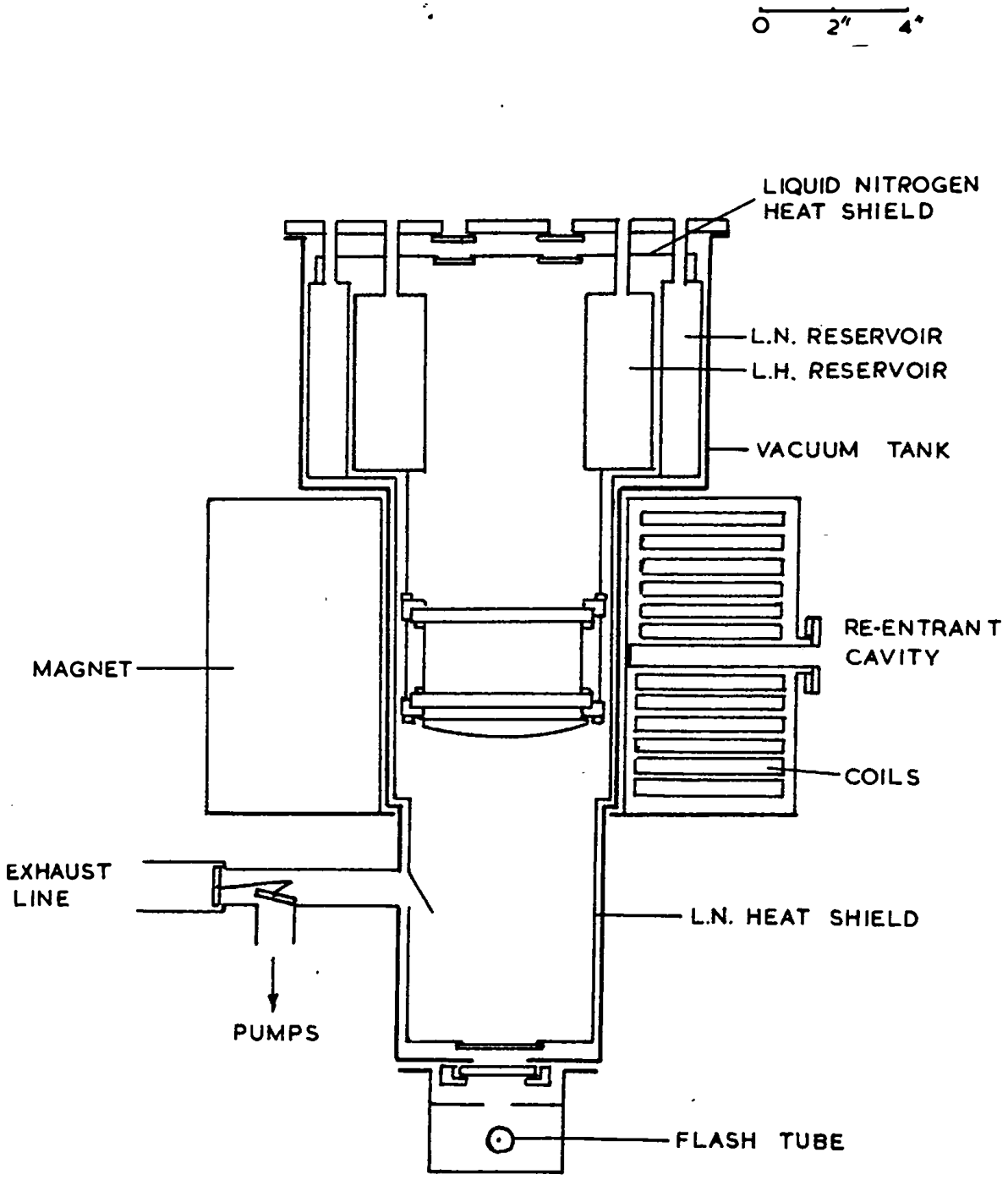

MAIN ASSEMBLY

designed to prevent hydrogen gas leaking into the experimental room. The rapidly changing chamber pressure during the expansion and recompression is monitored by a pressure transducer in the form of a capacitor (Linlor, Kerns and Mark,1957). The variation in chamber pressure changes the deflection of a diaphragm that acts as one electrode of a condenser. This capacitor forms one arm of an a.c. bridge, and the out-of-balance current in the bridge is displayed on a monitoring oscilloscope.

(ii) The cryogenic and high pressure system

The main cryogenic features are designed to minimise heat input to the chamber and hence to reduce loss of liquid hydrogen. Heat transfer to the chamber takes place by conduction along the support rods and through the surrounding gas and by radiation from warmer parts of the apparatus. Conduction along the supports is minimised by making them of stainless steel and suspending them from the liquid hydrogen reservoir (Figure 22). Gaseous conduction is reduced by surrounding the liquid hydrogen system by a vacuum. As seen from Figure 22, the chamber and reservoir system are suspended from the top plate into a large vacuum tank inside of which the pressure is maintained by a 2" diffusion pump. For a vacuum of 10^{-5}mm of Hg. or better the heat input to the

chamber is insignificant, but above this value the heat transferred rises rapidly. The vacuum tank is designed to withstand a pressure of 10 atmospheres; however, if the pressure rises above 1 atmosphere a valve opens up the tank to a 2" vent line, which passes upwards through the roof of the experimental room. The valve also protects the diffusion pump and the rotary oil pump which backs it. Because of the strong dependence of heat transferred by radiation on the temperature difference, it is necessary to surround the liquid hydrogen system by a heat shield at liquid nitrogen temperature. The heat shield is made of copper so that heat received is conducted easily to the liquid nitrogen reservoir from which it is suspended. The shield is split vertically to reduce eddy currents induced in the magnetic field. The reservoirs are made of stainless steel in the form of a cylindrical anulus with a 6" wide circumferential gap They lie concentric with each other, the outer containing liquid nitrogen and the inner liquid hydrogen. Both are suspended from the top plate by 3 thin-walled stainless steel tubes, which provide access for filling, boil-off and a level indicator. In the liquid hydrogen case the level is monitored by the change in capacitance of a condenser, in the form of two vertical concentric metal tubes, immersed in the liquid. The whole low temperature system is suspended from the top

plate, which is convenient for assembly purposes since it may easily be raised or lowered by a pulley system attached to the roof.

The chamber is filled by condensing high purity gas into it at pressures up to the final operating value of about 75 p.s.i.g. This gas is passed through a de-oxidising unit which removes oxygen.by forming water. The gas then passes through a charcoal trap at liquid nitrogen temperature which removes the water vapour and other impurities. From the charcoal trap it traverses 10 ft. of narrow bore tube immersed in the liquid nitrogen reservoir. When the chamber is full of liquid this filling line is closed and a larger bore one is used to give adequate control of the chamber pressure. This pipe also serves as an exhaust line and the chamber can be evacuated through it. A solenoid operated valve in this line is closed during expansion of the chamber, thus preventing comparatively warm gas from being drawn into the chamber system. A spring loaded safety valve isconnected to the chamber system and preset to blow off at a chamber pressure of about 100 p.s.i.g. The exhaust from this valve passes into the 2" diameter vent pipe through the roof. This valve is by-passed by two lines which are, of course, normally closed. One of narrow bore contains a low temperature trap which is used during operation to bleed off small amounts of gas from the chamber. The other

FIGURE 23

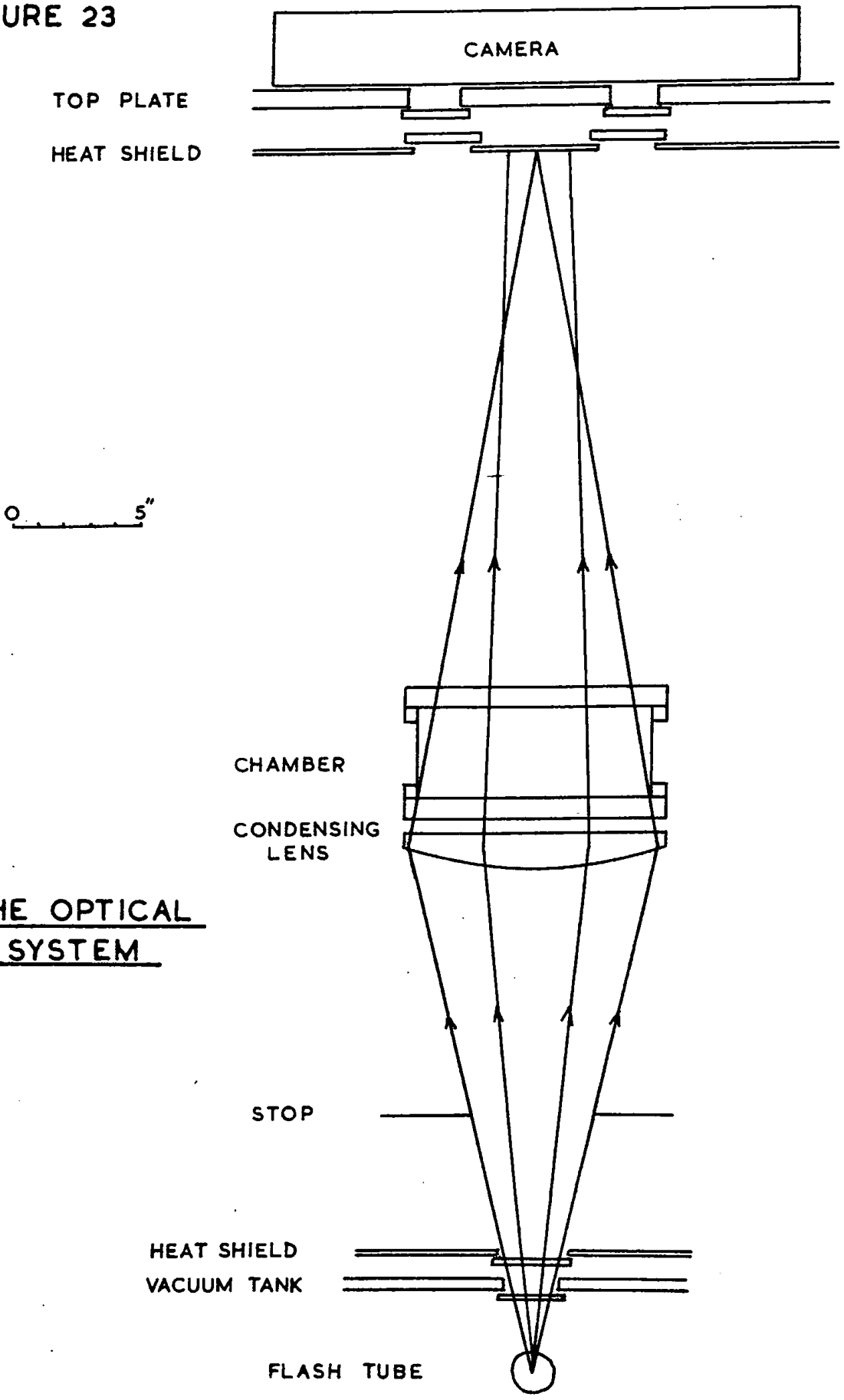

THE OPTICAL SYSTEM

larger bore line allows the chamber to be emptied quickly at the end of an experimental run.

(iii) The optical system

The scattering of light from a bubble in liquid hydrogen is strongly peaked in the forward direction due to the low refractive index of the liquid (1.08). The optical system employed is therefore a straight through type giving dark field illumination. A condenser lens attached to the bottom of the chamber converges the light from a source at the bottom of the vacuum tank to a region between the 3 camera lenses located on the top plate (Figure 23). Any light passing into the cameras is scattered from the main light beam. This is so for bubbles in the body of the chamber liquid, so that tracks appear as a bright string of dots against a dark background.

The source is a xenon filled flash tube (by Siemens Edison Swan Ltd.) located at the bottom of the vacuum tank in a brass box. It is effectively a point source since the electrode separation is only 5mm. This brass box is external to the tank and thus accessible when the main tank is evacuated. The flash tube illuminates the chamber through windows in the heat shield and vacuum tank. The latter is made from 3/8" toughened glass and designed to withstand a

tank pressure of 10 atmospheres. As an additional precaution the flash box is also designed to withstand the same pressure. The plano-convex condenser lens, of nominally 16" focal length, is attached to the bottom clamping ring of the chamber. Its paraxial focus lies 44" above the top plate but no light enters the camera lenses (Figure 23). Because of spherical aberration, light from the peripheral region of the lens is brought to a focus around the plane of the cameras. This is advantageous since ideally all light should be brought to a focus in the camera plane, so that there is a minimum variation in scattering angle from a bubble against position across the chamber. Any large variation is unfortunate because of the strong dependence of light intensity on scattering angle. Photographs are taken by 3 cameras positioned on the top plate. Two of these cameras are located in one unit and subtend an angle of about 16^{o} at the centre of the chamber. The third camera is displaced perpendicular to the vertical plane through the other two lenses and makes an angle of 8^{o} to it at the chamber. This third camera is intended to reduce scanning losses, and to enable better measurements to be made on some tracks. The cameras contain Dallmeyer wide angle lenses formerly used in the diffusion cloud chamber cameras (Chapter I, section 1). Photographs of the chamber taken through optically flat windows in the heat

shield and top plate are recorded on 35 mm. film. From the point of view of film speed and contrast Ilford 5G91 and Kodak "Plus X" have proved most satisfactory. Film is exposed in 100 ft. lengths in each camera unit and lasts 80-90 minutes in the large unit, which takes pairs of photographs every 10 seconds. The film in both camera units is wound on between photographs by a 12 r.p.m. electric motor controlled by a cam wheel on a sequence timer (section 3).

(iv) The magnet

The excitation system for the pulsed magnetic field is the same as that used for the diffusion cloud chamber (Batson et al., 1956) except for small differences. The high field of 15-20,000 oersted required for accurate curvature measurements, means that it is necessary to draw much larger currents from the 500 kilowatt generator in order to energise the air-cored magnet of the bubble chamber. In the old system the current was initiated in the magnet coils by firing a BK44 ignitron in order to give precise timing. However, because of the increase in heat dissipated in the valve due to the higher mean current, ithas been replaced by a larger BK34 ignitron with extra cooling. At present a further modification is being made in the form of a second BK34 valve in parallel with the first and a relay to alternate the firing of the

valves on alternate pulses.

The magnet solenoid consists of 12 layers of copper, each layer containing 72 turns of 1.25 x 0.1 inch copper strip. Insulation between turns is made of 0.01 inch thick Presspahn paper and the coils are separated by 1/8" thick bakelite sheets in the form of webs, which serve to direct the flow of cooling oil. When all layers are connected in series the solenoid has a total resistance of 0.32 ohms. The solenoid is enclosed in a stainless steel container and insulated from it by bakelite spacers and oil-resistant plastic sponge. The two central layers are separated by 1" bakelite rods, in order to fit over a re-entrant cavity which provides a beam entry port (Figure 22). The whole assembly is mounted on a rigid trolley which can easily be moved about.

Cooling is achieved by passing transformer oil at 2000 g.p.h. through the coils under a pressure head of 30 p.s.i.g. and then through two water-cooled heat exchangers (by Serck Radiators Ltd.) in parallel. This pressure head is maintained by a centrifugal pump (by Saunders Valve Co.Ltd.,). With the coils connected in series a peak current of 900 amperes may be drawn from the generator and gives a field of 14,500 oersted. Pairs of coils may also be connected in parallel giving a series-parallel arrangement. In this case the effective number of turns is halved when compared to the series

arrangement, so that twice the current is needed to give the same field. However, with this configuration it is possible to draw a peak current of 2,500 amperes which corresponds to a field of 20,000 oersted. Under these conditions with a 10 second pulse rate the mean power dissipation in the magnet is 100-120 kilowatts. With this high field the heat input to the chamber due to eddy currents is 10-20 watts; nevertheless the chamber can be operated satisfactorily by making an appropriate adjustment to the heater supplies.

The magnetic field has been measured over the chamber volume under pulsed and d.c. conditions. The variation of field strength with current was obtained using a small search coil of turns area 39.45 turns cm^2 and a Grassot fluxmeter. For these measurements the generator supplied direct current so that high fields could not be measured because of over-heating the magnet coils. It was seen that the field strength is proportional to current and, with the series arrangement of coils, a current of 900 amperes gives a field of $14,470 \pm 50$ oersted. The spatial variation of magnetic field was observed using a difference coil technique. Measurements were made in the vertical planes along and perpendicular to the particle beam direction. A maximum variation of less than $\pm 2\%$ of the central value was noted over the chamber volume. A large search coil of turns area 8.31×10^5 turns cm^2 was used for

the pulsed field measurements. The voltage developed across this coil was integrated using a simple Miller integrator circuit, the output of which was displayed on an oscilloscope. Knowing the constants of the integrator circuit and the calibration of the oscilloscope, the peak field was deduced from the maximum voltage. These measurements agreed with the corresponding ones due to steady currents to within the experimental accuracy.

During normal operation the magnetic field strength is controlled with reference to a carefully calibrated ammeter which measures the magnet current. A large search coil with turns area 1.7×10^6 turns cm^2 encircling the vacuum tank monitors the magnetic field with respect to time. The integrated output from this coil is displayed on a double-beam oscilloscope with a long time base, thus enabling suitable adjustment to be made with respect to the time of entry of the particle beam (section 3).

SECTION 3

Operation of the Bubble Chamber

(i) Timing

In order to relate the sequence of operation of the bubble chamber to the synchrotron cycle, timing is derived from the mirror system available from the accelerator. This system is briefly described in Chapter I, section 1. A suitable mirror pulse is applied to 4 variable delay circuits in parallel, two of which are used to control the expansion system. These two signals, separated by a known time of several milliseconds, are applied to a control circuit which operates the Barksdale valve (section 2(i)). The duration of the expansion is varied by adjusting the time interval between the two pulses, A third delay box triggers the flash circuit mentioned in section 2(iii). The fourth delay box provides a trigger for the oscilloscope on which the pressure transducer output is displayed (section 2(i)). On the other beam of this oscilloscope are shown a pulse from a scintillation counter in the particle beam and the pulse triggering the flash circuit. With reference to this trace adjustment is made of the time between the instants of particle entry and photography.

Where very precise timing is not essential a sequence

timer is used. An 8 r.p.m. electric motor drives a system of wheels, each one of which carries two overlapping adjustable cams operating microswitches. Each revolution the wheels are stopped by an electrically operated pawl, and a slipping clutch allows the motor to continue running. The sequence timer is related to the synchrotron cycle by a signal from a synchronous motor used for timing the radiofrequency power amplifier on the synchrotron (Chapter I, section 1). Three of the wheels operate relays controlling the excitation system for the magnetic field (section 2(iv)). One switches on and off the field current to the pilot exciter; a second relay reverses this current, and a third initiates the anode firing circuit for the ignitron. The maximum field is adjusted to coincide with the proton beam by displaying on the oscilloscope used to show the integrated output from the field monitoring coil, the pulse from the scintillator in the beam. This adjustment is not critical as the magnetic field has a fairly broad peak. The timer is also used to close the solenoid valve in the pressure control line to the chamber (section 2(ii)) and to start the motors which wind on the film between pulses.

(ii) Preparation

Preparatory to an experimental run the chamber is evacuated to remove impurities and filled with hydrogen gas

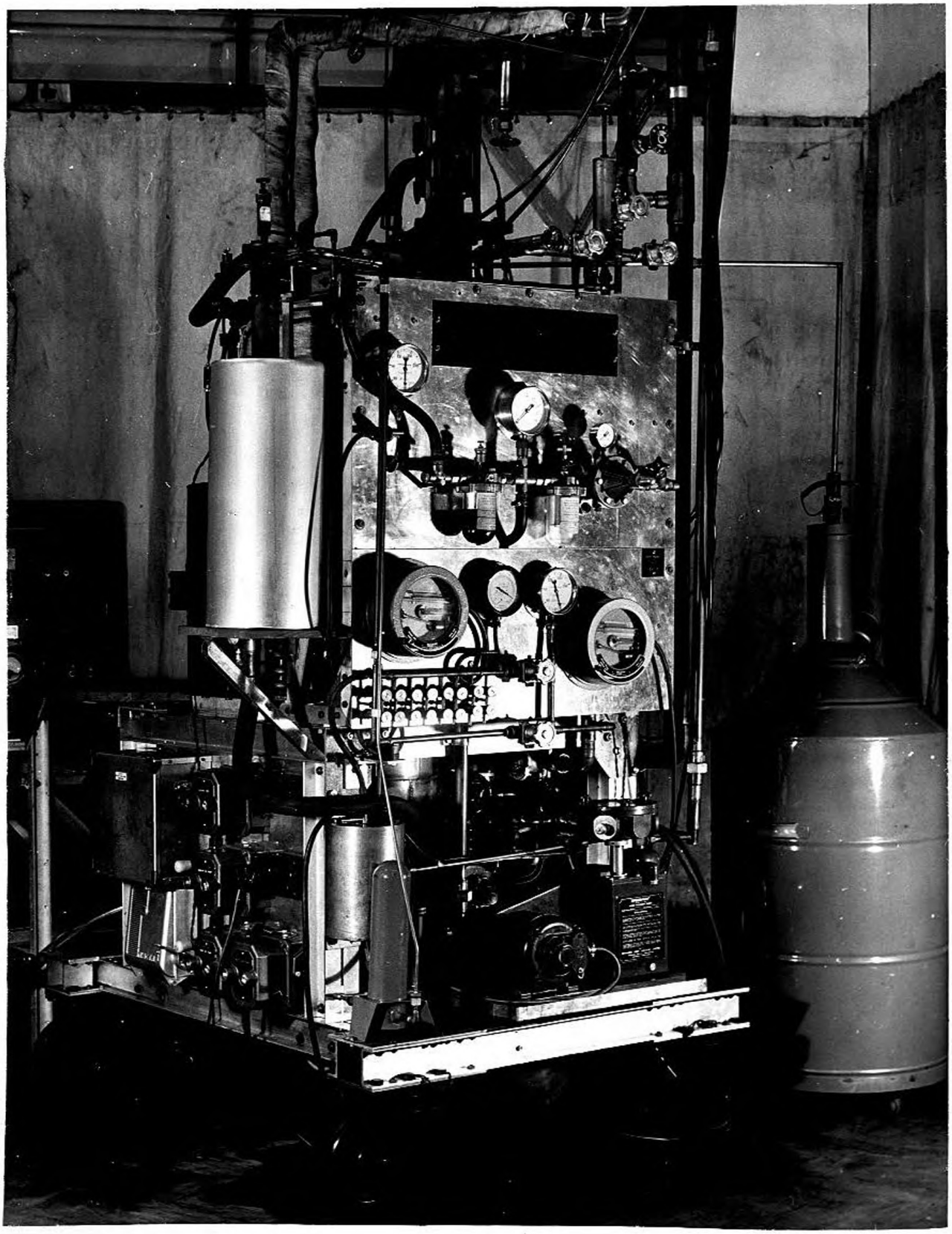

PLATE IV

several times. Provided there is a good vacuum ($\sim 10^{-5}$mm. of Hg) in the main tank both reservoirs are filled with liquid nitrogen to precool the chamber to 77°K. Plate IV shows a general view of the chamber installation with a liquid nitrogen dewar in position. Liquid nitrogen temperature is reached after about 2 days; cooling takes place by radiation to the surrounding heat shield, conduction along the heat leak and support rods and by gaseous convection in the chamber. At the end of this period the inner tank is emptied and the vent pipe is closed. The reservoir is then evacuated to a pressure of a few mm. of Hg and flushed with hydrogen gas. This process is repeated once or twice and finally the inner tank is left under one atmosphere of hydrogen. A 50 litre dewar (by Superior Air Products Co.) is connected to the inner reservoir by means of a double-walled transfer tube and liquid hydrogen is forced over using a rubber balloon as a pump. A liquefier manufactured by S.E.C.M.E.R. (Grenoble) supplies about a 100 litres of liquid hydrogen a day when required. As remarked upon earlier (section 2(ii)) the chamber is filled by condensing precooled high purity gas under pressure. Condensation takes place in the bellows which is kept at 21°K by liquid hydrogen in the reservoir. The chamber is cooled by liquid running down the expansion pipe and evaporating. When the chamber and expansion system are full of liquid, several hours

after the first condensation, the heaters are switched on to bring the temperature of the chamber to its operating value of about 27°K.

(iii) Operation

The chamber pressure is usually maintained at 10-15 p.s.i. above the liquid vapour pressure; that is at about 75 p.s.i.g. For a starting pressure of only a few p.s.i. above the vapour pressure, a bubble forms in the chamber after a few expansions. Under these conditions the sensitivity of the chamber is impaired and distortions become serious. On the recompression stroke bubbles at the top of the chamber condense thus releasing heat which leads to undesirable temperature gradients. According to the signal from the pressure transducer the chamber pressure falls to almost one atmosphere on expansion. The initial fall takes place in 10-15 milliseconds after which time the pressure can be held steady for any period up to a few hundred milliseconds. Repressurisation does not take place at once because the bellows is not fully extended; the chamber behaves therefore asif pressure defined. Under normal operation recompression occurs a further 10-15 milliseconds after the initial fall in pressure. Experience with the full energy proton beam from the Birmingham synchrotron has indicated that a small flash delay should be employed to

minimise distortions. In practice, the delay is usually set at 2 milliseconds since the beam has a width of 1-1.5 milliseconds and jitters in time by about 1-2 milliseconds. As mentioned earlier in this section, the flash delay is monitored by reference to an oscilloscope carrying signals from a scintillation counter in the beam and a delay box triggering the flash circuit. The latter signal is adjusted to take place just before recompression so that the chamber remains expanded for a minimum time, thus reducing the liquid hydrogen consumption. No tracks have been observed for beams entering the chamber in the first 5-10 milliseconds after the initial fall in pressure, so that the total time necessary for the expansion-recompression cycle is rather more than 30 milliseconds.

Under static conditions liquid hydrogen is boiled off at the rate of one litre per hour, but, when operating fully in a pulsed magnetic field of 16,000 oersted, consumption rises to about 6 litres per hour. The heat input to the chamber due to the $\int p\, dv$ work must be small, otherwise the operating temperature could not be maintained with the existing heat leak. The extra loss of liquid hydrogen is probably due to splashing at the back of the bellows, and may be reduced by installing baffles in the bellows container. If the chamber is run for 8 hours a day and kept under static conditions for

the remaining 16 hours, then about 75 litres of liquid per day are required, which can easily be supplied by the liquefier. However, initially about 40 litres are required to cool the chamber from liquid nitrogen temperature. Sufficient liquid hydrogen can be ensured before an experimental run as there is storage capacity for 200 litres.

(iv) Safety Precautions

Concentrations of hydrogen in air between 4% and 94%, by volume, are dangerous if ignited because of the resulting explosion. It is necessary therefore to prevent such a build-up and to ensure that the risk of sparks, etc. near the apparatus is negligible. Consequently electric motors are of the induction type and the electronic control circuits are some distance from the chamber assembly. In order that a slow leak of hydrogen into the air around the apparatus does not go undetected a katharometer is used, which sounds a warning bell if the concentration exceeds 1%. As a further precaution the apparatus is surrounded by a tent of asbestos cloth and a fan in the roof changes the air every few minutes. Since the reservoir and dewar system are not pressurised a sudden release of hydrogen from them is unlikely to occur. As referred to in section 2(ii), the main vacuum tank is designed to cope with a sudden surge of hydrogen gas in the

event of a rupture in the chamber.

SECTION 4

The Deuterium Filling System

(i) Introduction

The results of an experiment performed in the diffusion cloud chamber with a gas filling of deuterium (Batson et al., 1959; see Appendix) have stressed the interest in operating the bubble chamber with liquid deuterium. The cloud chamber experiment showed that the deuteron behaves as two free nucleons at this energy, thus enabling proton-neutron as well as proton-proton interactions to be studied. Further, a knowledge of both types of proton-nucleon inelastic cross sections makes possible a test of the validity of the charge independence of nuclear forces. As indicated in section 1, results of greater statistical accuracy and experimental certainty should be possible with the bubble chamber.

The boiling point of deuterium is 23.6°K which is a few degrees higher than that of hydrogen (20.4°K), consequently, to obtain a sufficient degree of superheat the operating pressure and temperature must be higher with liquid deuterium. A group at Brookhaven (Courant et al., 1959) have made a systematic comparison of the operating conditions in a piston-expanded bubble chamber with fillings of hydrogen and deuterium. They find the chamber sensitive to ionising radiation for a

temperature range of 26.1 - 28.9°K in hydrogen, which agrees with the observations on the present chamber. The upper limit was set by the method of temperature control which employs a pressurised hydrogen bath. In deuterium they find a temperature range of 30.5 - 32.6°K; again, the upper limit is determined by the apparatus. Also of interest is their investigation into the effect of the increased background in deuterium due to tritium; they observed that conditions were not noticeably worse than for hydrogen. At Berkeley, chambers 4" and 15" in diameter have been operated for extended periods with deuterium fillings. An optimum operating temperature range of 33.2 - 33.5°K is reported for the 15" chamber (Gow, 1958); the apparently higher operating temperature when compared to the piston-expanded chamber at Brookhaven is possibly due to the use of a gas expansion.

Deuterium is expensive and difficult to obtain in large quantities; consequently the apparatus that has been developed to fill the present chamber is designed as an enclosed system, thus enabling recovery and storage of the gas. About six and a half litres of liquid are required to fill the chamber and bellows system, which represents 220 cu.ft. of deuterium at N.T.P. A large storage tank of about 100 cu.ft. has been manufactured and will enable at least twice this amount of gas to be stored at a few atmospheres pressure. A high

FIGURE 24

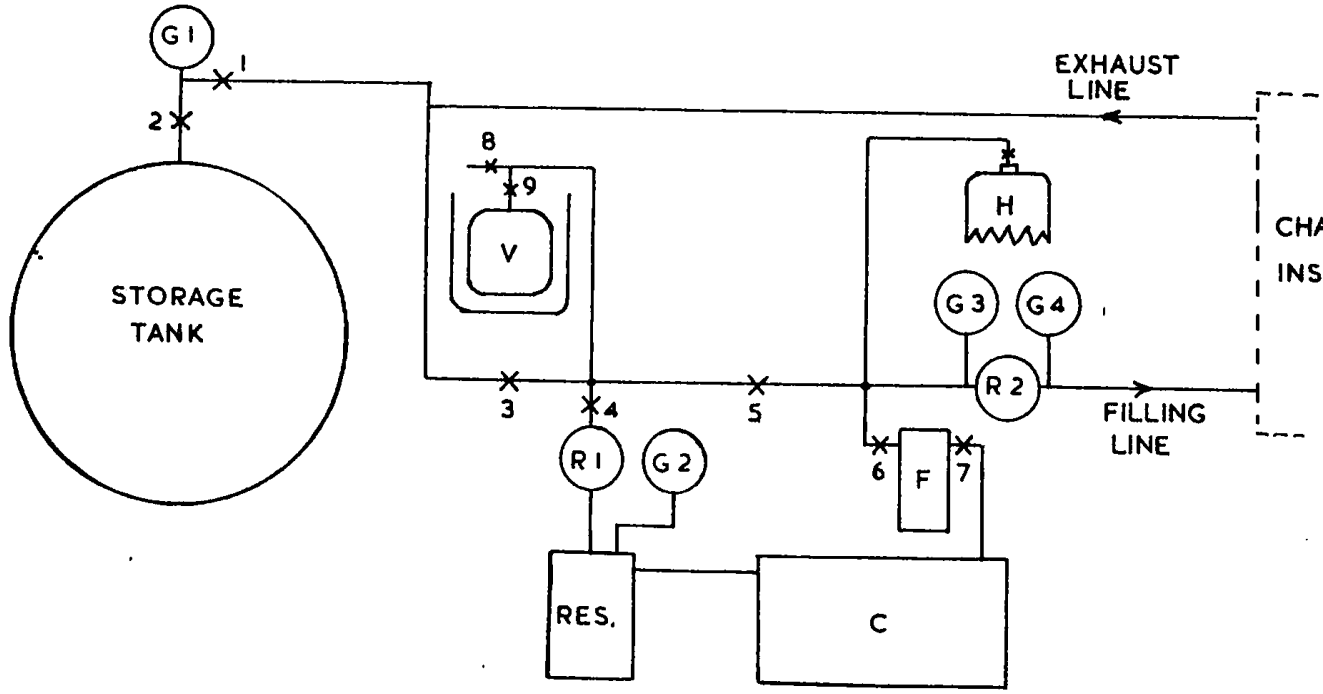

THE DEUTERIUM FILLING SYSTEM

X TAP

G PRESSURE GAUGE

R PRESSURE REGULATOR

F OIL FILTER

C COMPRESSOR

H HIGH PRESSURE CYLINDER

V VIBRAC CYLINDER

RES. RESERVOIR

pressure storage was decided against as this would necessitate a large compressor, which was absolutely leak tight, for restorage of gas between experiments. A small totally enclosed compressor has been embodied in the system to provide pressure control when operating the chamber. The large vessel will also serve as a "dump" tank for gas from the chamber if an emergency arises during operation. A small compressor has been installed to collect the gas pumped from between the chamber sealing gaskets and to return it to the main tank. A vacuum oil pump, as used for hydrogen operation, cannot be made sufficiently leak tight to prevent contamination of deuterium and also it will not operate against a head pressure of 2-3 atmospheres in the storage tank. Figure 24 shows a schematic diagram of the filling system which has been used for several experimental runs with hydrogen.

(ii) The apparatus

The storage vessel, which is cylindrical in shape with dished ends, is 4' in diameter with an overall length of 8'. It is constructed from steel sheet 3/16" thick welded at the joins, and designed for a working pressure of 56 p.s.i.g. However, the makers (Rubery Owen and Co.Ltd.) subjected the vessel to a test pressure of 170 p.s.i.g. before delivery. It is mounted on wheels with the axis horizontal and there

are 3 ports on the top of the curved surface. Referring to Figure 24, a ½" internal diameter copper pipe connects the compressor unit and exhaust line from the chamber to one of the tank ports. Valve 1 isolates the storage vessel from the rest of the system and valve 2 is included as a safety precaution in the event of failure of the first valve. Valve 2 is normally open so the gauge G1 monitors the tank pressure.

The compressor (c), which provides the source of high pressure to the chamber is a totally enclosed type (by Marco Refrigerators Ltd.) normally used in a refrigeration unit. It is driven by a 1½ H.P. motor and produces an output pressure of 200 p.s.i.g.; at this pressure a switch stops the motor. Since the input line is common to the outer casing of the compressor it is necessary to prevent the input pressure from rising too high, consequently, regulator R1 (by Hale Hamilton and Co.Ltd.) is set at 15 p.s.i.g. thus ensuring no pressure, measured on gauge G2, in excess of this value. Both the input and output connections to the compressor contain flexible metal tubing (by the Power Flexible Tubing Co.Ltd.) to minimise transmission of motor vibration to the rest of the unit. The high pressure gas from the compressor passes through a large capacity oil separator (F) (by Carter Refrigeration and Airconditioning Ltd.) which incorporates a mechanism for returning the oil to the sump. Tests have been

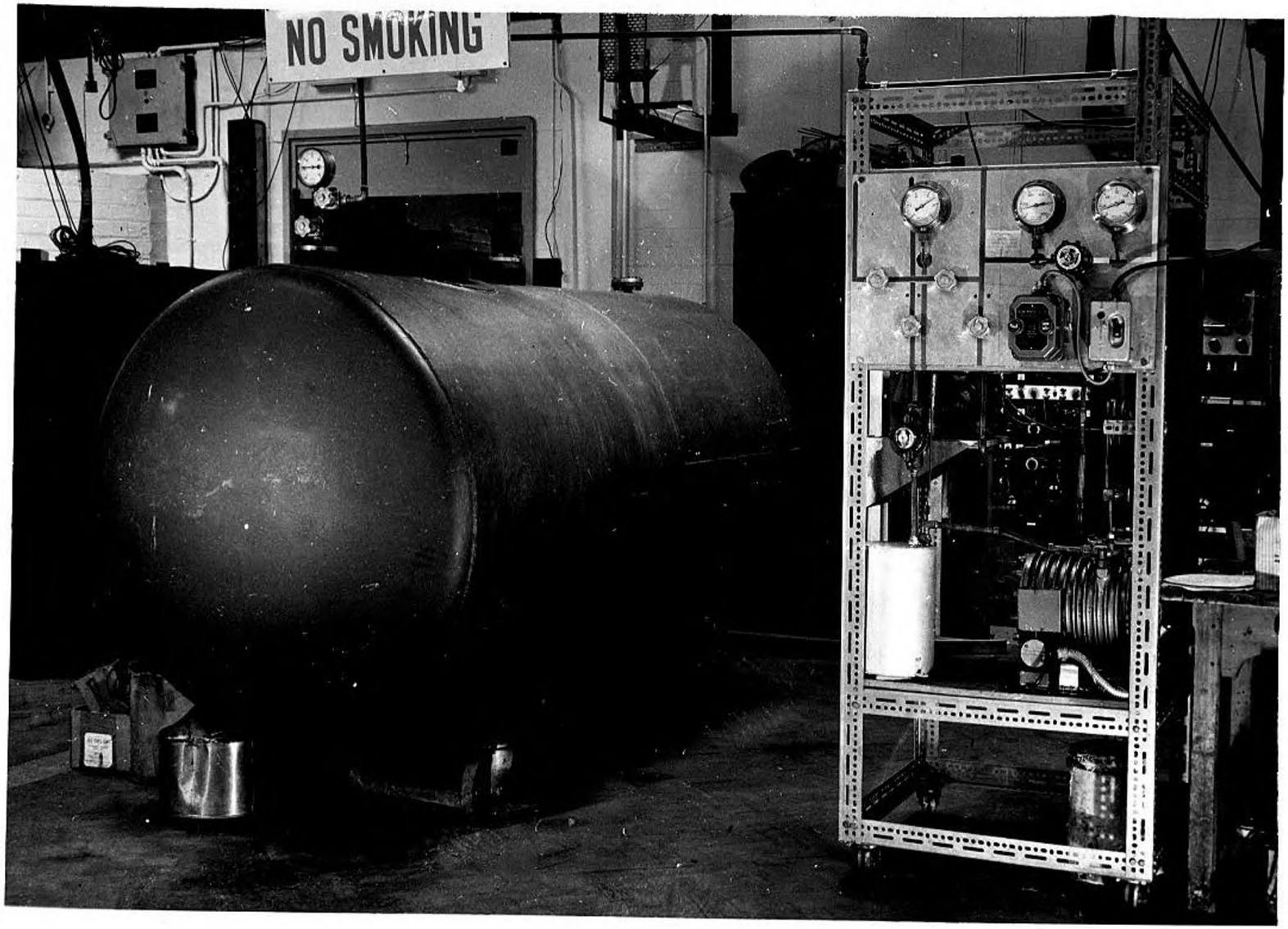

PLATE V

carried out with a deuterium gas sample, to show that exchange with hydrogen in this oil is unimportant. After leaving the filter (F) the gas passes into a high pressure storage bottle (H), of capacity 0.8 cu.ft., the pressure in which is noted from gauge G3. When filling this cylinder (H) to a pressure of 200 p.s.i.g. valves 1, 3, 4, 6 and 7 are open and valve 5 is closed. It is essential to close valve 7, when the compressor stops, to prevent gas leaking from the high pressure to the input side. The variable regulator R_2 (by Hale Hamilton Co.Ltd.) controls the pressure, monitored on gauge G4, to the 3/16" internal diameter copper filling line, which feeds gas to the purifiers on the chamber installation (section 2(ii)). With valves 4 and 6 closed and 5 open the storage tank is connected directly to the filling regulator (R_2). However, the tank pressure is normally too low for operational purposes. The tank and compressor assembly are shown on Plate V. As described in section 2(ii) the chamber system is protected by a spring loaded safety valve, from which gas will pass into the exhaust line shown in Figure 24 during operation with deuterium. The chamber is also connected to this line when either of the two valves by-passing the safety valve is opened. For ease of mobility, the complete filling unit is mounted on a trolley.

A small 1/8 H.P. compressor (by Edwards High Vacuum Ltd.)

which is completely enclosed collects gas from between the double gaskets sealing the chamber windows, and returns it to the main storage vessel. It maintains a pressure of a few m.m. of Hg between the gaskets and its output is connected to the exhaust line which is normally at the pressure of the tank.

A Vibrac steel cylinder of four litres capacity (by Vickers Armstrongs Ltd.), filled with activated charcoal, may be used as a source of high pressure in the event of the large compressor failing. Experience with the deuterium filling system for the cloud chamber (Batson et al., 1957) showed that on filling the cylinder to one atmosphere at 77°K and sealing it, a pressure of 900 p.s.i.g. is obtained at room temperature. However, because of the small capacity of the cylinder, filling the bubble chamber by the above method would be tedious. During operation of the chamber it may be necessary to dismantle part of the enclosed system, in which case it is desirable to transfer all deuterium gas to the storage tank. If the filling and chamber systems are opened to the storage vessel, then a few cu.ft. only of gas lie outside the tank. By closing the filling line and isolating the tank, the compressor may be used to evacuate the system to a few hundred m.m. of Hg. pressure. Alternatively, a few cu.ft. of gas at a time may be absorbed by the Vibrac cylinder, its contents being transferred to the tank between absorptions.

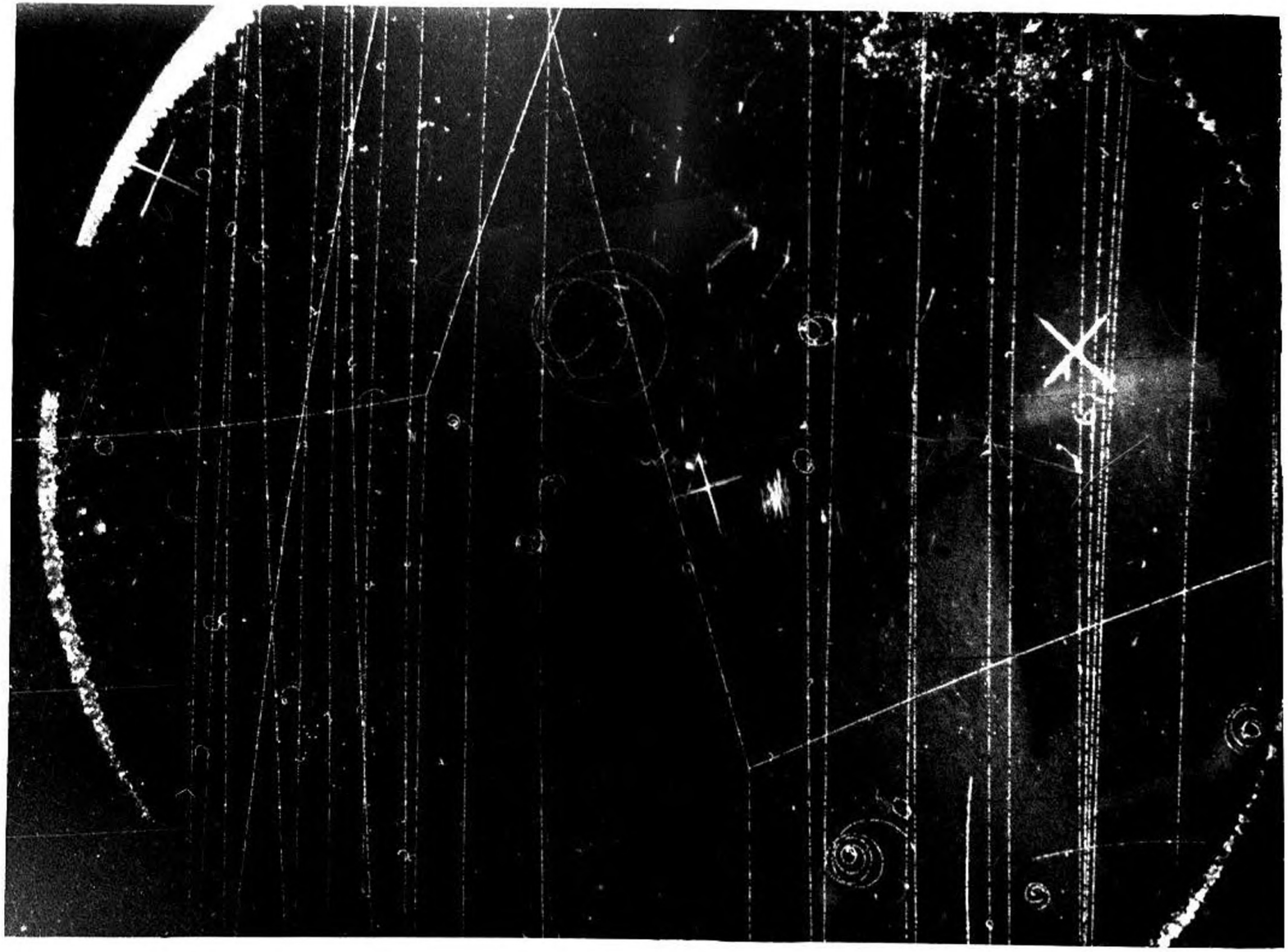

PLATE VI

SECTION 5

Experiments with the Bubble Chamber

So far the chamber has been operated with liquid hydrogen exposed to the full energy proton beam from the synchrotron. About 20,000 stereoscopic sets of photographs have been taken which should yield 6000 events. Examples of an elastic scattering (on the right) and an inelastic interaction, in which a meson is produced at a large scattering angle, are shown in Plate VI. Plate VII is a photograph of an event in which one of the secondaries interacts. The beam arrangement that has been used is almost identical to that employed in the cloud chamber experiment described in Chapter I, except that no analysing magnet was included. Scanning of photographs has begun in preparation for the detailed analysis of events. Measurements will be made on the track images using a semi-automatic scanner developed by B.B. Culwick and S.J. Goldsack of this laboratory. The information will be fed into a computer programmed to convert it into angles and curvatures in space.

The cloud chamber experiment showed that the elastic to inelastic ratio was just over unity, so that of the above total number of events approximately 3000 are elastic. Interesting information should be obtained in the near

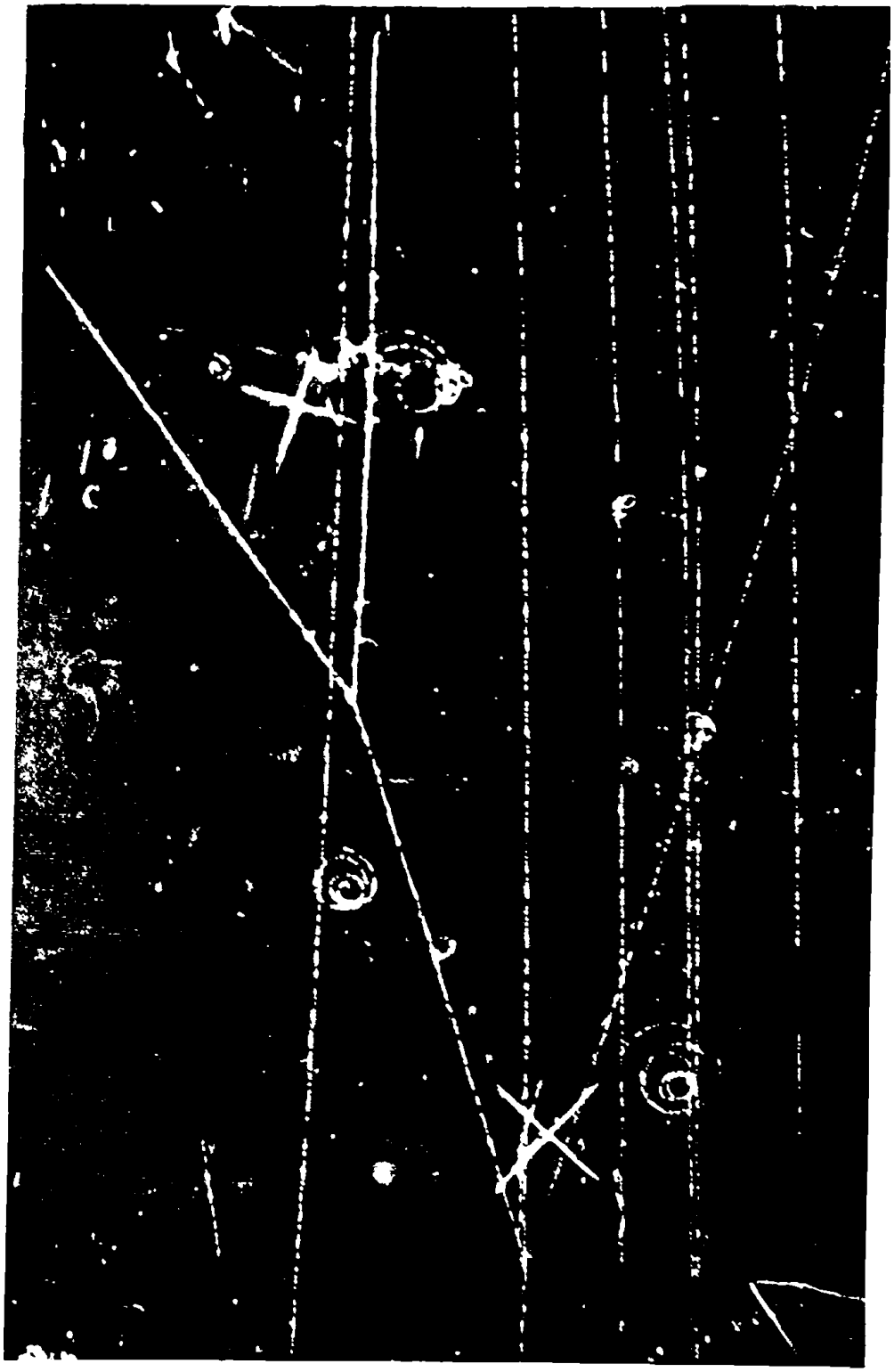

PLATE VII

future from these events which are easily identified and measured. More certain results on the elastic differential cross section at small angles should enable better comparisons to be made with the simple optical model and Brown's model mentioned briefly in Chapter I, section 2(v). The left-right asymmetry in elastic scattering described in Chapter I, section 3(i) should be confirmed with greater statistical certainty. Although the variation of polarisation with angle may be deduced from these events, such information is most satisfactorily obtained using a counter technique, where the very large numbers of events necessary for significant asymmetries are more easily accumulated. However, in the absence of a counter experiment measuring polarisation in hydrogen at this energy, such an analysis is probably worthwhile.

An estimate should be readily acquired of the partial cross sections for interactions giving 4-prong stars, since such events are easily recognised on the scanning table. In single meson production the comparatively rare decay mode of the neutral meson giving an electron pair (Dalitz, 1951) will lead to this type of event. Also in this category and perhaps of greater interest is double charged meson production.

When detailed information on all inelastic processes becomes available a confirmation or otherwise of the results of the cloud chamber experiment should be possible. Of

particular interest will be an analysis of single neutral meson production where the earlier experiment showed, on the basis of poor statistics, a disagreement with isobar theory. Along the lines of the further analysis described in Chapter I, section 3, it may be possible to obtain significant information on the spin of the postulated isobar.

If it proves possible to operate the chamber in a pencil beam of protons then, due to the increased rate of accumulation of events, a rapid study of certain features of large angle scattering can be made. For example, small angle elastic scattering may be investigated by an analysis of the recoil protons.

Now that 350 cu.ft. at N.T.P. of deuterium are available a study of interactions between protons and neutrons becomes possible. The cloud chamber experiment with a deuterium gas filling (Batson et al., 1959, see Appendix) yielded a large proportion of uncertain events. This was partly due to the limited sensitive volume and undesirable background resulting from the beta activity of the tritium contamination. It will be interesting to confirm whether or not the cross section for the reaction

$$p + n \longrightarrow p + n + \pi^{\circ}$$

is greater than expected on the basis of charge independence.

The possibility of exposing the bubble chamber to neutrons exists, but such beams have broad energy spectra and

the analysis of photographs is difficult when the incident particle cannot be seen. For these reasons p-n interactions are more satisfactorily studied by bombarding deuterium with protons, since the incident particle energy is well known. However, some work may be done on negative pion and double meson production, since these events appear as 3-prong stars. With a deuterium filling n-n interactions will occur but only events such as

$$n + n \longrightarrow n + p + \pi^-$$

will be seen. Nevertheless, a test of charge symmetry is possible when the above reaction is compared with the process

$$p + p \longrightarrow n + p + \pi^+$$

Now that about 5% of the internal beam of the synchrotron can be extracted, it becomes feasible to produce pion beams. A new range of experiments will be possible enabling the interactions of 500 - 600 Mev pions with nucleons to be studied.

ACKNOWLEDGEMENTS

I wish to express my sincere gratitude to Dr.L. Riddiford, my supervisor, who has encouraged me at all times. During the cloud chamber experiment I worked in close collaboration with Dr. A.P. Batson, who gave me valuable advice. The group as a whole thank the synchrotron staff for reliable operation of the accelerator, and acknowledge the useful work of Miss B. Hillman, Miss P. Cole and Mr. M.E. Boll.

In recent work on the liquid hydrogen bubble chamber, I have cooperated closely with Dr. G.A. Doran and Mr. J.B. Kinson. The bubble chamber group, who have also included Dr. D.C. Colley and Dr. A.W. Williams, are indebted to Mr. C. Barrow for his excellent technical assistance, and to Mr. G. Guest for the efficient running of the hydrogen liquefier.

Professor P.B. Moon has always shown a keen interest in the work for which I wish to thank him. The cost of the research was borne by the Department of Scientific and Industrial Research, to whom I am grateful for a maintenance grant.

REFERENCES

Baldin, A.M. and Kabir, P.K., 1958, Nuovo Cimento, IX (3), 547

Barker, K.H., 1954, Supplement to Nuovo Cimento, 11, 312.

Batson, A.P., Cooper, P.N. and Riddiford, L., 1956, J.Sci.Instrum, 33, 302.

Batson, A.P., Culwick, B.B., Klepp, H.B. and Riddiford, L., 1957, J.Sci.Instrum., 34, 17.

Batson, A.P., Culwick, B.B., Klepp, H.B. and Riddiford, L., 1959, Proc.Roy.Soc.A, 251, 233.

Batson, A.P. and Riddiford, L., 1956, Proc.Roy.Soc.A, 237, 175.

Block, M.M., 1956, Phys.Rev., 101, 796.

Booth, N.E., Hereford, F.L., Huq, M., Hutchinson, G.W., Law, M. Segar, A.M. and White, D.H., 1958, Nuclear Physics,7, 284.

Borelli, V., Bergia, , Perez-Ferreira, and Waloschek, P., 1959, Kiev Conference Report (Preprint).

Brown, G.E., 1958, Phys.Rev., 111, 1178.

Brueckner, K.A., 1952, Phys.Rev., 86, 106.

Brueckner, K.A. and Watson, K.M., 1952, Phys.Rev., 86, 923.

Chambers, E.E. and Hofstadter, R., 1956, Phys.Rev.,103,1454.

Chen, F.F., Leavitt, C.P., and Shapiro, A.M., 1956, Phys.Rev., 103, 211.

Colley, D.C., Kinson, J.B. and Riddiford, L. 1959, Nucl.Instrum. and Methods, 4, 26.

Cork, B., Wenzel, W.A. and Causey, C.W., 1957, Phys.Rev., 107, 859.

Courant, H., Jensen, J.E., Louttit, R.I. and Sanford, J.R., 1959, Rev.Sci.Instrum., 30, 280.

Crawford, F.S., Cresti, M., Good, M.L., Solmitz, F.T. and Lynn Stevenson, M., 1959, Phys.Rev.Letters, 2(1), 11.

Culwick, B.B., 1957, J.Sci.Instrum., 34, 154.

Dalitz, R.H., 1951, Proc.Phys.Soc.A, 64, 667.

Davies, O.L., 1957, Statistical Methods in Research and Production. London: Oliver and Boyd.

Dowell, J.D., 1958, Ph.D. thesis, University of Birmingham. Also to be published: 1959, Proc.Phys.Soc.

Duke, P.J., Lock, W.O., March, P.V., Gibson, W.M., McEwen,J.G., Hughes, I.S. and Muirhead, H., 1957, Phil.Mag., 2, 204.

Durbin, R., Loar, H. and Steinberger, J., 1951, Phys.Rev., 84, 581.

Dzhelepov, V.P., Moskalev, V.I. and Medved, S.V., 1955, Dokl.Acad.Nauk. S.S.S.R., 104, 380.

Eisler, F., Plano, R., Prodell, A., Samios, N., Schwartz, M., Steinberger, J., Bassi, P., Borelli, V., Puppi, G., Tanaka, H., Waloschek, P., Zoboli, V., Conversi, M., Franzini, P., Manelli, I., Santangelo, R., Silvestrini, V., Brown, G.L., Glaser, D.A. and Graves, C., 1958, Nuovo Cimento, VII(2), 222.

Fermi, E., 1950, Prog,Theor.Phys.(Japan), 5, 570.

1953, Phys.Rev., 92, 452.

1954, Phys.Rev., 93, 1434.

Fernbach, S., Serber, R. and Taylor, T.B., 1949, Phys.Rev., 75, 1352.

Fields, T.H., Fox, J.G., Kane, J.A., Stallwood, R.A. and Sutton, R.B., 1954, Phys.Rev., 95, 638.

Fowler, W.B., Shutt, R.P., Thorndike, A.M. and Whittemore, W.L., 1954, Phys.Rev., 95, 1026.

Friedman, J.I. and Telegdi, V.L., 1957, Phys.Rev.,105, 1681.

Garwin, R.L., Lederman, L.M. and Weinrich, M., 1957, Phys.Rev., 105, 1415.

Glaser, D.A., 1952, Phys.Rev., 87, 665.

1953, Phys.Rev., 91, 762.

Gow, J.D., 1958, University of California, Radiation Laboratory Report UCRL 8545.

Heer, E., Roberts, A. and Tinlot, J., 1958, Phys.Rev.,111, 645.

Hildebrand, R.H. and Nagle, D.E., 1953, Phys.Rev., 92, 517.

Holmquist, F.N., 1958, University of California, Radiation Laboratory Report UCRL 8559.

Hughes, J.S., March, P.V., Muirhead, H. and Lock, W.O., 1957, Phil.Mag., 2, 215.

Huq, M., 1958, Ph.D. Thesis, University of Birmingham.

Kalbach, R.M., Lord, J.J. and Tsao, C.H., 1959, Phys.Rev., 113, 325.

Kovacs, J.S., 1956, Phys.Rev., 101, 397.

Lattes, C.M.G., Muirhead, H., Occhialini, G.P.S. and Powell, C.F., 1947, Nature, 159, 694.

Law, Margaret E., Hutchinson, G.W. and White, D.H., 1958/59 Nucl.Phys., 9, 600.

Lee, T.D. and Yang, C.N., 1956, Phys.Rev., 104, 254.

Lindenbaum, S.J. and Sternheimer, R.M., 1957, Phys.Rev., 105, 1874.

Linlor, W.I., Kerns, Q.A. and Mark, J.W., 1957, Rev.Sci.Instrum., 28, 535.

Mandelstam, S., 1958, Proc.Roy.Soc.A, 244, 491.

Mescheryakov, M.G. and Neganov, B.S., 1955, Dokl.Akad.Nauk. S.S.S.R., 100, 677.

Mescheryakov, M.G., Nurushev, S.B. and Stoletov, G.D., 1957, J.Exp. and Theor.Phys., 33, 37.

Moon, P.B., Riddiford, L. and Symonds, J.L., 1955, Proc.Roy.Soc.A, 230, 204.

Morpurgo, G., 1958, Nuovo Cimento, IX(3), 564.

Morris, T.W., Fowler, E.C. and Garrison, J.D., 1956, Phys.Rev., 103, 1472.

Parmentier, D. and Schwemin, A.J., 1955, Rev.Sci.Instrum., 26, 954.

Peaslee, D.C., 1954 a, Phys.Rev., 94, 1085.

1954 b, Phys.Rev., 95, 1580.

Serber, R. and Rarita, W., 1955, Phys.Rev., 99, 629.

Smith, L.W., McReynolds, A.W. and Snow, G., 1955, Phys.Rev., 97, 1186.

Stadler, H.L., 1954, Phys.Rev., 96, 496.

Sternheimer, R.M., 1954, Phys.Rev., 93, 642.

Tanner, N., 1957, Phys.Rev., 107, 1203.

Wallenmeyer, W.A., 1957, Phys.Rev., 105, 1058.

Wilkinson, D.H., 1958, Phys.Rev., 109, 1603.

Wolfenstein, L., 1956, Ann.Rev.Nucl.Sci., Vol.6, 43.

Wood, J., 1954, Phys.Rev., 94, 731.

Wright, R.W., Saphir, G., Powell, W.M., Maenchen, G. and Fowler, W.B., 1955, Phys.Rev., 100, 1802.

Wu, C.S., Ambler, E., Hayward, R.W., Hoppes, D.D. and Hudson, R.P., 1957, Phys.Rev., 105, 1413.

Yamaguchi, Y., 1958, Progr.Theor.Phys., 19, No.6, 622.

Yukawa, H., 1935, Proc. Phys.-Math.Soc.(Japan), 17, 48.